STIMULATION DESIGN AND EVALUATION OF HIGH TEMPERATURE SAGD WELLS

A Thesis

by

VIACHESLAU YURYEVICH KUDRASHOU

Submitted to the Office of Graduate and Professional Studies of
Texas A&M University
in partial fulfillment of the requirements for the degree of

MASTER OF SCIENCE

Chair of Committee,	Hisham A. Nasr-El-Din
Committee Members,	Maria A. Barrufet
	Mahmoud M. El-Halwagi
Head of Department,	A. Daniel Hill

August 2015

Major Subject: Petroleum Engineering

ABSTRACT

This thesis presents an experimental approach to design, perform, and evaluate stimulation treatments for SAGD producers completed with slotted liners.

Heavy oil production from a high temperature sandstone reservoir declined due to the blockage of slots in horizontal liners. Blocking materials were mainly presented by silicon-based scales, migrated fines, and numerous iron species. Previously, wells were mainly treated by HCl and a high pH chelating agent. These treatments did not improve the production significantly but corroded liners even more.

Three liners were pulled out from the wells. Blocking and scaling materials were collected from the slots and walls of these liners for analysis. The experimental process included static acid solubility tests using 15 wt% HCl at room temperature, SEM, and XRD analysis. Also, it was proved that hydrochloric acid is not an optimal solution for blockage removal in these producers. Additionally, organic solvent preflush proved to be an effective potential improvement in the treatment design.

Oil sand samples were collected from the reservoir. The mineralogy of these samples was analyzed in detail. Organic matter was removed, and the rock samples were separated in sand, silt, and clay fractions. Presence of kaolinite, illite, muscovite, incomplete hydroxide interlayer smectite was proved by XRD, SEM, TEM, FTIR, and AAS. Also, interstratification of mica and kaolinite was observed. These results were used to make a decision concerning the choice of compatible treatment fluid.

Seven stimulation treatments were conducted in five different wells using foamed chelating agent (GLDA). Flowback emulsion was separated and prepared for analysis which included ICP and GLDA titration. Additionally, the decomposition of GLDA at reservoir conditions was mimicked using aging cells. Decomposition products were identified using GC-MS and were found to be glutaric and aminodiacetic acids. Possible improvements in the treatment's program and recommendations were formulated based on the obtained data. For example, the soaking time was reduced from 6 to 4 hours after the first treatment. Production data analysis proved the effectiveness of the treatment design.

Overall, it was shown that only a systematic approach could be useful to design a successful treatment and achieve a positive impact.

DEDICATION

I dedicate this work to my family. To my dear parents, Yuri and Valentina Kudrashovy, and to my beloved brother – Igor Kudrashov.

ACKNOWLEDGEMENTS

I am very thankful and indebted to my advisor Dr. Hisham Nasr-El-Din for the constant guidance, support, and motivation, which he provided during these years. I treasure the opportunity to be part of such a great team.

I would like to thank Cenovus Energy for the financial support of this work and cooperation on this project. I strongly appreciate the help and feedback provided by Zied Ouled Ameur and Jeff Forsyth.

I am very grateful to my friends, colleagues, and the department faculty and staff for a great time at Texas A&M University.

Finally, I am forever thankful to my family.

NOMENCLATURE

D	Outer diameter of the liner, in
h	Distance between parallel slots, in
L	Length of the liner, in
l	Distance between slots' sections, in
$M_{initial}$	Mass of the scale before reaction with HCl, g
$M_{unreacted}$	Mass of the scale after reaction with HCl, g
S	Length of the slot, in
T	Thickness of the liner's wall, in
w	Width of the slot, in

GLOSSARY

AAS	Atomic absorption spectroscopy
DTS	Distributed temperature sensing system
ESI	Electrospray ionization
GC-MS	Gas chromatography-mass spectrometry
GLDA	Glutamic acid N, N-Diacetic acid
HCl	Hydrochloric acid
HF	Hydrofluoric acid
ICP	Inductive coupled plasma
SAED	Selected area electron diffraction
SEM	Scanning electron microscope
TEM	Transmission electron microscope
XRD	X-ray diffraction

TABLE OF CONTENTS

Page

Page

Page

LIST OF FIGURES

FIGURE Page

FIGURE Page

FIGURE Page

FIGURE Page

FIGURE Page

FIGURE Page

LIST OF TABLES

TABLE Page

1. INTRODUCTION

SAGD is a well-known and reliable enhanced oil recovery method, which is widely used for development of heavy oil reservoirs (Nasr et al. 1998). This technique leads to a reduction in the crude oil viscosity, and, as a result, oil recovery increases. Additional positive actions of the steam injection are the thermal expansion in the rock-fluid system, gravitational segregation into the steam (Kumar et al. 1992), and the effects of distillation and miscibility (Lim et al. 1992). However, this method can be a cause of severe formation damage due to the interactions of injected fluids with formation fluids and reservoir rocks. These problems include scale deposition and fines migration. Bennion et al. (1992) stated that the wettability alteration was the third form of formation damage associated with thermal recovery projects. One of the indicators of normal SAGD operations is a constant differential pressure (DP) between the injector and producer wells. An increase in this parameter may indicate a variety of restrictions present in the well or in the reservoir rocks. Usually, one of these restrictions is scale deposition which causes a production well to operate at a decreased pressure, which consequently increases the DP.

Serious formation damage occurs during steam injection because of the complex chemical reactions and hydrothermal effects in the reservoir (Okoye et al. 1990, 1991). This is especially important for poorly consolidated and high clay-content sandstones (Hajdo et al. 1994). The degree of damage is a function of the composition and properties of injected fluid, flow rate, and mineralogy of the reservoir. Fines migration

problems can be caused by inadequate clay control because clay minerals often serve as a cementing material in sandstones. Sand production is a result of the cement damage which can be caused by clay swelling. Hower et al. (1974) characterized the clays which are most common to hydrocarbon-bearing reservoirs. Clays can be a cause of formation damage associated with water-promoted disintegration, dispersion, and migration of clays. Young et al. (1980) described two basic types of clays: expanding and low water absorbing clays. Bennion et al. (1992) described two forms of damage because of mineral dissolution: re-precipitation of the solubilized minerals and release of fines, which can migrate into the flowing fluid stream and plug pore throats. Okoye et al. (1990) showed that the amount and type of solid material which form scales depends on factors such as pH, temperature, flow rate, and ionic makeup of reservoir fluids. Okoye et al. (1992) used the results of previous authors (Thornton and Radke 1988; Kia et al. 1987) and applied their results for the kinetic, electrostatic forces, and mass action theories.

Scales could be formed on the walls of the horizontal wells and on the surfaces of pumps. Most of the time, carbonate and silicate scales are predominant there. Davies et al. (1996) described that carbonate scales originate from the interaction of injected hot fluid and formation fluids. Ions that form carbonate scales usually originate from formation waters. Carbonate scales are the result of reactions at elevated temperatures between divalent ions and bicarbonate ions (HCO_3^-), carbonates (CO_3^{2-}), or even from carbon dioxide which can be dissolved in water. Chakrabarty and Longo (1994) claimed that swelling clays can fill up pore spaces, and CO_2 can dissolve calcite away from the

wellbore and lead to calcite precipitation in the near-wellbore region because of pressure reduction. Carbonate scales usually form because of the mixing of incompatible fluids (Ostroff 1981) and/or because of the change of pressure and temperature which is common for steam injection projects (Erno et al. 1991). An important point is that carbonate scales precipitate around the formation sand grains as a circumgranular cement that significantly reduces the permeability, while the effect on the open pore space is not significant. Silicon-based salts have been described as one of the most difficult scales to remove, often requiring the use of mechanical and/or chemical methods or fluoride-based chemicals which present environmental and safety concerns. Davies et al. (1996) investigated that the silica content of the produced water increased as a result of steam operations and stated that silicate scales result from interactions of a hot fluid with the formation. Gill (1998) described silicate scales, their formation mechanisms, polymerization, and co-precipitation with other minerals and biological activity in water. Some of these processes may take place concurrently, so it is difficult to predict equilibrium solubility. As previously stated, the solubility of amorphous silica is also dependent on many other factors such as, pH, temperature, particle size, particle hydration, and the presence of other ions such as iron and aluminium. A hard silica scale is formed when calcium carbonate or other mineral precipitates provide a crystalline matrix in which silica can be entrapped.

Possible preventative strategies could be implemented such as an operation under conditions less conductive to scaling, removing of ions to prevent them from reacting, and allowing deposits to be accumulated and removed periodically by

chemical/mechanical means. An additional approach is to leave ions in a solution but apply chemical treatment to disperse precipitates or modify their crystal growth patterns. In the last decade, some preventative techniques using chemical inhibitors were presented (Darrell et al. 2008; Nengkoda et al. 2008; Wang et al. 2010; Guan 2013).

Chemical treatments are widely used for removal of the damaging material, but sandstone acidizing is a real challenge for petroleum engineers. Regular mud acid with 12:3 HCl:HF ratio is the most popular and traditional acid used for sandstone for years. Carbonate scales are soluble in HCl, and silica scales are soluble in HF. The depth of the damaged zone is also a very critical factor. For deep damage, a retarded HF acid is usually recommended (Gdanski 1985; Thomas and Crowe 1978; Al-Dahlan et al. 2001). Serious problems occur at high temperature applications because of high and uncontrolled reaction rates and corrosion to well tubulars. HCl can dissolve the rust and produce a significant amount of ferric (iron with an oxidation number of 3+). Fe^{3+} can easily precipitate and cause serious formation damage. It should be noted that inhibitors should always be used with HCl, especially at high temperatures. However, Schechter (1992) explained adsorption effects and changes in wettability connected with an excessive amount of inhibitors. Another critical aspect for the economics of the treatments is the cost of corrosion inhibitors. Additionally, for some cases, the mineralogy of a sandstone reservoir could limit possible options because an acid that is preferred for the removal of a specific mineral cannot be used due to an incompatibility with another mineral present in the same reservoir. For example, HCl acid is not compatible with illites (Thomas et al. 2001; Mahmoud et al. 2011) and zeolites (Rogers

et al. 1998). HF is very reactive with clays and some cementing materials (DeVine et al. 2002) which could cause sand production and formation damage. Organic acids could cause swelling in reservoirs with smectites.

Because of these challenges, alternatives to mud acid have recently been developed. For example, Yang et al. (2012) proposed organic-HF acids system. Zhou and Nasr-El-Din (2013) examined a single stage sandstone acid system based on HF and phosphonic acid. Stolyarov and Alam (2013) presented a HF-organophosphonate acid system. Another good solution for sandstone reservoirs could be chelating agents (Fredd and Fogler 1997 and 1998). For example, aminopolycarboxylic acids were used to stimulate sandstone formations (Ali et al. 2002; Ali et al. 2005; Parkinson et al. 2010). Chelants create complexes with di- and trivalent cations and minimize their precipitation. They are also much weaker than HCl and simple organic acids which means they dissolve less cementing materials and don't cause sand production after a treatment.

Acid stimulation of high temperature wells is a difficult task, mainly because of the high reaction rate and high corrosion rate induced by strong acids. Chelating agents possess an additional benefit because of their slow reaction rate which enables better placement in the target zone. Adenuga et al. (2013) studied the reaction of GLDA solutions with dolomite. They showed that GLDA reacted slower than simple organic acids. GLDA is better suited for retardation and deeper penetration into a dolomitic reservoir than simple organic acids. Li et al. (2008) conducted studies of reaction mechanisms and kinetics for organic acids and chelating agents. They reviewed most of

the models and described results for the reaction with calcite. An important conclusion is that the complexation effect mainly exists for calcite reaction with chelating agents. Rabie et al. (2011) also studied GLDA reaction kinetics. They identified the mechanism by which GLDA reacts with calcite by measuring percentage of complexation at different temperatures and disk rotational speeds.

Hydroxyathylaminocarboxylic acids (HACA) were used for stimulation of high temperature formations (Frenier et al 2001; 2003; 2004). Reyes et al. (2013) tested an aminopolycarboxylic acid (APCA) which was found to be a biodegradable chelating agent. One more important issue with the use of chelating agents is their thermal stability at high temperatures. (Sokhanvarian et al. 2012) examined the thermal stability of GLDA and other chelates at different temperatures and soaking time. According to Nasr-El-Din et al. (2012), relatively low concentrations of corrosion inhibitors for organic acids help to protect low carbon steels from a 20 wt% GLDA solution. Braun et al. (2012) investigated the environmental impact of GLDA and compared its toxicity with other chelating agents such as EDTA and NTA. They presented that GLDA is biodegradable in fresh and seawater. It also has the best in class eco-footprint of the most common chelating agents.

Combined systems of chelants and HF have also been applied in the field such as a system of phosphonic acid with HF (Rae and di Lullo 2003). Armirola et al. (2011) developed an acid system that is based on a chelate, HF, and boric acid.

From the previously cited literature, the use of chelating agents on their own or as part of more complex stimulation fluid provides a viable alternative to mineral acids

in high temperature applications as demonstrated by both laboratory and field applications. The objectives of this work are to: (1) discuss in detail a field treatment that was done using chelating agent (GLDA), (2) review laboratory tests conducted to identify the properties of the chelating agent, and (3) evaluate the treatment and GLDA performance for a horizontal SAGD well.

2. BLOCKING MATERIALS ANALYSIS

The procedure of scale sampling and experimental work, which was conducted in order to determine main properties of the scale, will be discussed in this chapter. The evaluation of chemical and physical properties of the scale is a critical task for the design of the stimulation. It is important to know what materials are blocking fluid flow and how they were formed. The next question to be answered is about the effectiveness of chemicals which are usually used to address the problem. Experimental work will be discussed in detail to formulate possible improvements to the treatment design.

2.1 Methodology

Scale samples from three different injectors and producers were analyzed. First of all, the size and main parameters of each liner were measured using calipers and a ruler. Sampling of the materials, which cover its surface, illustrated that scale is not uniform at different surfaces but varies. For example, the scale on the top part of the liner has differences in structure from the scale on the bottom part. Observations demonstrated that in all cases, scale which was collected from the inner surfaces is different from the scale which was formed on the outer part of the liner. For these reasons, samples located on different surfaces of the liner were carefully collected for further analysis. In particular, to reach the blocking materials, the slots liners were carefully cut. Special isolating materials were used to not contaminate scale samples from the slots while cutting.

The next step after collecting numerous scale samples was to analyze those using SEM. The sample was coated with gold using a special sputter prior to the analysis to enhance the electron-sample interactions. This analysis revealed information about the sample including: external morphology (texture), chemical composition, crystalline structure, and orientation of the collected materials. Mainly, data was collected over a selected area of the samples' surfaces. For detailed description, a 2-dimensional SEM images and a qualitatively chemical composition spectrums were generated for each sample before and after acid solubility tests. This data helps to identify elements which were dissolved by 15 wt% HCl. Pictures of the reacting mixtures were also taken.

The percentage of the scale which were dissolved during the reaction with HCl was calculated by the next formula:

$$\text{Dissolved} = (1 - M_{unreacted}/M_{initial}) * 100\ \% \quad \text{(2.1)}$$

Where $M_{unreacted}$ is the dry mass of the materials which were collected after the reaction with HCl by filtering through 1 micron filter paper, and $M_{initial}$ is the mass of the collected scale before the reaction with HCl.

ICP was used for analysis of the fluids which were collected after the reaction. The preparation of fluids included: filtration and dilution (usually in range 1:250 – 1:1000 times) with deionized water.

Additionally, XRD was used to identify minerals which form scale collected from the slots. This data was used to understand whether blocking materials were formed inside the slots or were transported there by flow.

At the end of this phase, all of the experimental data was carefully analyzed in order to formulate the main conclusions.

2.2 Results and Discussions

2.2.1 Liner #1

Figure 2.1 presents the general view of liner #1. Slots are blocked and mainly not visible; however, the amount of slots could be evaluated from the cross section of the liner. Slot sections' proportions are shown in **Figure 2.2**.

Figure 2.1 – General view of liner #1

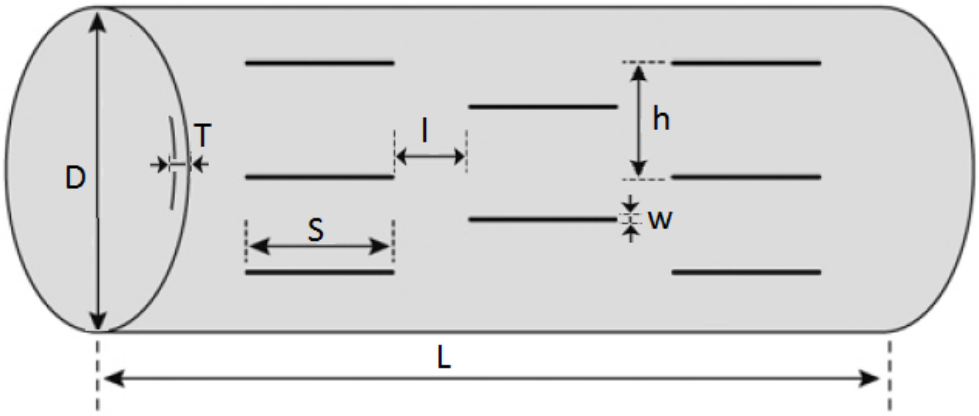

Figure 2.2 – Main parameters of liner #1

Table 2.1 contains the main parameters of liner #1 which were shown in Figure 2.2.

Table 2.1: Main parameters of liner #1

Main parameters of liner #1, in			
h	l	S	T
0.662	0.860	2.560	0.467

2.2.1.1 Outer scale samples

For liner #1, two samples of outer scale were collected. Blocking materials from the top semicircle part of liner #1 were mainly formed by corrosion products and scales

(scale sample #1). This part of the liner doesn't contain organic layers and is mainly blocked by silt sized grains (**Figure 2.3**).

Figure 2.3 – Top part of liner #1

For the bottom semicircle part of the liner, samples were also collected (scale sample #2). This part contains scale and corrosion products which consolidated by layers of organic material (**Figure 2.4**):

Figure 2.4 – Bottom part of liner #1

The textures of these two samples are very different (**Figure 2.5**). The sample from the top part of liner #1 is unconsolidated and powdery, while the sample from the bottom part is consolidated by organic materials which are "baked" together with scale and sand particles.

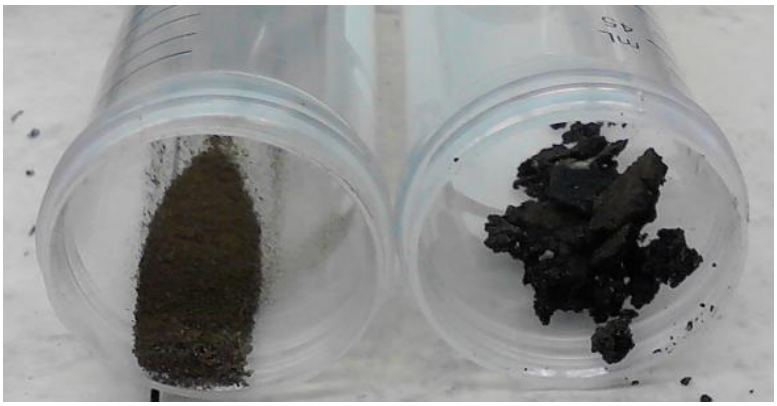

Figure 2.5 – Samples of the blocking materials taken from the outer surface of liner #1

First of all, samples were carefully grained, dried, and mounted in the SEM powder holder. **Figures 2.6** and **2.7** show electron microscope pictures with a magnification of 200 for both of the powdery and organic layered scale samples. Big grains both angular and rounded are cemented by the tiniest particles of scale from the top.

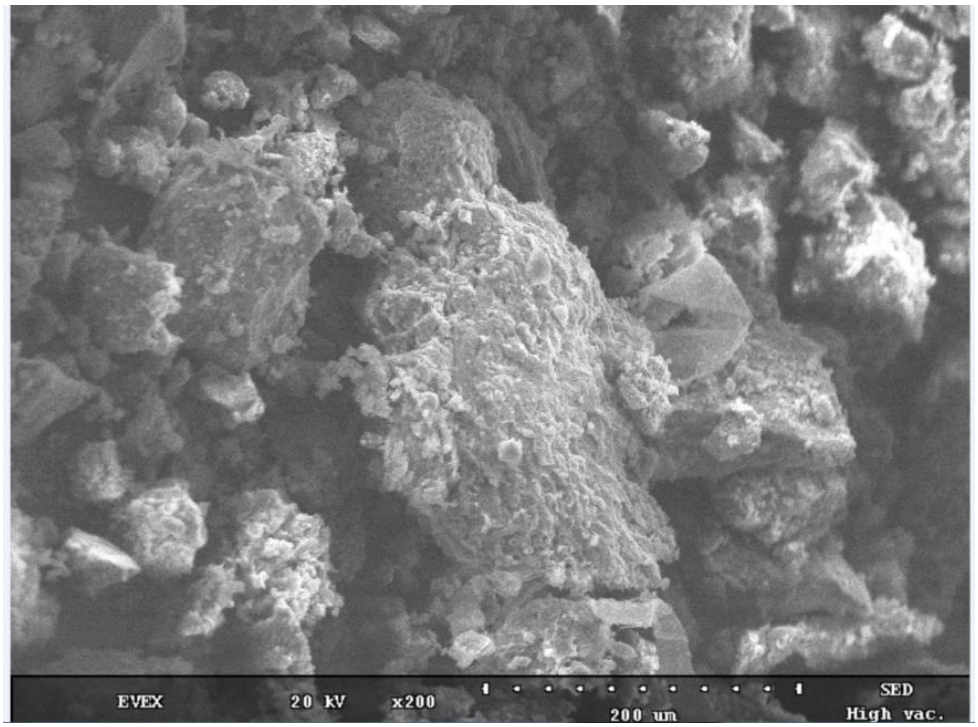

Figure 2.6 – Outer scale (top) electron microscope picture (magnification is 200)

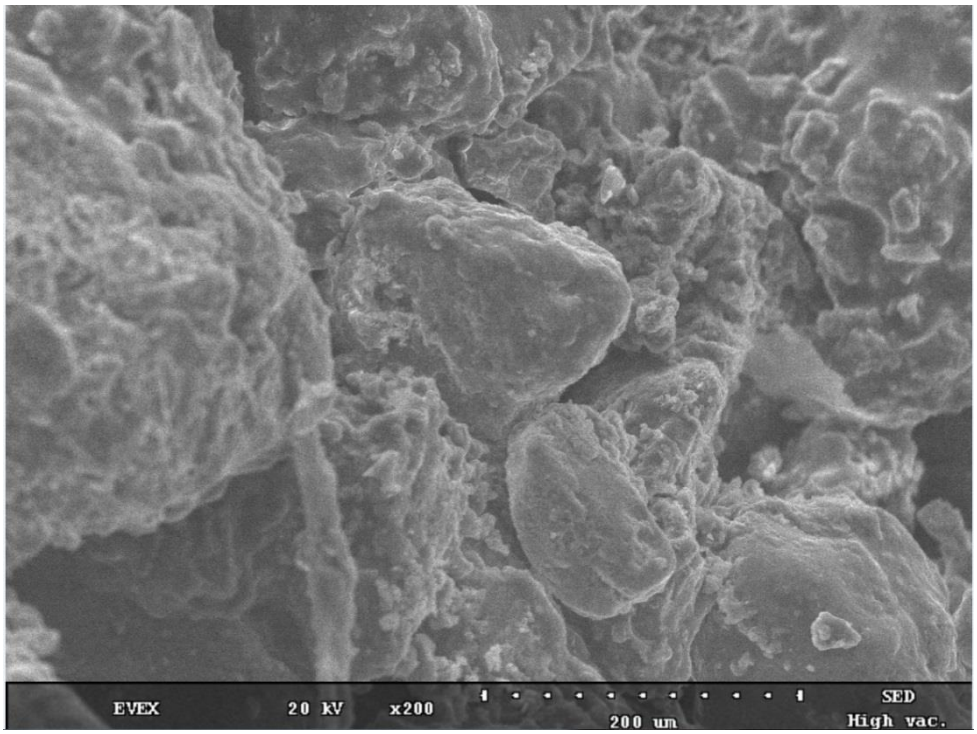

Figure 2.7 – Outer scale (bottom) electron microscope picture (magnification is 200)

The quantitative data about the chemical composition for these two samples are shown in **Figures 2.8** and **2.9**. Based on these results, the silicon content is higher for the sample with organic layers. This can be explained by the fact that big quartz grains are better cemented in the presence of organic material. At the same time, the amount of iron is relatively higher for the powdery sample from the top of liner #1 which is caused by the relatively higher amount of corrosion products in these blocking materials. Uncovered by organic materials, walls of liner tend to corrode faster than those of covered walls at the same conditions.

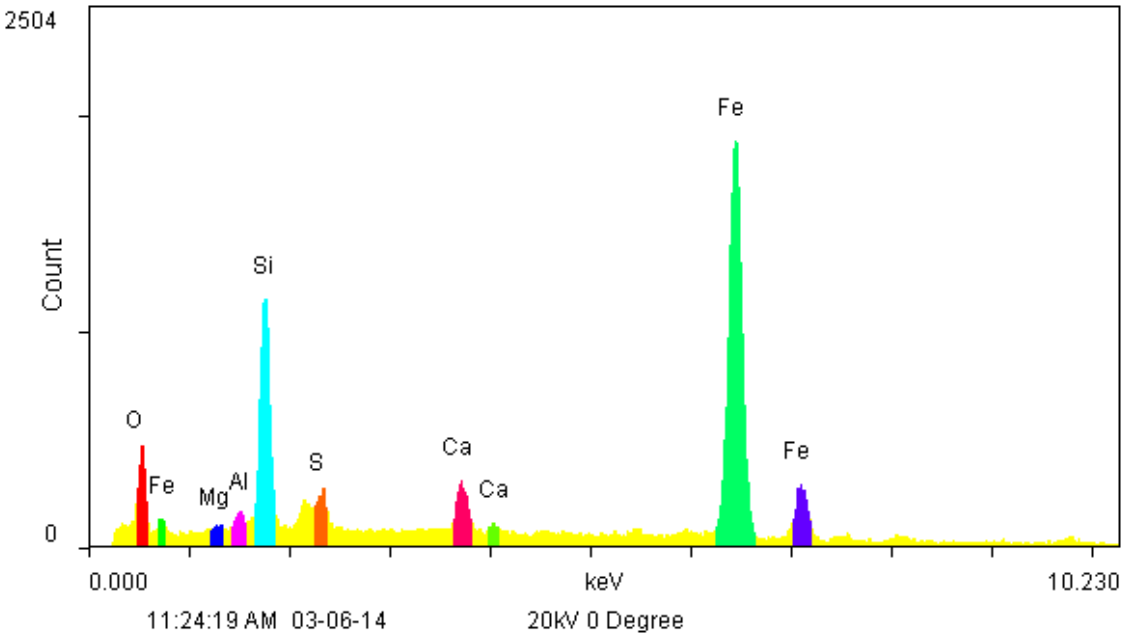

Elements:	WT%	AT%	K_A	K_F	K_Z	Intensity	P/bkg
O K	35.73	60.09	0.197	1	1.074	11.209	6.2
FeL	9.54	4.6	0.558	1	0.92	2.721	1.4
MgK	0	0	0.161	1.002	1.029	0	0
AlK	1.28	1.27	0.234	1.004	0.999	2.148	0.5
SiK	14.81	14.19	0.314	1.001	1.028	36.508	8.2
S K	2.32	1.94	0.426	1.002	1.02	6.575	1.4
CaK	2.09	1.4	0.811	1.013	1.002	8.989	2.4
FeK	34.25	16.5	1.006	1	0.912	92.202	22.4

Figure 2.8 – EDS data for the outer scale (bottom)

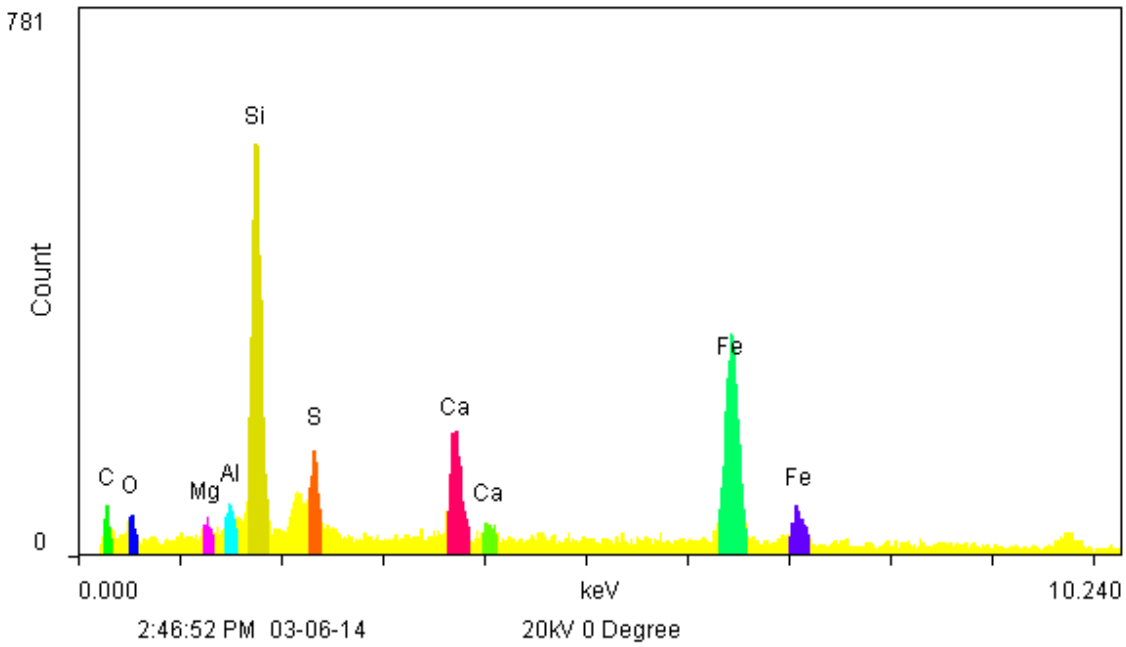

Elements:	WT%	AT%	K_A	K_F	K_Z	Intensity	P/bkg
C K	43.22	62.62	0.117	1	1.042	1.764	3
O K	17.72	19.28	0.132	1	1.025	1.57	2.7
MgK	0	0	0.282	1.003	0.983	0	0
AlK	0.99	0.64	0.407	1.006	0.954	1.226	0.5
SiK	14.29	8.85	0.526	1.002	0.982	24.875	11.6
S K	3.05	1.66	0.584	1.002	0.967	4.959	2.5
CaK	4.07	1.77	0.91	1.006	0.954	8.18	5.3
FeK	16.65	5.19	1.024	1	0.866	19.104	11.6

Figure 2.9 – EDS data for the outer scale (top)

Acid solubility tests were conducted using 15 wt% HCl. The masses of the scale samples collected from the top and bottom part of liner #1 are, respectively, 0.230 g and 0.897 g. **Figures 2.10** and **2.11** present the reaction process during the solubility test. It is interesting to note that the scale sample from the top, which is not mixed with oily materials, was reacting fast with gas evolution, while the sample from the bottom part wasn't significantly reacting with HCl. This can be explained by the fact that organic

matter acts as a barrier between acid and scale particles. This means that in order to remove organic layers from the scaling materials, a preflush with organic solvent is needed before the scale dissolution by HCl.

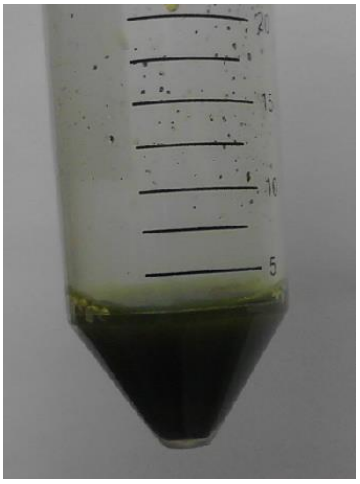

Figure 2.10 – Acid solubility test for outer scale from the top part of liner #1

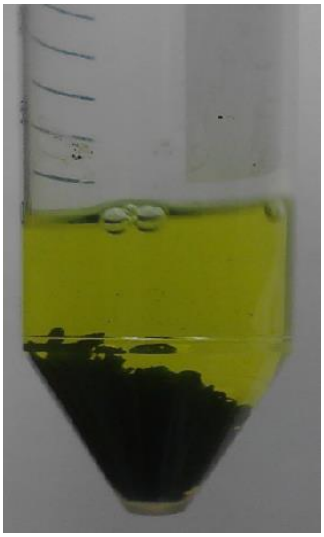

Figure 2.11 – Acid solubility test for outer scale from the bottom part of liner #1

After acid solubility reactions, samples were filtered with 1 micron filter paper. Solids were separated, washed with deoinized water, and dried, while liquids were diluted and analysed using ICP.

Table 2.2 summarizes acid solubility tests for both scale samples. ICP results are presented in **Table 2.3**.

Table 2.2: Acid solubility tests results

	Scale sample #1	Scale sample #2
Initial mass, g	0.230	0.897
Unreacted mass, g	0.157	0.807
% dissolved by HCl	31.7	10.0

Table 2.3: ICP results for the outer scale of liner #1

Sample #	Element concentration, mg/l					
	Ca	Mg	Si	Al	Fe	S
Scale #1	3114.5	213	1	420.5	10285	2865
Scale #2	520	30.5	8	209	4154	2878

After the mass measurements, the unreacted scale was further analyzed using SEM. **Figure 2.12** presents both scale samples after the reaction with 15 wt% HCl. Scale sample #1 (left) changed color and mainly contains sand sized quartz, while scale

sample #2 (right) is still black and covered with organic material. The only observable change in the second sample is texture; before the reaction, this sample was consolidated in bigger blocks, while after the reaction, it is more powdery.

Figure 2.12 – Outer scale for liner #1 after acid reaction

Figures 2.13 and **2.14** present an electron microscope picture with a magnification of 200 for both scale samples. First, samples are presented by quartz grains of different sizes. The texture of the second sample is different because grains of all sizes are consolidated by interlayered organic matter.

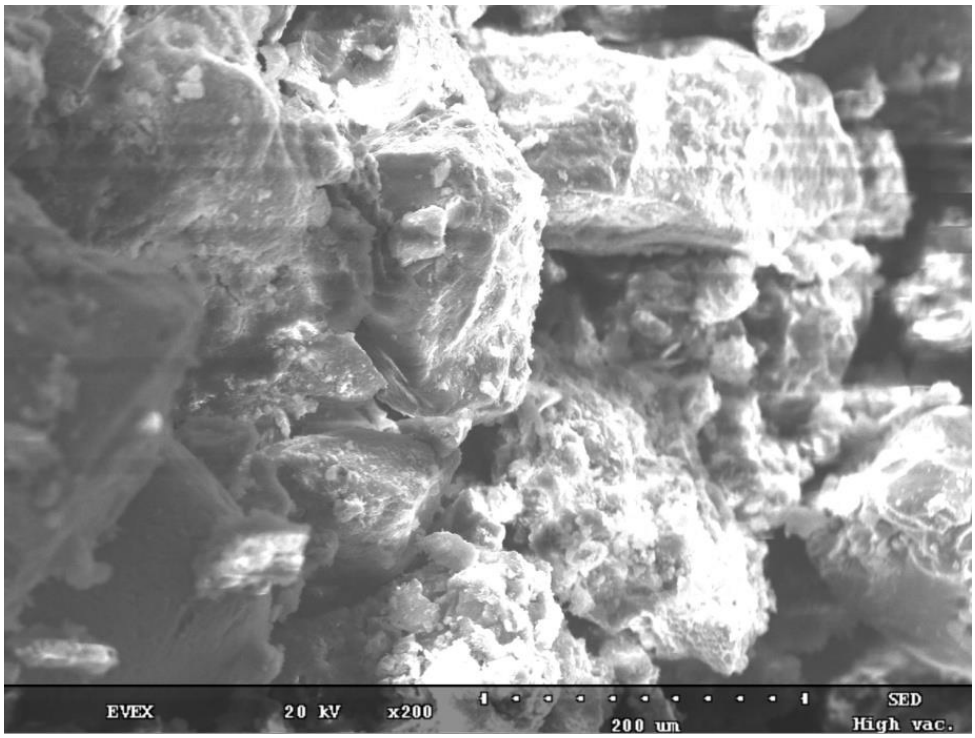

Figure 2.13 – Outer scale #1 after the acid reaction, electron microscope picture (magnification is 200)

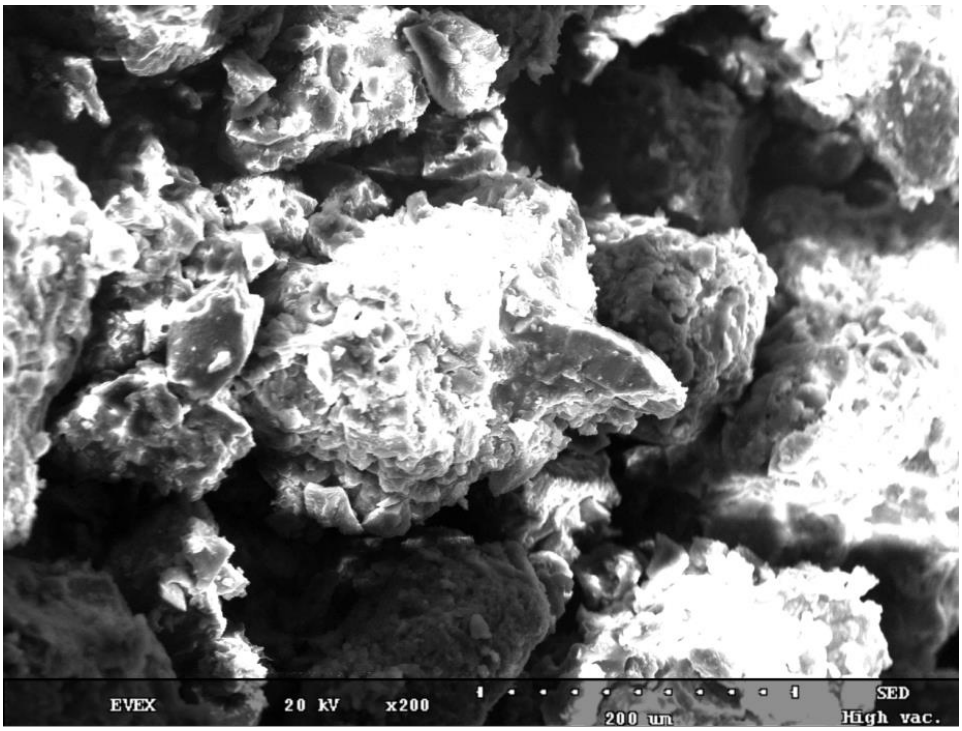

Figure 2.14 – Outer scale #2 after the acid reaction, electron microscope picture (magnification is 200)

The quantitative data about the chemical composition for these two samples is shown in **Figures 2.15** and **2.16**. It is clear that both samples contain a dominant amount of quartz because silicon is not soluble in HCl. However, such elements as iron, calcium, manganese, and aluminum were successfully dissolved. Although such a high HCl concentration is not reasonable at high temperatures because of the reaction rate, corrosion, and other issues, but, in theory, blocking materials could still be mobilized without the dissolution of quartz. These grains of quartz are usually consolidated by iron oxides, iron sulfides, and calcium and magnesium carbonates. These minerals could be

dissolved which would make quartz unstable and wash it out with flow. Additionally, organic matter should be removed by an organic solvent to break the barrier between minerals and acid. This approach is intentionally oversimplified in order to develop the conceptual direction for further development. Grain size distribution, corrosion rates, sand production, formation damage, and other issues should be accounted in detail before field application, but these topics are not focused on in this chapter.

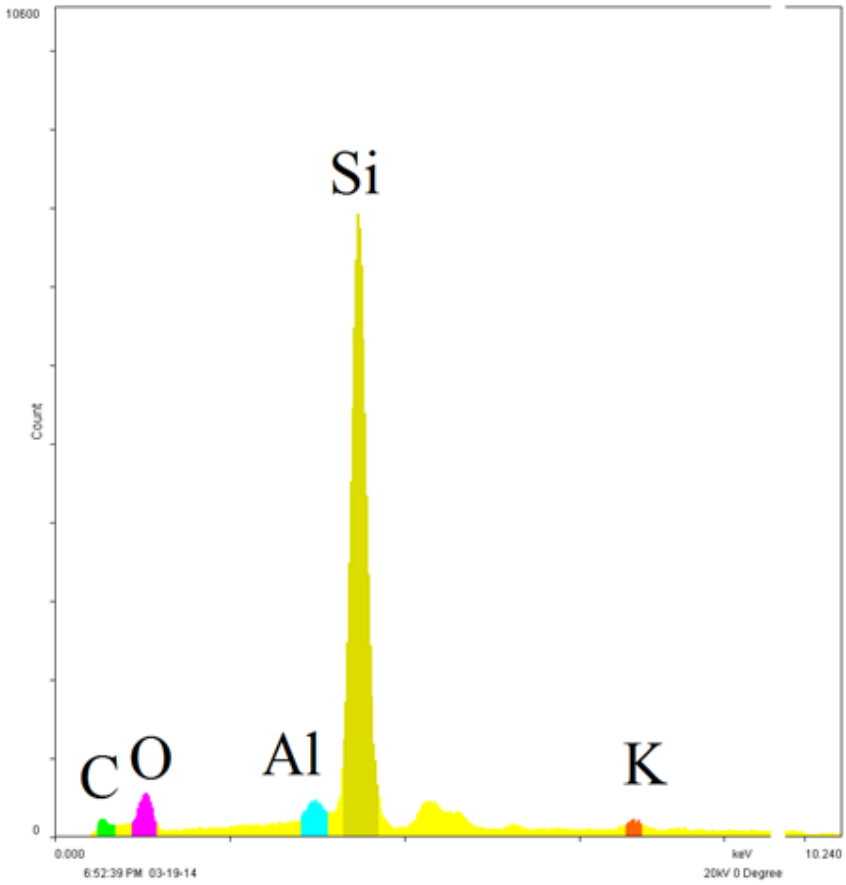

Elements:	WT%	AT%	K_A	K_F	K_Z	Intensity	P/bkg
SiK	100	100	1	1	1	494.186	37.2

Figure 2.15 – EDS data for the outer scale after the reaction (top)

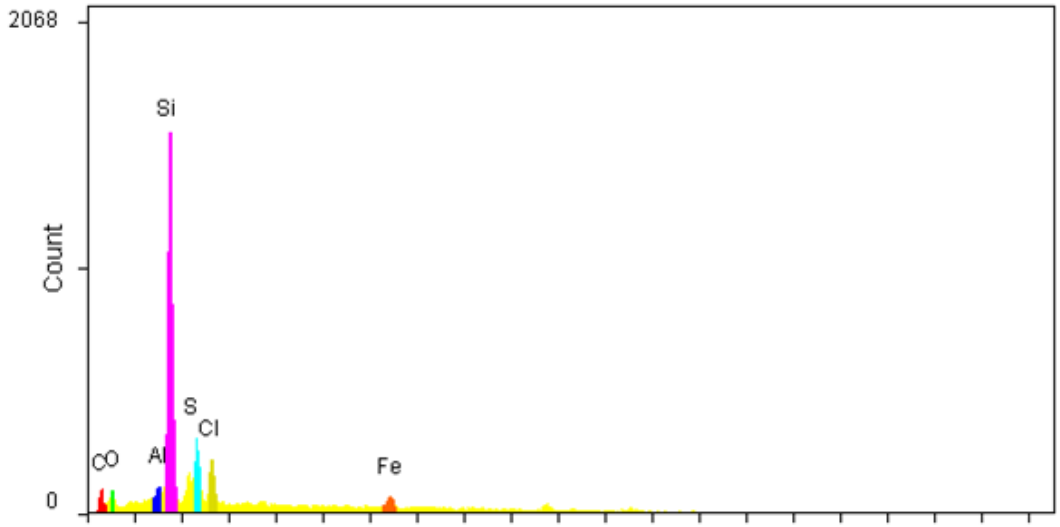

Elements:	WT%	AT%	K_A	K_F	K_Z	Intensity	P/bkg
SiK	52.83	57.23	0.853	1.01	1.013	95.327	25.2
S K	25.11	23.83	0.361	1.008	1.004	16.202	4.9
ClK	22.07	18.94	0.324	1	0.959	11.296	3.5

Figure 2.16 – EDS data for the outer scale after the reaction (bottom)

2.2.1.2 Inner scale samples

The inner surface of liner #1 is mainly covered by corrosion products and rust (**Figure 2.17**).

Figure 2.17 – The inner surface of liner #1

These corrosion products are very simillar at all the inner locations of the liner. That is why only one inner rust sample was collected. This sample was mainly presented with silt sized particles (**Figure 2.18**).

Figure 2.18 – Inner rust sample of liner #1

According to the usual methodology of the analysis, the sample was grained, dried, and mounted in the SEM powder holder. **Figures 2.19** and **2.20** show an electron microscope picture with a magnification of 200 and quantitative EDS data about the chemical composition for this sample accordingly. As expected, the dominant element in these corrosion products is iron. An amount of silicon is present, mainly because of the fine quartz particles.

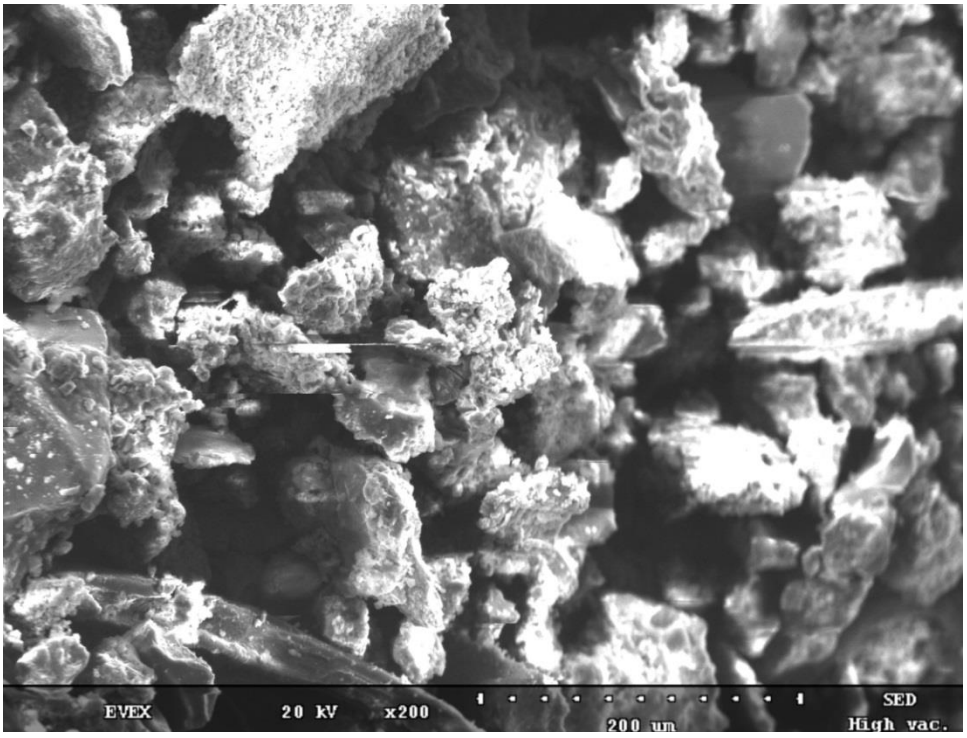

Figure 2.19 – Inner rust sample electron microscope picture (magnification is 200)

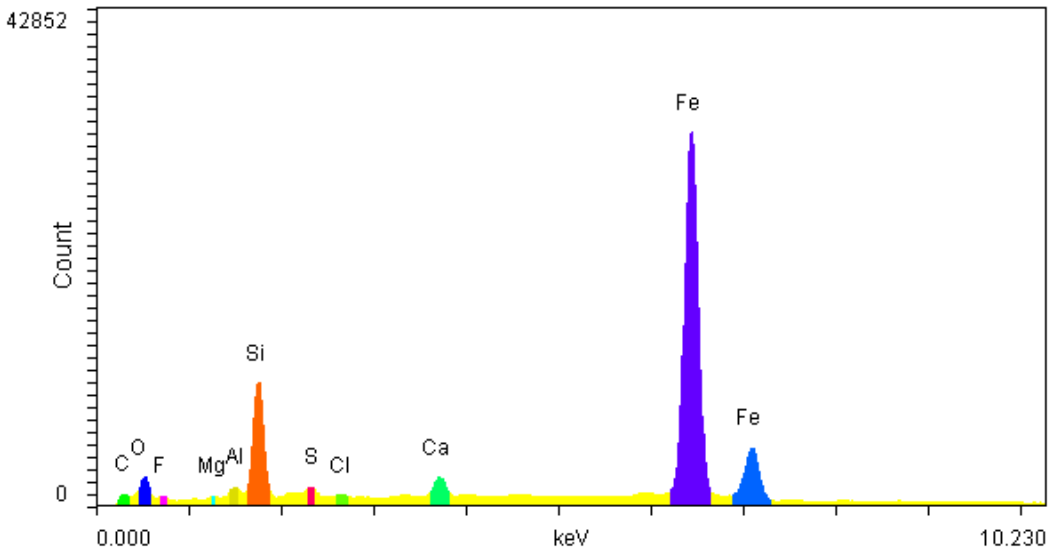

Elements:	WT%	AT%	K_A	K_F	K_Z	Intensity	P/bkg
C K	19.67	38.56	0.085	1	1.087	27.778	1
O K	18.45	27.16	0.163	1	1.069	95.576	3.2
F K	2.92	3.62	0.169	1	1.004	27.913	0.9
MgK	0.42	0.41	0.168	1.001	1.025	9.323	0.2
AlK	1.38	1.21	0.242	1.003	0.995	47.958	0.9
SiK	10.63	8.91	0.323	1.001	1.024	538.532	8.9
S K	0.87	0.64	0.466	1.002	1.015	53.595	0.8
ClK	0.19	0.13	0.582	1.004	0.97	13.039	0.2
CaK	1.2	0.7	0.851	1.015	0.997	108.088	1.4
FeK	44.27	18.66	1.02	1	0.908	2409.078	39.7

Figure 2.20 – EDS data for the inner rust sample

Acid solubility tests were conducted using 15 wt% HCl. The mass of the sample collected from the inner surface of liner #1 was 0.157 g. After the reaction with 15 wt% HCl, it was calculated that 50.1% of sample was dissolved. This value is higher than those of the previous samples which can be explained by the good solubility of iron and corrosion products in HCl.

Table 2.4 presents ICP results for the inner surface sample of liner #1. The highest concentration is for iron which was expected.

Table 2.4: ICP results for the inner surface sample of liner #1

Sample #	Element concentration, mg/l					
	Ca	Mg	Si	Al	Fe	S
Inner #1	1116	176	108.8	160.8	13960	2412.4

After the mass measurements, the unreacted scale was further analyzed using SEM. **Figures 2.21** and **2.22** present an electron microscope picture with a magnification of 200 and EDS results for the unreacted part of the sample, respectively. It is clear that after iron was almost fully dissolved, silicon became the dominant element in these unreacted corrosion products mixed with quartz grains.

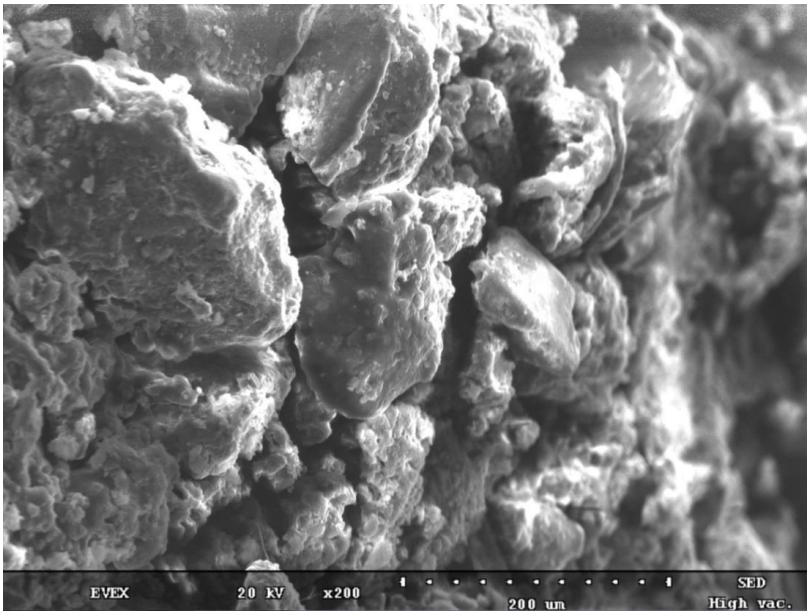

Figure 2.21 – Inner scale after the acid reaction, electron microscope picture (magnification is 200)

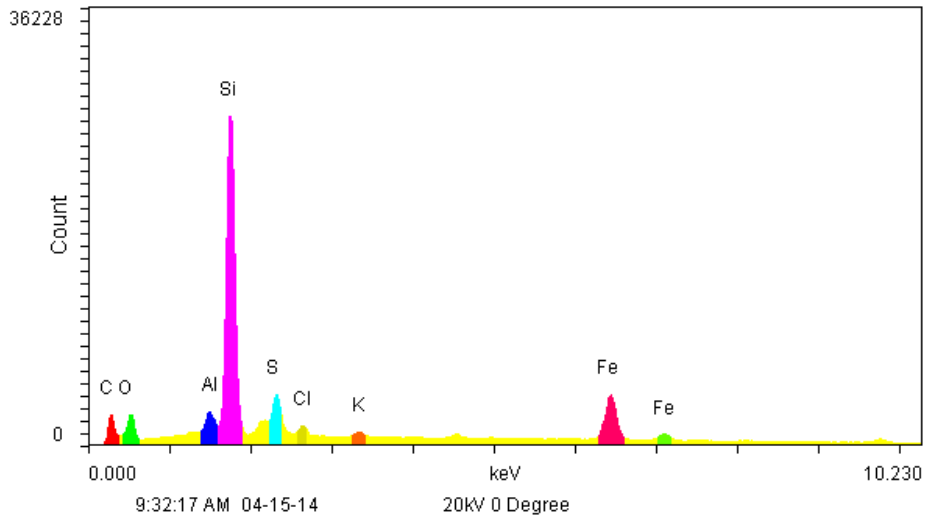

Elements:	WT%	AT%	K_A	K_F	K_Z	Intensity	P/bkg
C K	47.92	62.59	0.134	1	1.026	83.407	3
O K	24.35	23.88	0.147	1	1.009	90.189	3.3
AlK	1.52	0.89	0.533	1.007	0.94	92.63	1.5
SiK	16.37	9.14	0.648	1.001	0.968	1313.639	18.3
S K	2.86	1.4	0.621	1.001	0.949	184.683	2.6
ClK	0.66	0.29	0.702	1.001	0.908	43.213	0.7
K K	0.31	0.12	0.872	1.002	0.916	24.347	0.4
FeK	6	1.69	1.043	1	0.851	262.025	5.9

Figure 2.22 – EDS data for the inner sample after the reaction

2.2.2 Liner #2

Figure 2.23 represents the general view of liner #2. The shape of the openings is different for this liner and presents a dense metal net inside a circular channel. This net is supposed to let fluids enter the liner and prevent sand production at the same time. However, because of the pressure and temperature gradients which occur during the filtration process, these openings become blocked by precipitates and scales.

Figure 2.23 – General view of liner #2

Table 2.5 contains the main parameters of liner #2 which are shown in **Figure 2.24**.

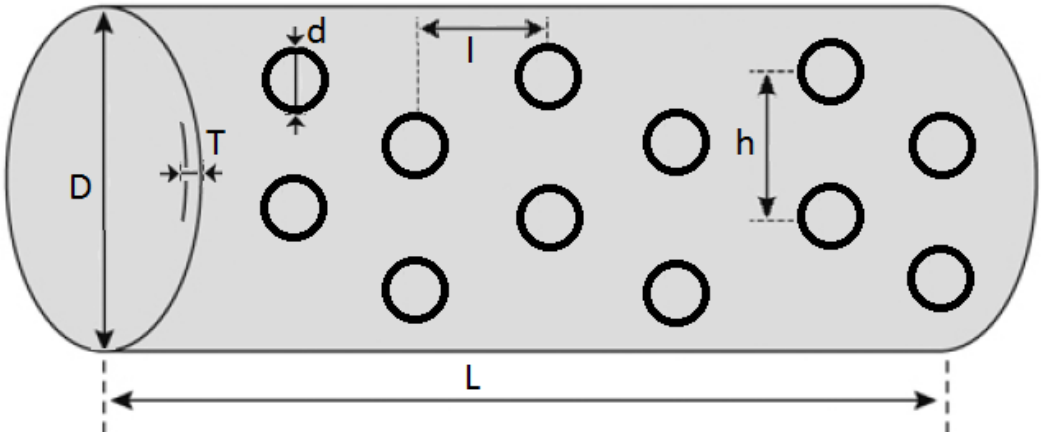

Figure 2.24 – Main parameters of liner #2

Table 2.5: Main parameters of liner #2

Main parameters of liner #2, in			
h	l	d	T
2.060	2.070	1.080	0.467

2.2.2.1 Outer scale sample

All of the blocking materials were found to be almost the same in content and structure for the whole analyzed interval (**Figure 2.25**). That's why only one sample of the outer scale will be discussed further in this chapter (**Figure 2.26**).

Figure 2.25 – Section of liner #2 with blocked openings

Figure 2.26 – Sample of the blocking materials taken from the outer surface of liner #2

The procedure of the analysis remained the same for liner #1. SEM picture with a magnification of 200 and quantitative data about the chemical composition of the outer sample are present in **Figures 2.27** and **2.28**, respectively.

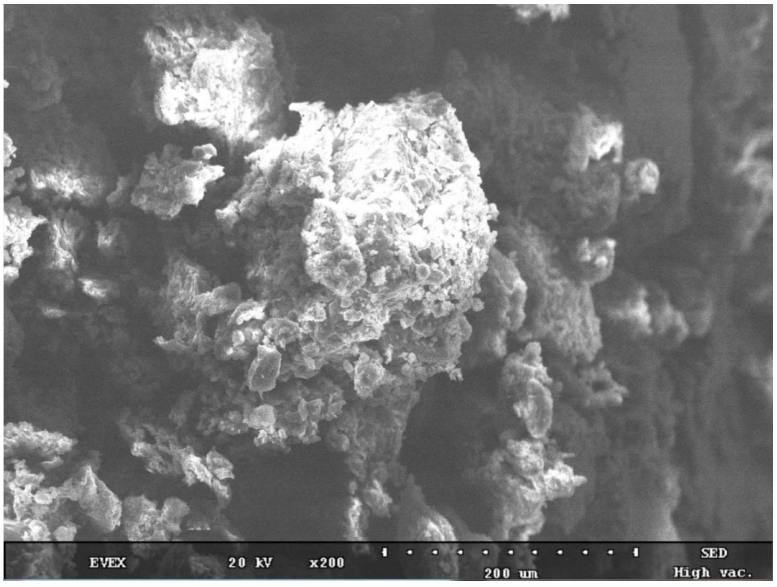

Figure 2.27 – Outer sample electron microscope picture (magnification is 200), liner #2

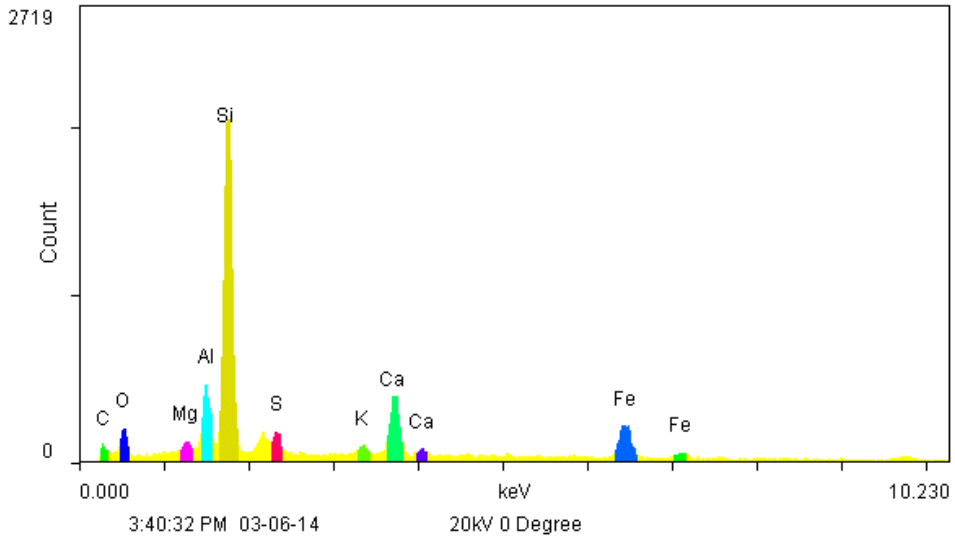

Elements:	WT%	AT%	K_A	K_F	K_Z	Intensity	P/bkg
C K	30.33	45.14	0.104	1	1.037	3.014	1.6
O K	27.23	30.42	0.147	1	1.02	7.312	3.8
MgK	1.55	1.14	0.361	1.006	0.979	4.251	1.1
AlK	5.17	3.42	0.488	1.009	0.95	21.018	5.2
SiK	23.14	14.73	0.534	1.001	0.978	111.723	26.4
S K	2.01	1.12	0.496	1.002	0.961	7.578	1.7
K K	0.71	0.32	0.801	1.007	0.926	3.752	1
CaK	4.37	1.95	0.859	1.002	0.948	22.601	6.2
FeK	5.49	1.76	1.011	1	0.861	17.006	5.2

Figure 2.28 – EDS data for the outer sample, liner #2

The amount of iron in this sample is relatively low in comparison with previous samples. Based on the chemical composition of the sample, the blocking materials are mainly formed by quartz and probably some aluminosilicate minerals which could be consolidated by carbonate minerals.

The mass of the sample collected from the outer surface of liner #2 was 0.340 g. Acid solubility tests were conducted using 15 wt% HCl. **Figure 2.29** shows the reaction process during the solubility test. The reaction process was fast and accompanied with gas bubbling. However, the amount of unreacted sample was observed to be significant

(black solids in the mixture in the **Figure 2.29**). The unreacted solids were subsequently collected, dried, and weighted. The mass of the unreacted outer sample was found to be 0.184 g which makes the percentage of the dissolved sample to be 46.0%. The ICP results for liquids collected after the acid solubility reaction with 15 wt% HCl are presented in **Table 2.6**.

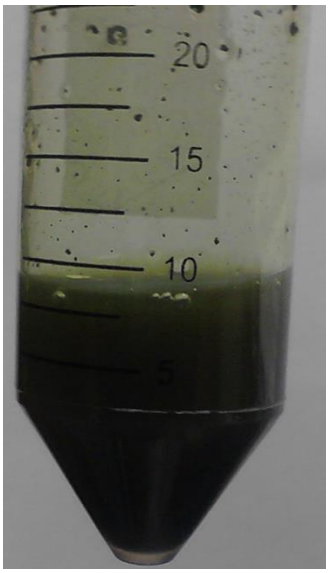

Figure 2.29 – Acid solubility test for the outer sample, liner #2

Table 2.6: ICP results for outer scale of liner #2

Sample #	Element concentration, mg/l					
	Ca	Mg	Si	Al	Fe	S
Outer #1	7245	238.5	20	1027.5	13005	2834

After the acid solubility test, the unreacted sample was further analyzed using SEM. **Figure 2.30** presents the scale sample after the reaction with 15 wt% HCl. The grains' average size became smaller after the reaction with HCl which was also observed for the previous samples.

Figures 2.31 and **2.32** present SEM pictures with a magnification of 200 and quantitative EDS data, accordingly, for the remaining after the reaction sample.

Figure 2.30 – Outer scale for the liner #2 after the acid reaction

It can be concluded that iron and calcium were mainly dissolved during the reaction with HCl. At the same time, magnesium and aluminum were treated in a lesser amount. The silicon remained untreated. The SEM image presents angular quartz grains covered with aluminosilicates and untreated carbonate minerals.

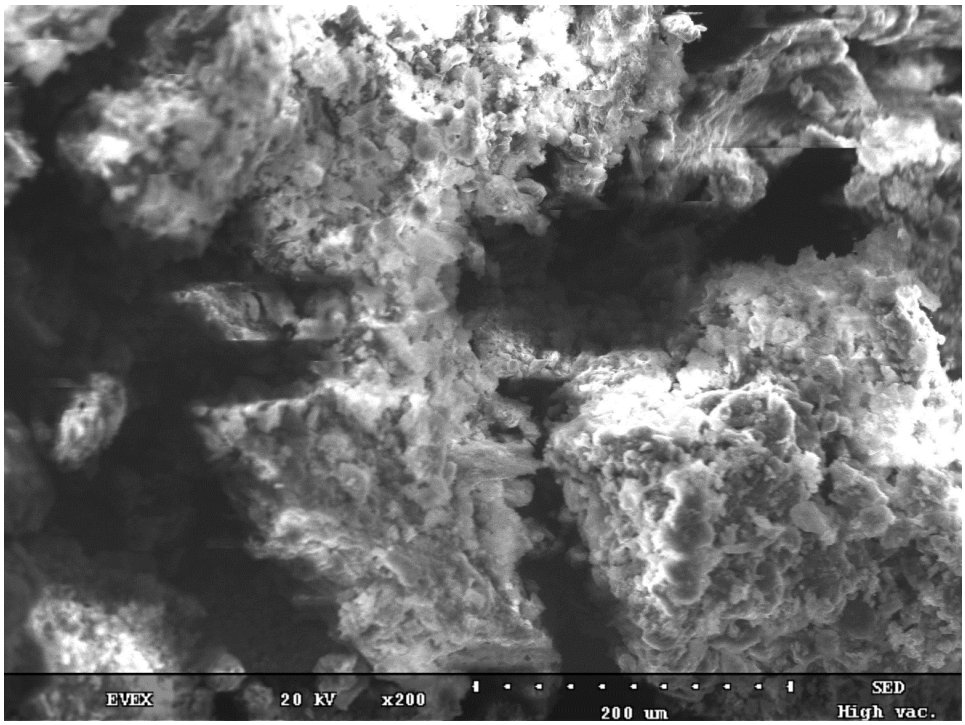

Figure 2.31 – Inner rust sample electron microscope picture (magnification is 200)

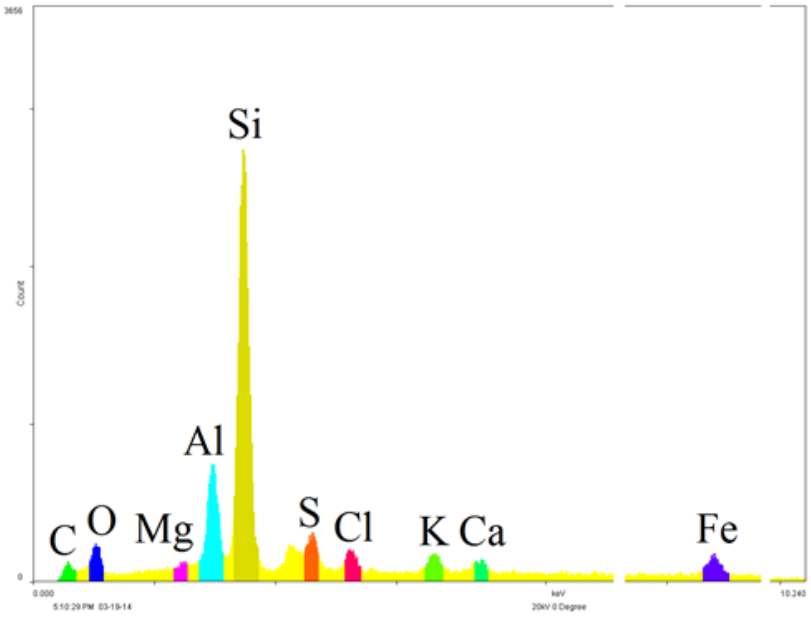

Elements:	WT%	AT%	K_A	K_F	K_Z	Intensity	P/bkg
AlK	14.19	14.69	0.893	1.038	0.976	36.069	6.2
SiK	85.81	85.31	0.574	1	1.004	147.451	23.4

Figure 2.32 – EDS data for the inner rust sample

This type of scale contains a high amount of quartz which could not be dissolved by HCl. The acid was mainly spent on cementing materials and iron species. Almost half of the scale mass was dissolved, but this is still not enough to remove the blocking materials.

2.2.2.2 Inner scale sample

One sample of scale and corrosion products was collected from the inner surface of liner #2 (**Figures 2.33** and **2.34**).

Figure 2.33 – Inner surface of liner #2

For this type, the liners materials on the inner surface are mainly corrosion products mixed with sand grains of different sizes. Organic matter was not observed here. However, quartz particles are consolidated and attached to the wall by smaller particles and corrosion products.

Figure 2.34 – Inner rust and scale sample of liner #2

This sample was grained, dried, and mounted in the SEM powder holder. SEM and EDS data is shown in **Figures 2.35** and **2.36**. As expected, the concentrations of iron and silicon are highest with minor inclusions of other elements. The structure of the sample is basically big grains of quartz consolidated and covered with each other by various types of corrosion products such as iron oxide and iron sulfides.

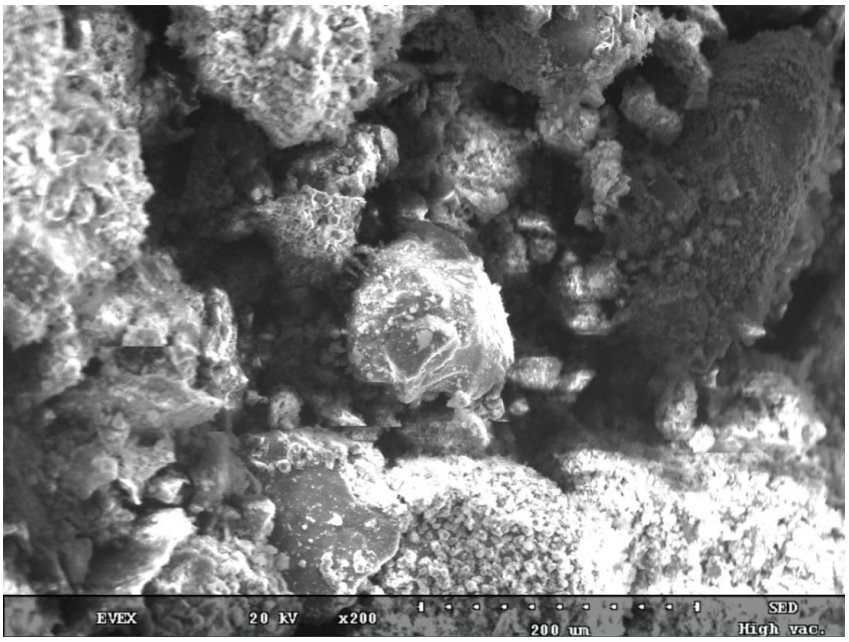

Figure 2.35 – Inner rust sample electron microscope picture (magnification is 200)

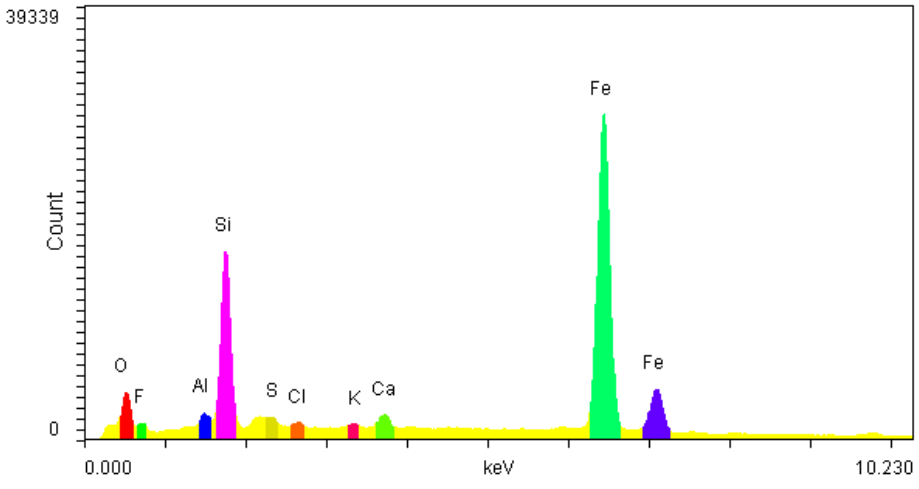

Elements:	WT%	AT%	K_A	K_F	K_Z	Intensity	P/bkg
O K	27.29	47.16	0.195	1	1.079	195.658	4.1
F K	5.89	8.57	0.157	1	1.014	60.137	1
Al K	2.49	2.55	0.236	1.005	1.004	97.701	1.1
Si K	18.42	18.13	0.309	1.001	1.033	1029.696	11.3
S K	1.27	1.1	0.397	1.002	1.025	77.604	0.7
Cl K	0.56	0.44	0.506	1.003	0.98	38.736	0.4
K K	0.3	0.21	0.711	1.009	0.984	28.599	0.3
Ca K	0.93	0.64	0.787	1.013	1.006	89.885	0.8
Fe K	42.83	21.2	1.003	1	0.917	2650.928	29

Figure 2.36 – EDS data for the inner rust sample

Acid solubility tests were conducted using 15 wt% HCl. The mass of the sample collected from the inner surface of liner #2 was 0.295 g. The unreacted mass was measured to be 0.166 g which means that 43.7% of the sample was dissolved. This number is close to 50.1% for liner #1 since the structures of the inner surface samples are very similar. The 6.4 % difference is due to the fact that the relative amount of quartz particles is higher for liner #2.

As expected, the high concentration of iron in the reacted fluid was identified using ICP (**Table 2.7**).

Table 2.7: ICP results for the inner surface sample of liner #2

Sample #	Element concentration, mg/l					
	Ca	Mg	Si	Al	Fe	S
Inner #2	291.2	26	275.2	39.2	12516	2306

The solid unreacted particles were separated, washed with deionized water after the reaction, and dried for further analysis. Visually, this sample was mainly filled by sand sized quartz (**Figure 2.37**).

Figure 2.37 – Inner materials sample for the liner #2 after the acid reaction

SEM pictures confirmed that rust and other cementing and covering materials were dissolved, while grains of quartz remained untouched (**Figure 2.38**). This could be clearly observed by a comparison of **Figures 2.35** and **2.38**.

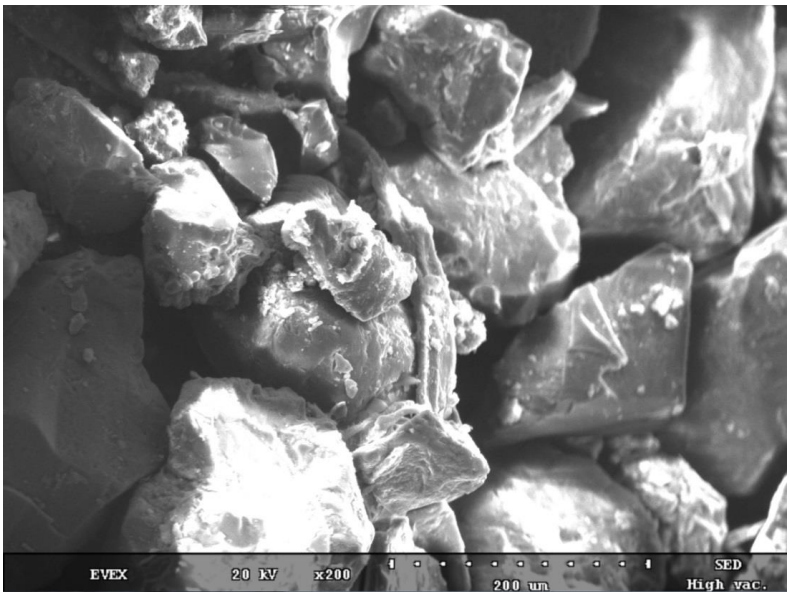

Figure 2.38 – Inner scale after acid reaction, electron microscope picture (magnification is 200)

Figure 2.39 confirms that quartz is the dominant component remaining in the materials collected from the inner wall of liner #2 after the reaction with 15 wt% HCl.

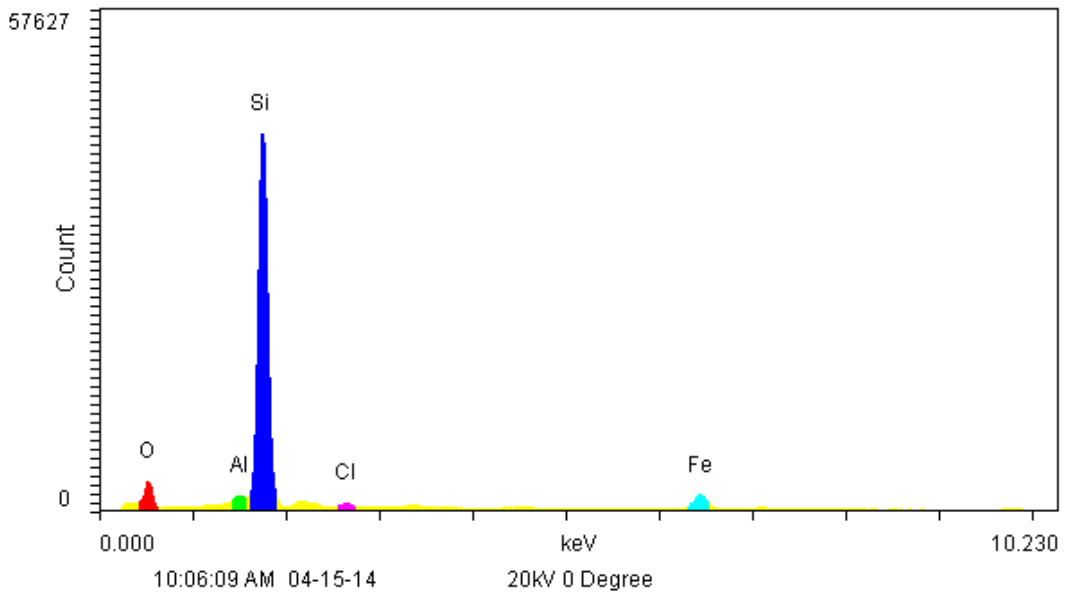

Elements:	WT%	AT%	K_A	K_F	K_Z	Intensity	P/bkg
O K	40.29	55.33	0.213	1	1.031	151.62	4.8
AlK	2.24	1.83	0.504	1.02	0.96	91.828	1.8
SiK	51.38	40.2	0.602	1	0.988	2693.667	50.9
ClK	1.11	0.69	0.444	1	0.931	32.161	0.6
FeK	4.98	1.96	0.994	1	0.872	146.359	3

Figure 2.39 – EDS data for the inner sample after the reaction

This type of liners differs from the slotted liners because of the openings' type. The blocking mechanisms depend on the minimum sizes of the net cells and slots. The pressure drops in the slot and circular opening are not the same which creates conditions for the formation of different minerals. Overall, scaling and blocking materials for liner #2 are heavily filled by quartz grains of different sizes which makes it hard to remove them by just dissolving the cementing materials.

2.2.3 Liner #3

Slotted liner #3 is shown in **Figure 2.40**. This liner has the same shape of openings as liner #1's. However, this liner was pulled from another well and has different scaling and corrosion materials covering its inner and outer surfaces. The sizes of the slot sections are summarized in **Figure 2.41** and **Table 2.8**.

Figure 2.40 – General view of liner #3

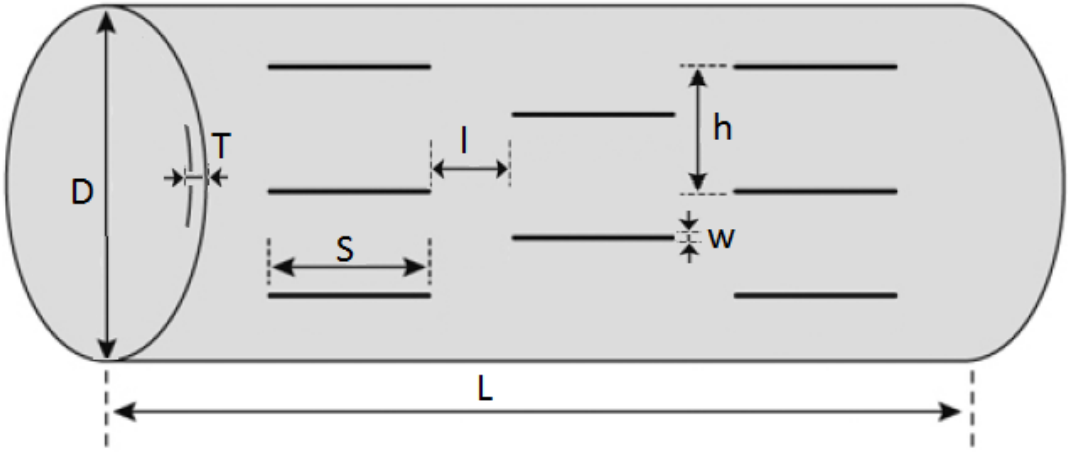

Figure 2.41 – Main parameters of liner #3

For this liner, distances between slots are bigger than those of liner #1. The slots are also a little longer.

Table 2.8: Main parameters of liner #3

Main parameters of liner #1, in			
h	l	S	T
0.890	0.575	2.625	0.467

2.2.3.1 Outer scale samples

For liner #3, two scale samples were collected. Similarly, like liner #1, the blocking materials were different for the top and bottom semicircles of liner #3. The outer sample #1 was collected from the top part which is shown in **Figure 2.42**. These blocking materials are mainly corrosion products. However, the outer scale sample #2 was much more numerous and greenish in color (**Figure 2.43**).

Figure 2.42 – Top part of liner #3

Figure 2.43 – Bottom part of liner #3

It should be noted that the structures of the samples are different (**Figure 2.44**). The outer sample from the bottom part is presented with consolidated particles which form blocks. However, sample #1 presents smaller sized black particles similar to rust.

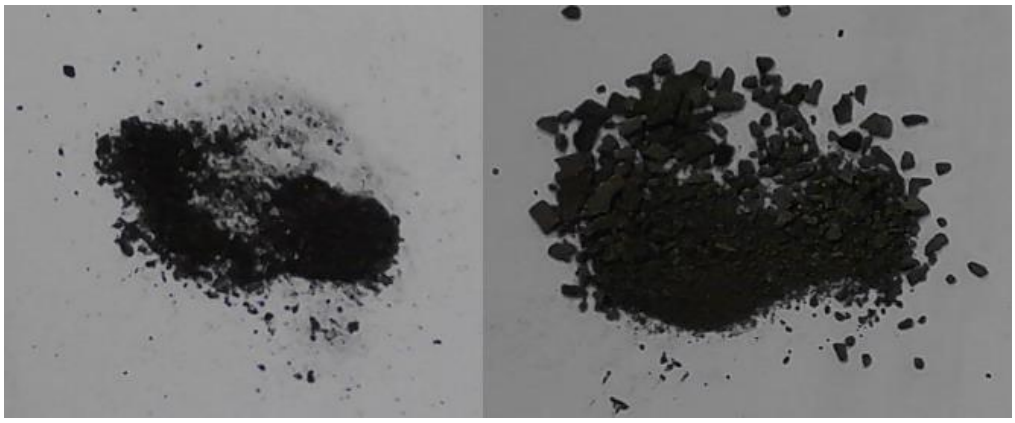

Figure 2.44 – Samples of the blocking materials taken from the outer surface of liner #3

Both samples were grained prior to the SEM analysis. **Figures 2.45 – 2.48** present SEM images and EDS data for samples #1 and 2, respectively. Angular particles of iron sulfide and quartz are the main minerals for sample #1.

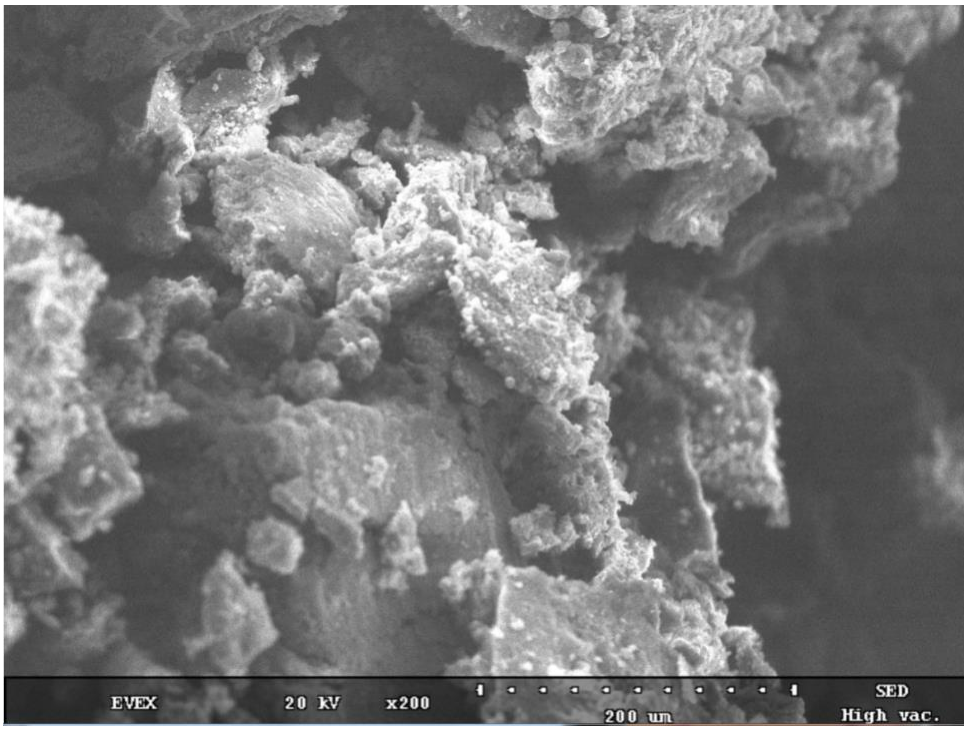

Figure 2.45 – Outer scale (top) electron microscope picture (magnification is 200)

For sample #2, iron sulfide is not a significant component. For this sample, quartz is mainly covered by iron oxides and insignificant amount of aluminosilicate minerals which play a role of cementing material for the bigger particles.

Figure 2.46 – Outer scale (bottom) electron microscope picture (magnification is 200)

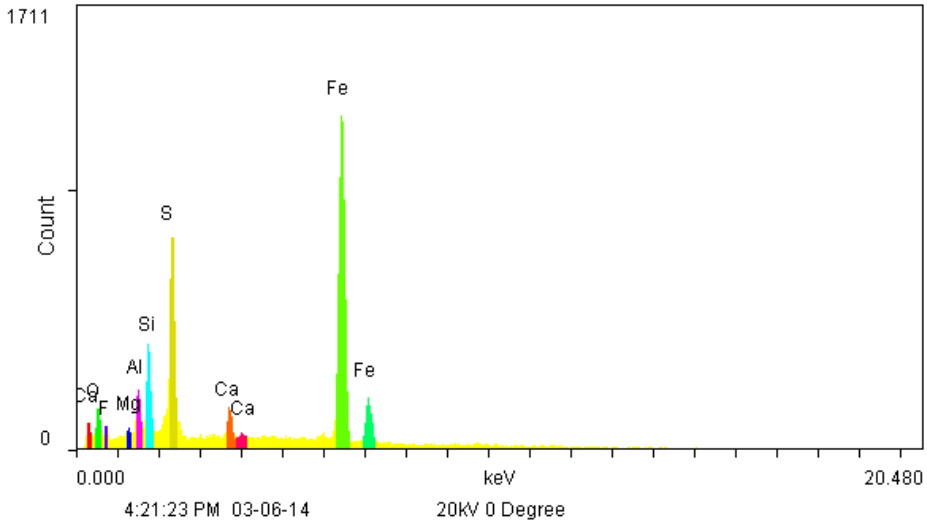

Elements:	WT%	AT%	K_A	K_F	K_Z	Intensity	P/bkg
O K	23.26	41.35	0.168	1	1.079	6.27	2.9
F K	6.55	9.81	0.156	1	1.014	2.917	1.2
MgK	0	0	0.169	1.003	1.035	0	0
AlK	4.95	5.21	0.246	1.004	1.004	8.845	1.7
SiK	8.07	8.17	0.305	1.004	1.033	19.575	3.5
S K	15.84	14.05	0.467	1.002	1.026	49.801	10.7
CaK	1.83	1.3	0.741	1.011	1.007	7.25	1.7
FeK	39.49	20.11	0.986	1	0.917	105.264	27.6

Figure 2.47 – EDS data for the outer scale (bottom)

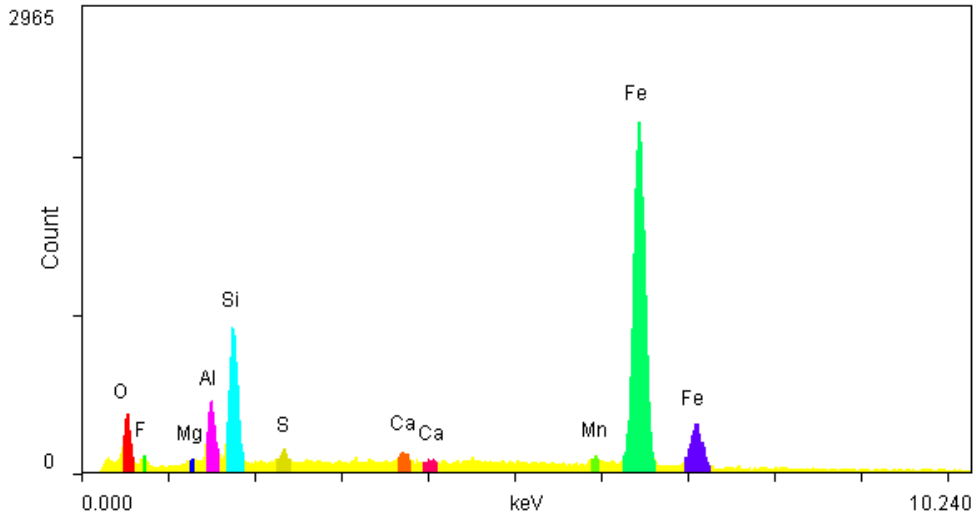

Elements:	WT%	AT%	K_A	K_F	K_Z	Intensity	P/bkg
O K	28.92	49.27	0.206	1	1.079	15.885	6.2
F K	5.22	7.49	0.152	1	1.014	3.754	1.3
MgK	0	0	0.163	1.003	1.034	0	0
AlK	7.37	7.44	0.237	1.003	1.004	21.079	3.6
SiK	13.95	13.54	0.282	1.001	1.033	51.817	8.8
S K	1.07	0.91	0.401	1.002	1.025	4.794	0.8
CaK	0.69	0.47	0.8	1.013	1.006	4.937	0.8
MnK	0.82	0.41	0.999	1	0.9	4.032	0.7
FeK	41.96	20.48	1.008	1	0.917	189.821	33.1

Figure 2.48 – EDS data for the outer scale (top)

For these samples, 15 wt% HCl was used to conduct acid solubility tests. The masses of the samples #1 and #2 were measured to be 0.058 g and 0.233 g, respectivelly. **Figures 2.49** and **2.50** present the reaction process during the solubility test. It is important to mention that during the reaction of the first sample (**Figure 2.49**), hydrogen sulfide was evolving. This could be a serious problem because of safety and well integrity issues. Safe iron sulfide dissolution could be performed by using H_2S-scavengers.

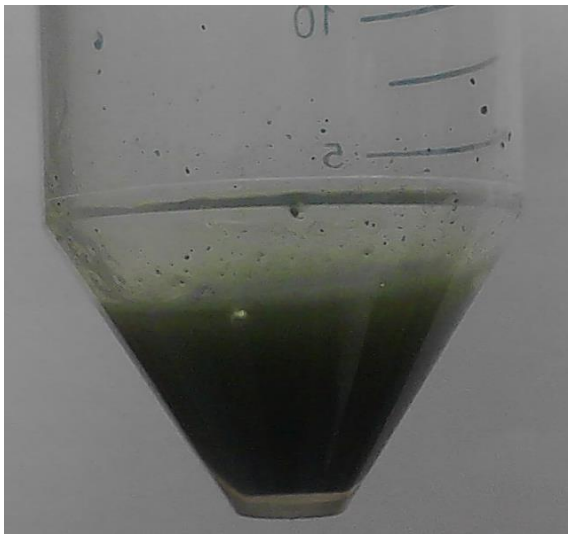

Figure 2.49 – Acid solubility test for the outer scale from the top part of liner #3

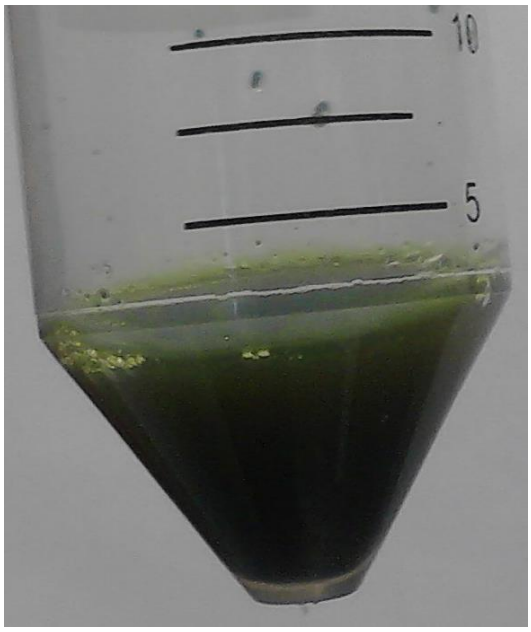

Figure 2.50 – Acid solubility test for the outer scale from the bottom part of liner #3

After the reactions, the solids were separated, washed with deoinized water, dried, and weighed to determine how much of the sample was dissolved by HCl. **Table**

2.9 summarizes acid solubility tests for both scale samples. It should be noted that these samples have the highest capacity to be dissolved by HCl.

Table 2.9: Acid solubility tests results

	Scale sample #1	Scale sample #2
Initial mass, g	0.058	0.233
Unreacted mass, g	0.017	0.090
% dissolved by HCl	70.7	61.4

Liquids were filtered, diluted, and analyzed using ICP (**2.32** – EDS data). As it was expected, iron and sulfur have the highest concentrations after the liquid reaction related to sample #1. For sample #2, iron and aluminum have high concentrations.

Table 2.10: ICP results for the outer scale of liner #3

Sample #	Element concentration, mg/l					
	Ca	Mg	Si	Al	Fe	S
Scale #1	335.5	10.5	88.5	172.5	34845	2927.5
Scale #2	731	619	263	4586.5	30825	2883

The unreacted solids for both samples are shown in **Figure 2.51**. The main change is that consolidated blocks were broken during the reaction because of the

significant amount of iron and cementing minerals were dissolved. However, both samples preserved its colors. A SEM analysis was conducted to identify any other changes that occurred after the solubility test.

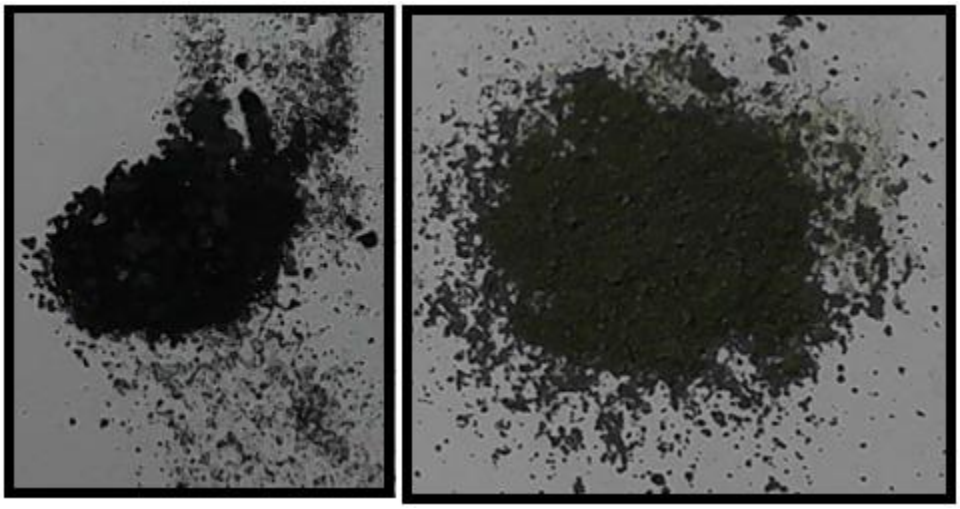

Figure 2.51 – Outer scale for liner #3 after the acid reaction

SEM images with a magnification of 200 are presented in **Figures 2.52** and **2.53**. Sample #1 initially contained a big amount of iron sulfide and iron oxide species which were almost completely dissolved. Calcium and magnesium, which fixated particles between each other, were also fully dissolved together. The main component that remained untreated is silicate oxide which forms quartz. Because of the high sulfur content, hydrogen sulfide utilization should be accounted for in the safe treatment of this well.

The second sample is very similar in terms of dissolved materials; however, the sulfur content is relatively smaller (**Figures 2.54** and **2.55**).

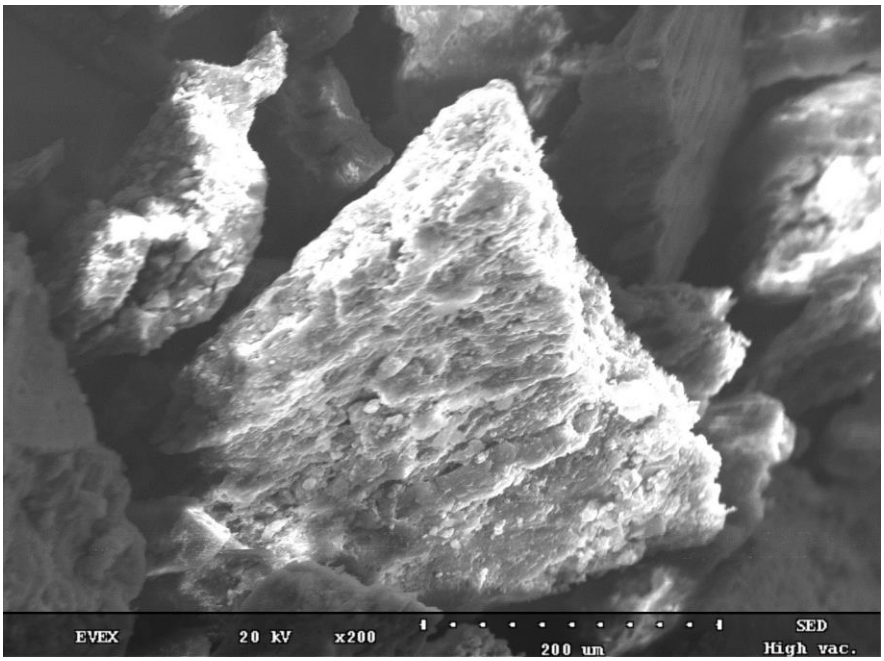

Figure 2.52 – Outer scale #1 after the acid reaction, electron microscope picture (magnification is 200)

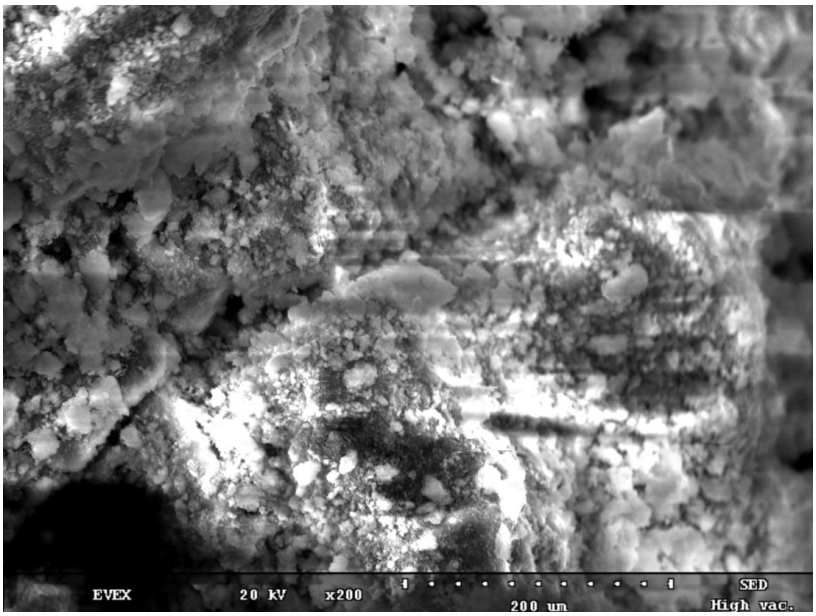

Figure 2.53 – Outer scale #2 after the acid reaction, electron microscope picture (magnification is 200)

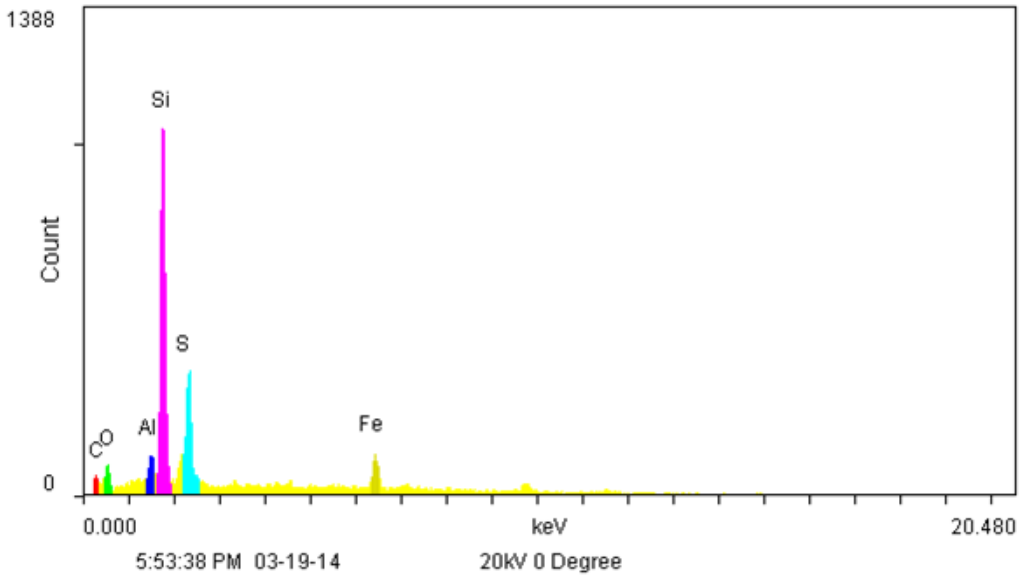

Elements:	WT%	AT%	K_A	K_F	K_Z	Intensity	P/bkg
O K	34.08	49.93	0.174	1	1.038	4.436	5.8
AlK	3.33	2.9	0.473	1.015	0.966	5.404	1.5
SiK	35.86	29.93	0.552	1.005	0.994	73.317	18.4
S K	19.36	14.16	0.405	1	0.981	24.405	7.6
FeK	7.36	3.09	0.976	1	0.879	8.999	3.7

Figure 2.54 – EDS data for the outer scale after the reaction (top)

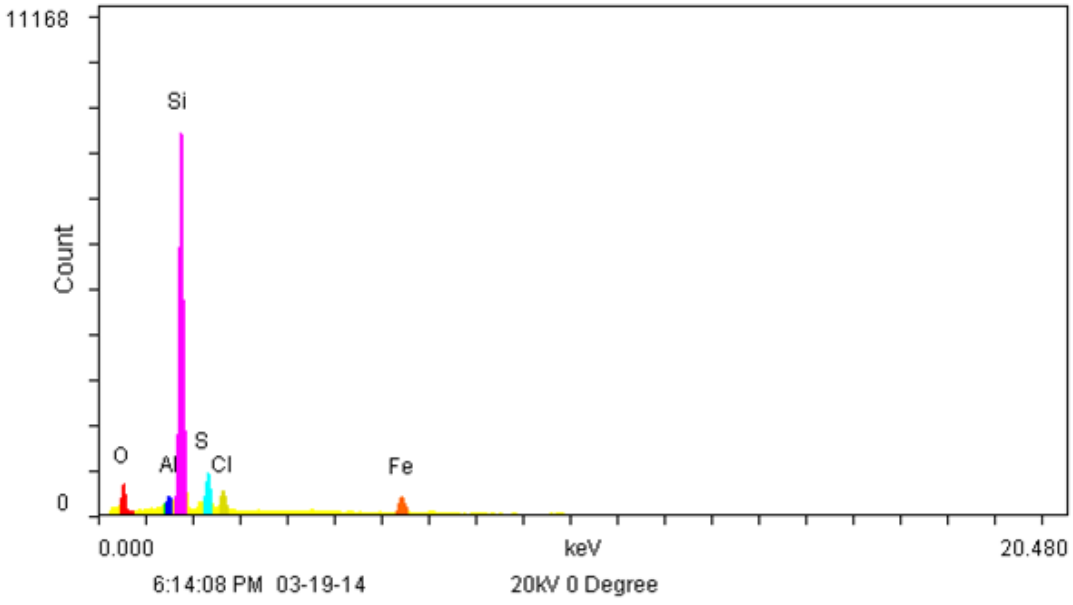

Elements:	WT%	AT%	K_A	K_F	K_Z	Intensity	P/bkg
O K	38.54	54.18	0.186	1	1.034	15.979	4.7
Al K	2.31	1.93	0.496	1.017	0.963	11.746	2.1
Si K	41.48	33.22	0.593	1.003	0.991	271.455	49.4
S K	8.21	5.76	0.381	1.002	0.977	29.068	5.9
Cl K	4.76	3.02	0.433	1	0.934	17.06	3.3
Fe K	4.7	1.89	0.982	1	0.875	17.217	3.5

Figure 2.55 – EDS data for the outer scale after the reaction (bottom)

2.2.3.2 Inner scale samples

The inner surface of liner #3 is covered by a few different materials. The whole inner surface is a little corroded, but some zones are also covered by sand sized particles of quartz (**Figure 2.56**). The blocking materials are presented by corrosion products, and quartz particles were collected for further analysis (**Figure 2.57**).

Figure 2.56 – Inner surface of liner #3

Figure 2.57 – Inner rust sample of liner #3

SEM images with EDS data were first made for the collected and prepared sample (**Figures 2.58** and **2.59**). Based on this data, quartz is the dominant mineral

which fills the sample. There is also some iron species which will probably be the main aim of the HCl solubility test.

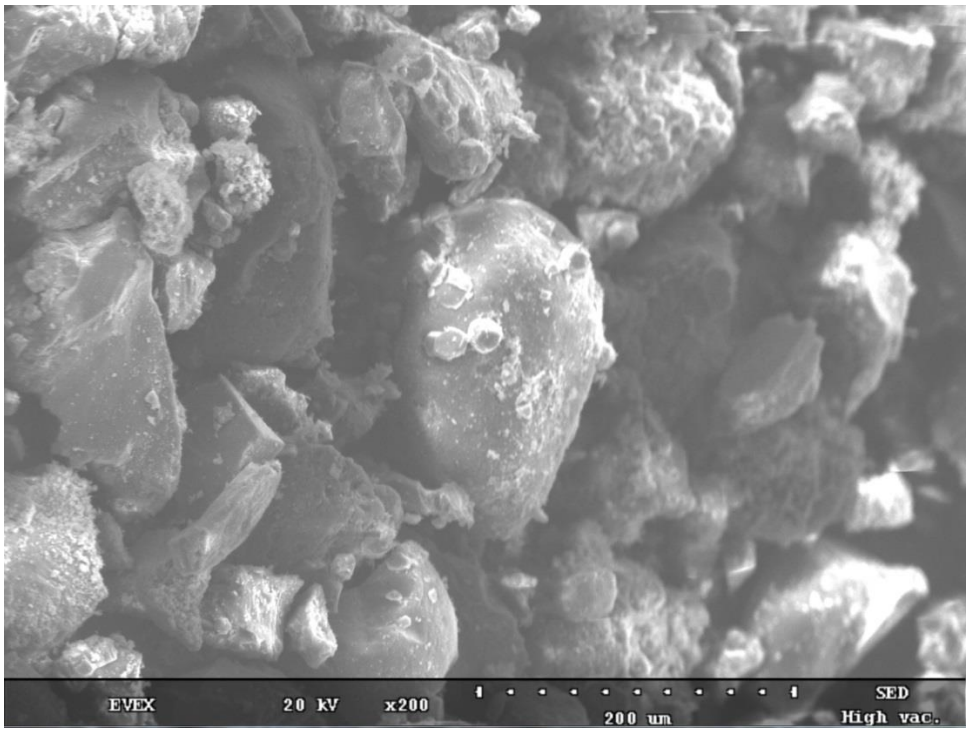

Figure 2.58 – Inner rust sample electron microscope picture (magnification is 200)

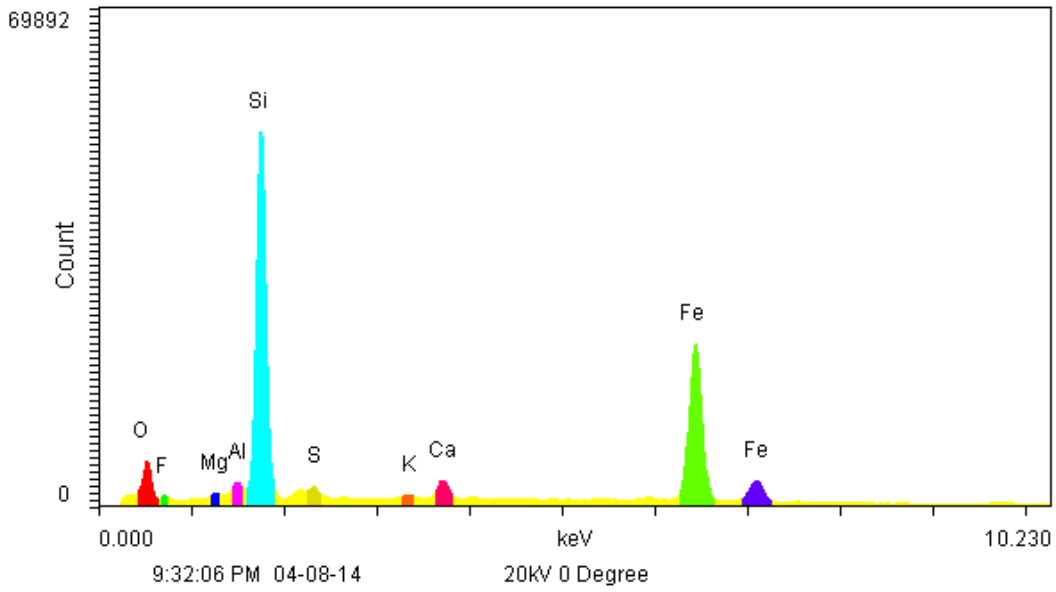

Elements:	WT%	AT%	K_A	K_F	K_Z	Intensity	P/bkg
O K	32.66	50.2	0.197	1	1.054	182.059	4.6
F K	3.49	4.51	0.143	1.001	0.991	25.117	0.6
MgK	1.33	1.34	0.223	1.005	1.011	34.781	0.6
AlK	2.2	2.01	0.313	1.01	0.981	89.064	1.6
SiK	33.49	29.32	0.403	1.001	1.01	1886.719	29.4
S K	1.48	1.14	0.367	1.001	0.999	64.095	0.9
K K	0.36	0.23	0.684	1.006	0.96	25.079	0.4
CaK	1.48	0.91	0.764	1.007	0.982	105.573	1.6
FeK	23.51	10.35	0.995	1	0.894	1111.706	16

Figure 2.59 – EDS data for the inner rust sample

An acid solubility test was conducted using 15 wt% HCl. The mass of the sample collected from the inner surface of liner #3 was 0.584 g. After the reaction, the mass of the unreacted solids was measured to be 0.425 g. This means that only 27.3% of the sample was dissolved. This sample was mainly formed by quartz, and this explains the low soluble amount. Based on ICP data (**Table 2.11**), iron was the main element dissolved by HCl which is in agreement with expectations.

Table 2.11: ICP results for the inner surface sample of liner #3

Sample #	Element concentration, mg/l					
	Ca	Mg	Si	Al	Fe	S
Inner #1	801.6	271.2	115.6	82	12096	2356

The unreacted scale sample was separated and dried. This sample clearly contains different sized quartz particles mixed with black material which could be remained after the reaction with iron sulfide (**Figure 2.60**). Further analysis of unreacted solids was conducted using SEM. **Figures 2.61** and **2.62** present electron microscope pictures with magnification of 200 and EDS results for the unreacted part of the sample, respectively.

Figure 2.60 – Inner materials sample for liner #2 after the acid reaction

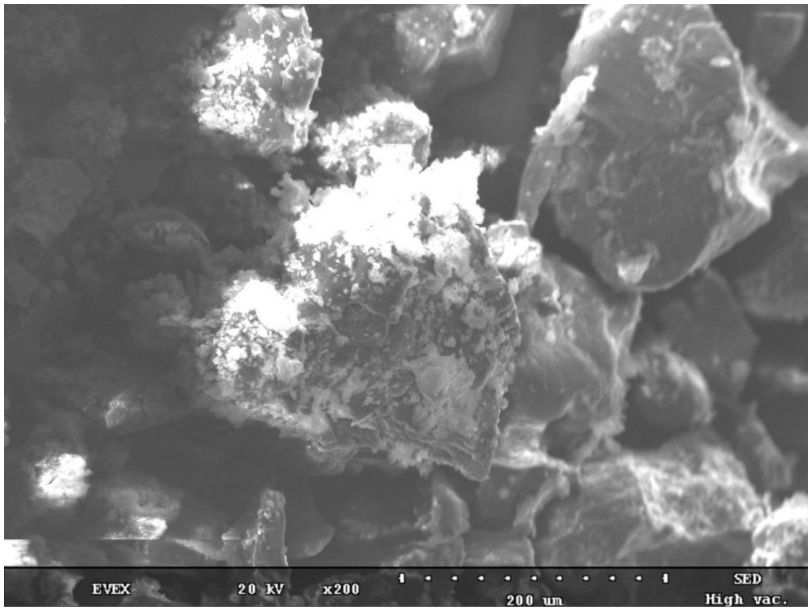

Figure 2.61 – Inner scale after the acid reaction, electron microscope picture (magnification is 200)

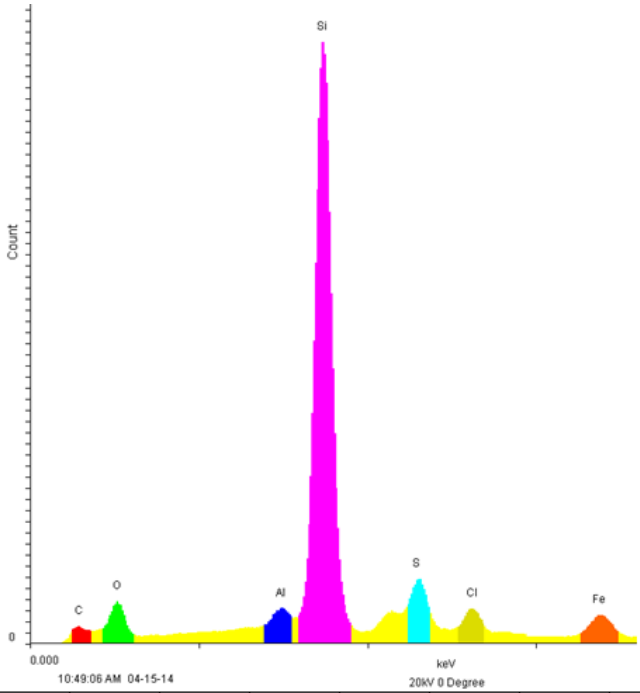

Elements:	WT%	AT%	K_A	K_F	K_Z	Intensity	P/bkg
SiK	72.18	74.76	0.93	1.006	1.002	1992.944	34.2
S K	27.82	25.24	0.288	1	0.992	199.652	3.5

Figure 2.62 – EDS data for the inner sample after the reaction

As it was expected, iron, calcite, and aluminum were almost completely dissolved. Silicon oxide was the main mineral remaining after the HCl solubility test. This result shows that hydrochloric acid is not the best option in terms of an actual dissolution of the scaling and blocking materials because, even at a very high concentration, it doesn't dissolve main components. However, HCl does remove cementing materials which usually consolidates silicon-based scales.

2.2.4 Blocking materials from the slots

Actual production problems are caused by the blocking of slots. However, it is not an easy task to reach this samples because of the very small width of these slots (**Figure 2.63**). It is almost impossible to collect a representative amount of the scale sample from the slot without cutting the liner. Samples from the slots were collected by cutting the liner. It was decided to cut the liner according to the scheme shown in **Figure 2.64**. Red lines present cuts.

Figure 2.63 – Blocked slots

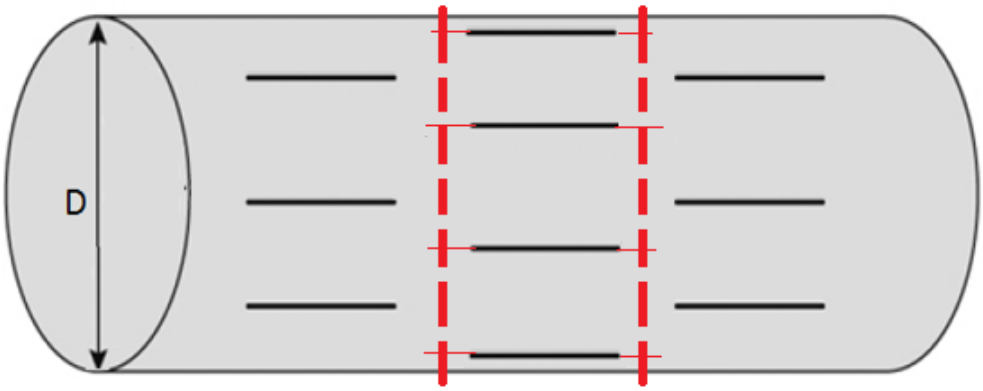

Figure 2.64 – Scheme of cutting the liner

It should be noted that the usual saws use oil for lubrication and cooling of the cutting parts; however, it could contaminte the actual sample. That is why a special saw was used for the actual cutting procedure which was performed without lubricants and overheating. Also, slots were isolated by tape to prevent contamination by metal sawdust.

2.2.4.1 SEM

As a result, the inner surface of slots was exposed (**Figure 2.65**). The structure of the blocking materials is different for different samples. Some of them have channels, and some are fully blocked. In some slots, grains of quartz were cemented by grey and black cement. SEM data for these samples is shown in **Figures 2.66** – **2.69**.

Figure 2.65 – Inner surface of the slot

SEM results showed the main components in both scales are iron and silicon. Samples similar to the sample in **Figure 2.66** are more abundant, and they usually cement bigger grains of quartz.

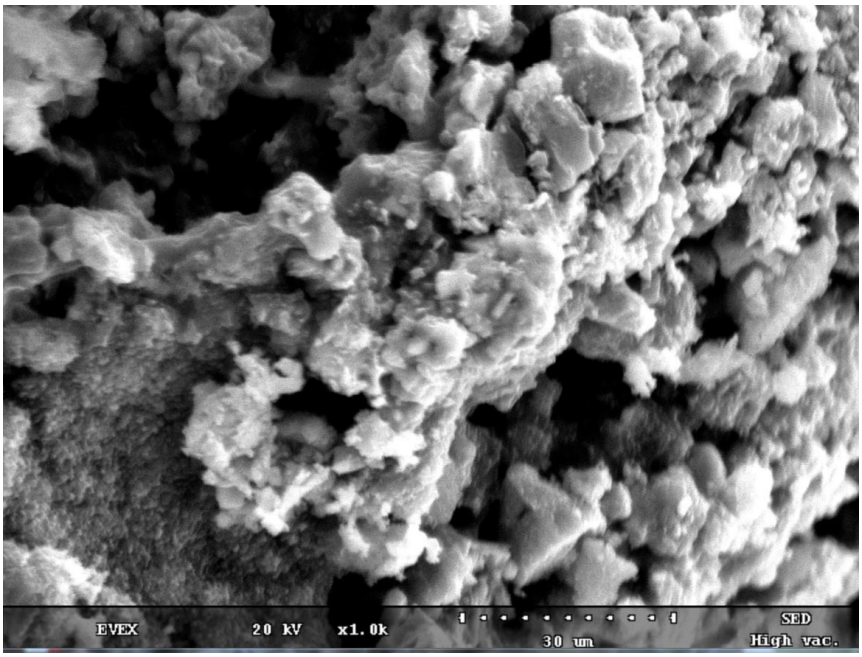

Figure 2.66 – Sample from slot #1, magnification 1000

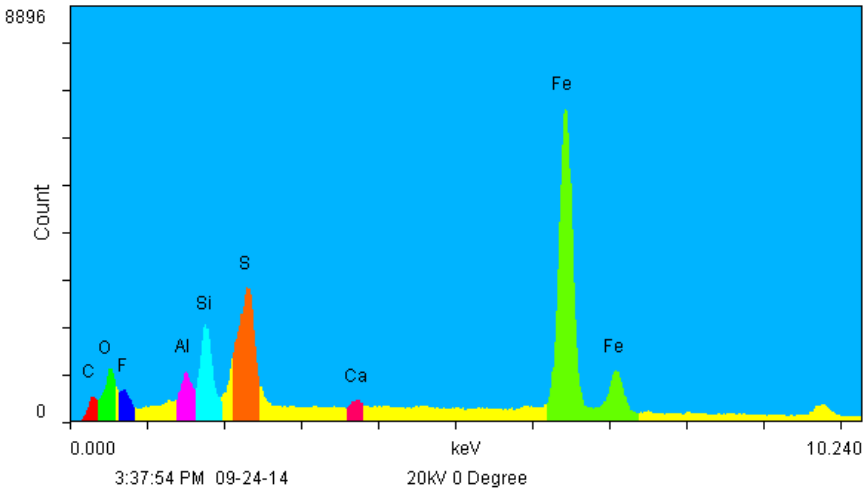

Figure 2.67 – EDS data for slot sample #1

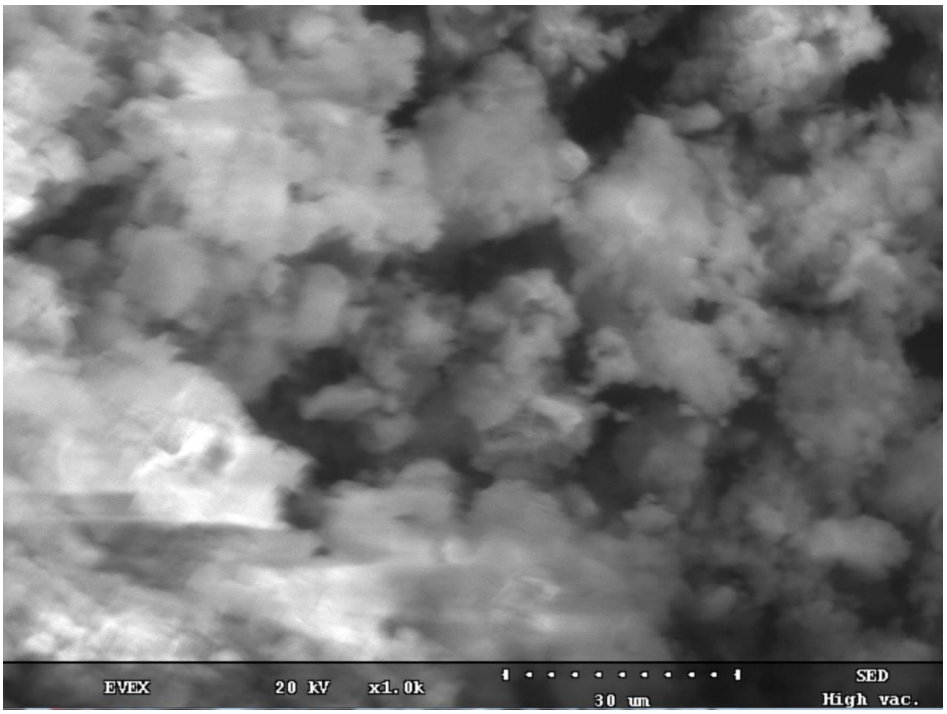

Figure 2.68 – Sample from slot #2, magnification 1000

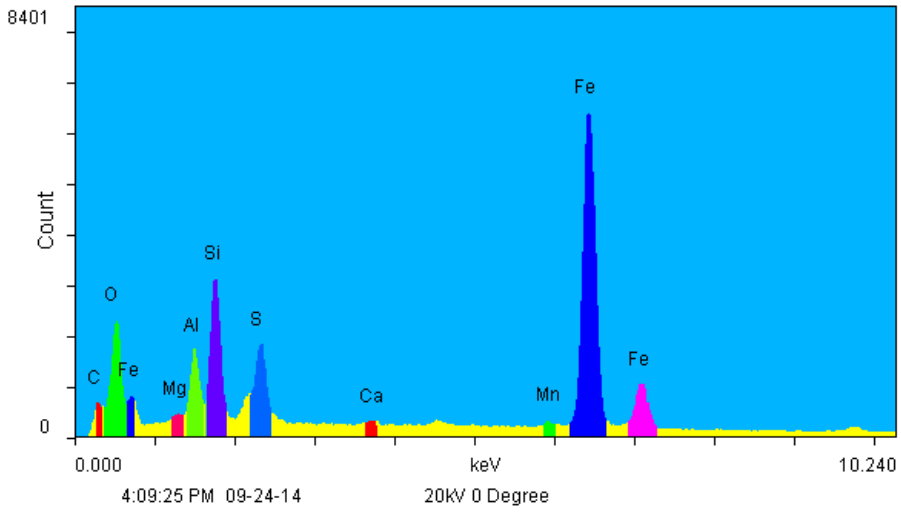

Figure 2.69 – EDS data for slot sample #2

From EDS data, it could be concluded that these samples contain a significant amount of iron silicates and sulfides together with aluminosilicates. It is very likely that the main source of iron is tubing corrosion and minerals dissolution (for example, clays with cation exchange). Aluminum and silicates are common for sandstone minerals, especially smectite, kaolinite, and feldspars.

2.2.4.2 XRD

The XRD results for the scale from the inside surface of the slots are shown in **Figure 2.70**. This scale consist of purrhotite, antigorite, greenalite, and chlorite. The high background level indicates high amount of amprohous material. It is very important to know the structures and surface charges of the minerals to understand their solubilities in acid and other properties. Purrhotite is a redox sensitive mineral with a variable iron content from the iron sulfides group. The Fe:S ratio for this mineral is close to unity which means that this mineral can be dissolved in acid. Antigorite is a polymorph of serpentine which is very stable at high temperatures. Greenalite is another mineral from the kaolinite-serpentine group. Both antigorite and greenalite are 1:1 layer phyllosilicates with mainly Si^{4+} as a tetrahedral cation and Mg^{2+} as an octahedral cation, but in both cases, Al^{3+} substitution is possible. The surface charge of these minerals depends on the pH because of the attached to the octahedrals H^{+} which can be easily dissolved with respect to the Mg^{2+} in the magnesium oxide octahedral sheet. Feng et al. (2013) showed that the removal of magnesium ions from the serpentine surface by acid leaching results in a decrease of serpentine iso-electric point. Chlorite is a common phyllosilicate mineral

with a 2:1 layer structure and an excess of negative charge. This negative charge is partially compensated by a positively charged interlayer octahedral hydroxide sheet.

Overall, minerals and their distribution in slot-filling material are an important issue which should be futher investigated. This analysis is useful for the understanding of the structure and origin of the scale particles. It was found that some samples contain abundant quartz and iron oxides together with a range of iron silicate phases including: Fe-rich, Al-rich, Ca-bearing, and S-bearing varieties. Calcite presents only locally, while other minor minerals have trace phases including: K feldspar, Ca-siderite, and kaolinite. It should be noted that quartz with minor K feldspar occurs as fine to medium sand grade and rounded detrital grains. The same could be stated about calcite grains which indicates a common origin. Dolomite inclusions are not significant and noted within the calcite mainly. The grains of kaolinite are detrital in origin because they are associated with the rounded quartz grains. All detrital grains are cemented and coated with both iron oxides and iron silicates. Iron oxides are the most prevalent in direct contact with the slot wall and may also extend into the slot wall due to the progressive corrosion and replacement of the steel. Iron silicates typically coat the iron oxides on the slot wall but also occur as a pore-filling material and cement. S-bearing phases are typically concentrated towards the inside diameter of a liner. Lateral variations in the Fe and Ca content along the length of the slot are also noted. Siderite occurs as common pore-filling crystals that typically occupy larger pores, especially in close proximity to the slot wall.

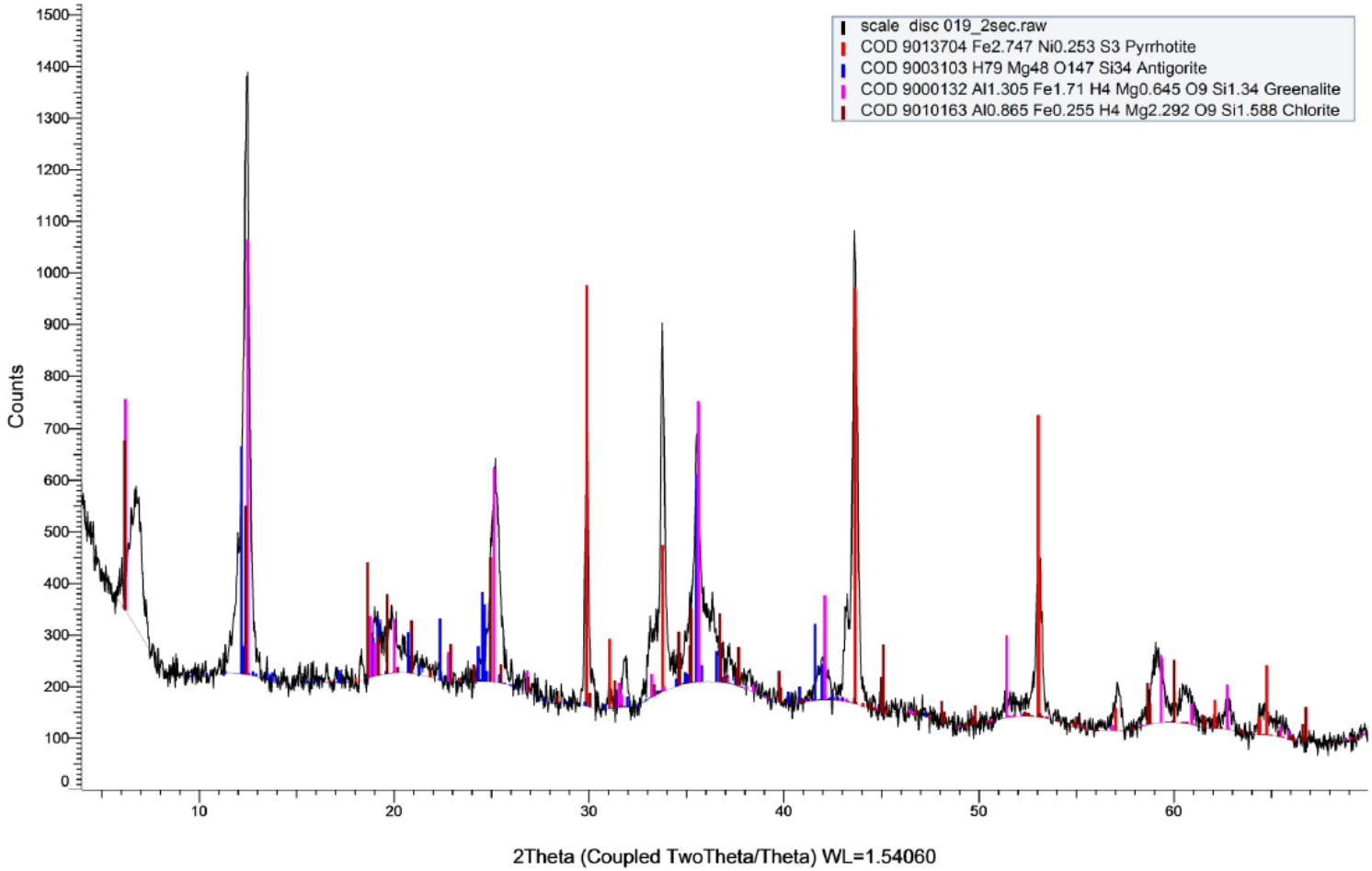

Figure 2.70 – XRD results for the sample from a slot

2.2.5 Additional solubility test

It was shown previously that the outer scale sample from the bottom part of liner #1 almost didn't react with HCl during the normal acid solubility test. The solubility for these materials was 10%. It was decided to try to dissolve the organic matter in xylene. The reaction occurred instantly (**Figure 2.71**). It was measured that the dissolution of the sample in xylene is 12.4% by weight.

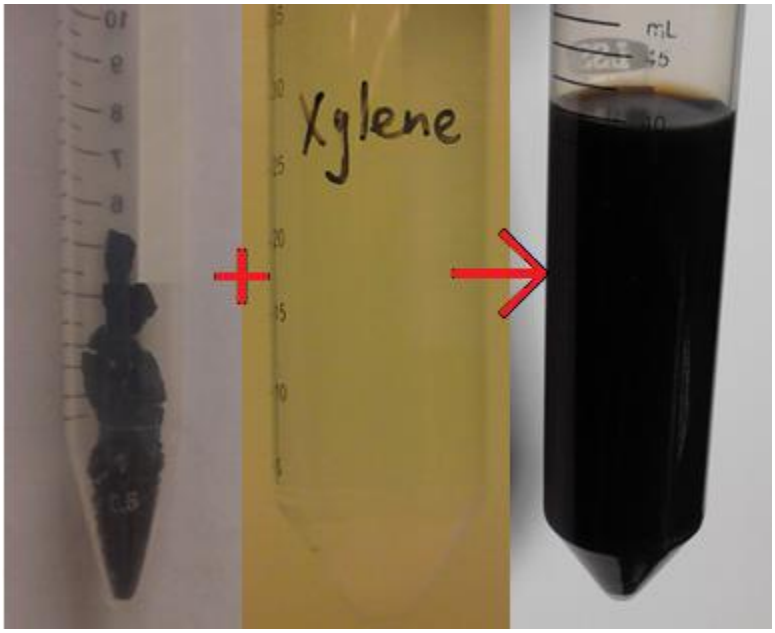

Figure 2.71 – Solubility of organic rich scale in xylene

After filtration and washing of the unreacted with xylene, part of the sample (**Figure 2.72**) solubility with 15 wt% HCl was found. After the reaction and

sedimentation of unreacted material (**Figure 2.73**), the solubility of the sample in HCl was determined to be 13.2 %.

Figure 2.72 – Sample from the bottom part of liner #1 after the reaction with xylene

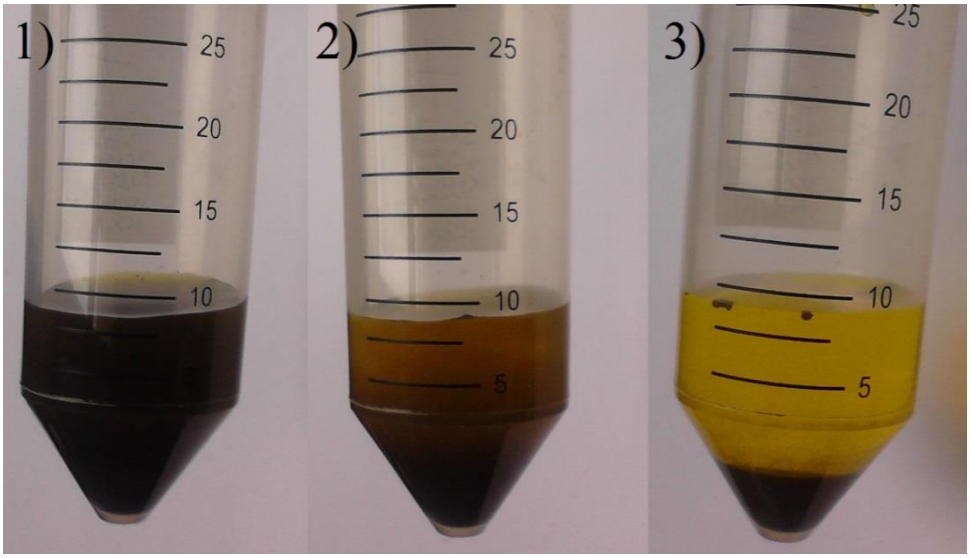

Figure 2.73 – Sample from the bottom part of liner #1 during the reaction with HCl

It should be stated that the solubility in HCl increased more than 30% after the xylene preflush. It is also important that 23.9 % of the initial sample was dissolved overall by xylene and HCl, which is more than twice higher than the 10 % dissolved by HCl only.

After the reactions with xylene and HCl, the unreacted material was washed and analyzed using SEM. **Figure 2.74** presents rounded particles of aluminosilicates. It should be noted that these particles are not so well cemented anymore.

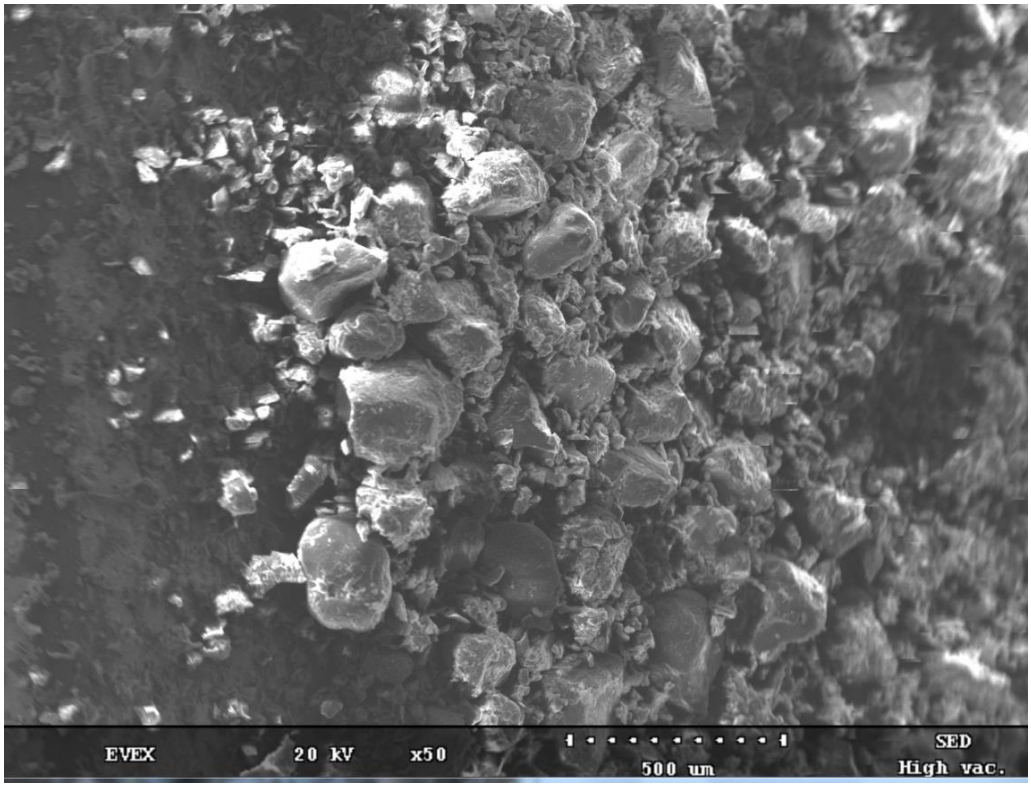

Figure 2.74 – Unreacted sample after xylene and HCl electron microscope picture (magnification is 50), liner #1

It was very unusual to identify a mercury peak in the unreacted sample (**Figure 2.75**). The source of mercury should be futher investigated.

Based on the ICP data (**Table 2.12**), the amount of Mg dissolved in HCl increased from 30.5 mg/l (table 2.3) to 200.2 mg/l. More cementing materials were dissolved in comparison with the HCl reaction without the organic solvent preflush.

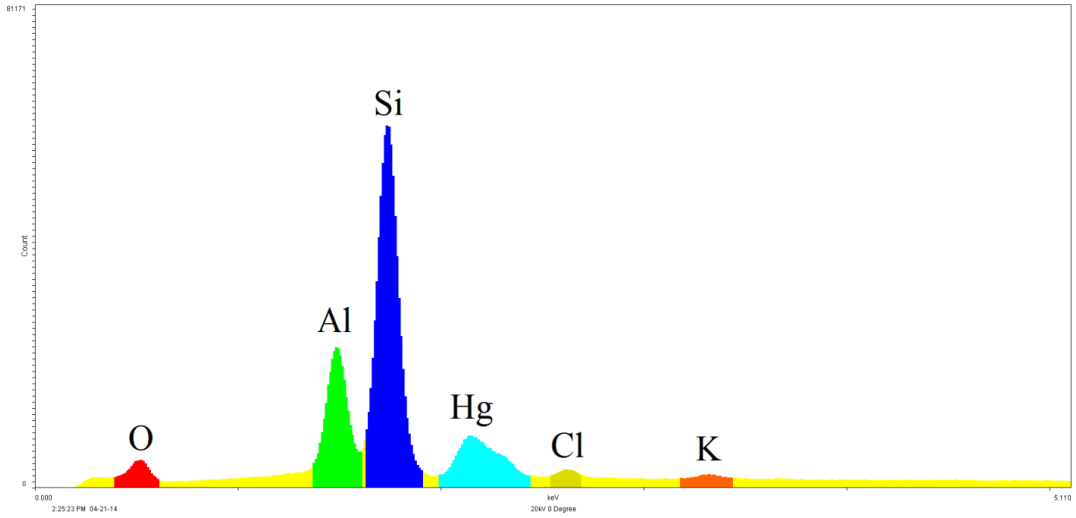

Figure 2.75 – EDS data for the unreacted sample after xylene and HCl, liner #1

Table 2.12: ICP results for reacted HCl after the xylene reaction, liner #1

Sample #	Element concentration, mg/l				
	Ca	Mg	Si	Al	Fe
Xylene and HCl, liner #1	608.8	200.2	10.8	634.8	4786

2.3 Conclusions

It was found that scales are formed by different minerals in injectors and producers. For injectors, scale is mainly formed by interlayers of silica polymorphs and organic materials. The main minerals in this type of scale are quartz, calcite, barite, and siderite. It should be noted that HCl is not able to dissolve such scale, especially when the scale is covered with organic materials which plays as a barrier between acid and minerals. That is why the solubility of these scales in 15 wt. % HCl is rarely higher than 50 wt. %. Scale from producers is strongly connected with tubing corrosion because it usually contains a lot of iron. The main minerals which are present in this scale are iron sulfides and oxides, aluminosilicates, carbonate minerals with magnesium and iron isomorphous substitution, and calcium sulfates. The solubility of these scales in HCl are slightly higher, but they are also usually covered by a crude oil which requires using an organic solvent as a preflush.

3. MINERALOGICAL ANALYSIS OF THE TARGET ZONE

The objective of this stage of the work is to analyze the samples of oil sands from a mineralogical point of view. The important task for a treatment design is to identify the structure, texture, and mineralogy of the samples to clarify physical and chemical properties of rocks in the target zone.

Additionally, a mineralogy analysis is a useful tool in order to investigate the mechanism of the steam-rock interactions in the reservoir and the potential sources of ions which form the scale. This work is necessary for a better understanding of clay stabilization mechanisms and migration control in the reservoirs with a similar mineralogy.

The sample for the analysis was taken from the McMurray formation in Alberta. The Lower McMurray comprises a variable succession of mudstone/coal, associated with blocky clean sands. The lithological content of the Lower McMurray is comprised of gravel, coarse sand, silt, and clay with mainly siderite as a cementing material. Clay minerals mainly include kaolinite and illite (Hein et al. 2000).

3.1 Methodology

3.1.1 Air dry and grind the sample

The oil sand sample was dried in the fume hood overnight. At the beginning, the sample was slightly consolidated, and some heterogeneity of the components such as different color lamella and structure was observable as shown in **Figure 3.1**.

After the crashing of these consolidated aggregates, the sample was passed through the 2-mm sieve without a strong pressure. Everything that remained in the sieve was again treated with a mortar and pestle. After a few repetitions, the sample was able to pass through the sieve completely. A significant amount of organic materials was observed during the crashing.

Figure 3.1 – The sample before and after the crashing

3.1.2 Moisture content quantification

Three aluminum weighing dishes were labeled and weighed before and after adding a few grams of the dried sample. The dishes were placed in the oven at 105 °C and left there overnight. The samples were removed from the oven and cooled down in a vacuum-type desiccator. Cooled dishes with the samples were weighed again. The moisture content was calculated using **Eq. 3.1**:

% Moisture = (Air Dry Weight – Oven Dry Weight)/Oven Dry Weight * 100 %..... (3.1)

3.1.3 Preliminary evaluation of carbonate minerals, sulfides, manganese oxides, and evaporates

About 0.5 grams of the sample was taken for a reaction with 1M HCl. The sample was in the micro weighing dish, and a few drops of 1M HCl were added. The reaction of calcite with HCl (**3.2**) is shown below:

$$CaCO_{3(Calcite)} + 2H^{+} = Ca^{2+} + CO_2\uparrow + H_2O \quad \text{.....(3.2)}$$

3.1.4 Preliminary evaluation of oxidizing/reducing components

Hydrogen peroxide was used to identify oxidizing/reducing components such as manganese oxides, sulfides, and reduced iron Fe^{2+} species. H_2O_2 can be both an oxidizer and a reducer and can react with organic matter, manganese oxides, sulfides, and reduced iron Fe^{2+} species such as siderite and pyrite.

3.1.5 Preliminary evaluation of magnetic minerals

A magnetic stir bar was used to pull out the magnetic minerals in the sample. The sample was spreading out in a weighing dish, and the magnetic bar was drawing back and forth to find some magnetic minerals. Any minerals exhibiting magnetic properties would stick to the bar.

3.1.6 Preliminary evaluation of evaporite minerals

40 grams of the sample were mixed with 200-mL of deionized water in the 250 ml centrifuge bottle. Then, the sample was placed on the reciprocating shaker for 30 minutes. After the elapsed time, the mixture was centrifuged at 2000 rotations per minute speed for 10 minutes. A cloudy supernatant indicates that the electrolyte content in the supernatant is low, and the cations in the solution are mostly monovalent. Afterwards, approximately 20 mL of the supernatant were filtered to measure the electrical conductivity (EC) and pH. The major evaporate minerals are gypsum and more soluble ones. When water is rich in halides, sulfates, nitrates, or borates, high EC will be identified. To check gypsum, 1 mL of supernatant was mixed with 1 mL of acetone in a 5-mL glass test tube. A formation of cloudy white precipitation is an indicator of the presence of gypsum. Sulfates were checked with a $BaCl_2$ solution and a chloride anion Cl- with $AgNO_3$ solution. In both cases, the presence of the cloudy white precipitates ($BaSO_4$ or AgCl) is an indicator of the SO_4^{2-} or Cl^- ions, accordingly.

The sample was kept for further experiments.

3.1.7 XRD of the bulk sample

A representative portion of the sample was taken, crushed using a mortar and pestle, and passed through a sieve (140 mesh). The sample was pressed in the cavity of the XRD mount for further analysis using a glass slide without orienting the grains in a preferred direction.

3.1.8 Removing of the flocculating and cementing materials

The flocculating materials are soluble salts. Polyvalent cations are adsorbed on the mineral surfaces, while cementing agents are carbonate minerals, Ca^{2+} and Mg^{2+}, organic matter, oxides and hydroxides of iron, and amorphous silica and alumina. These materials should be removed from the sample to enhance the dispersion of an individual particle and to facilitate size fractionation.

3.1.8.1 Removing of carbonate minerals

50 ml of a pH of 5 sodium acetate were added to the sample, and the mixture was shaken by hand in the 250 ml centrifuge bottle. Vigorous bubbling of CO_2 indicated the presence of clay-sized particles. The solution was heated up in the water bath at 90 ˚C for 30 minutes. The mixture was shaken every 10 minutes. The bottle was shaken by hand to suspend settled particles. Then, a centrifugation at 2000 rotations per minute for 5 minutes was done, and the supernatant was pipetted off. After adding 50 ml of fresh, pH of 5 sodium acetate, all steps were repeated 3 times.

3.1.8.2 Removing of organic matter

20 mL of pH of 5 sodium acetate were added to the 250 mL centrifuge bottle with the sample after the carbonate removing procedure. The bottle was shaken by hand

and with a vortex mixer. 10 mL of hydrogen peroxide were added to the bottle. Then, the bottle was placed in a 1000 mL beaker covered with a watchglass and left overnight.

More H_2O_2 was added, and the bottle was shaken and placed in a 70 ˚C water bath with a loosened cap. This process was repeated in about one-hour intervals 7 times. All of the black organic material was removed from the surface of the mixture during the heating process. After this, the temperature was increased up to 100 ˚C to decompose hydrogen peroxide; the bottle was cooled down and centrifuged at 2000 rotations per minute for 5 minutes. The supernatant was pipetted and decanted.

3.1.9 Size fractionation and XRD preparation

3.1.9.1 Sample dispersion

50 mL of sodium carbonate with a pH of 10 were added to the sample, and the bottle was shaken. After suspending the particles, the bottle was centrifuged at 2000 rotations per minute for 10 minutes. This procedure was repeated twice until the supernatant became cloudy which indicates that the silts and clays have started to disperse from the sample.

3.1.9.2 Separation of sand fraction (>53 μm)

First, the plastic funnel and sieve were installed. The centrifuge bottle was shaken and, then, was allowed to stand for a minute to let the sand particles settle. The upper suspension was poured onto the #270 mesh sieve until all the particles were washed out from the bottle and cap. Some amount of pH of 10 sodium carbonate was added to wash out the particles. After rinsing sand with deionized water, the sand was washed to a pre-weighed aluminum dish which was placed into the oven at 105 ˚C until

the sand is dried. The weight of dish with sand was measured after cooling them in the desiccator.

3.1.9.3 Separation of silt (2-53 μm) and clay fractions (<2 μm)

Silt and clay fractions were separated using the centrifugation method. A 250-mL centrifuge bottle was filled with pH of 10 sodium chloride solution to the 9-cm mark and, then, was shaken to suspend the particles. Then, the bottle was centrifuged at 820 rotations per minute for 3 minutes in an Allegra X14R centrifuge. The suspension between 0.5 and 9 cm contains the clay fraction, and it was siphoned. These actions were repeated until the upper solution became clear. All of the settled particles were transferred in the 250-ml bottle. This is the silt fraction. This fraction was centrifuged and transferred to the pre-weighed aluminum dish to be dried at 105 ˚C in the oven.

3.1.9.4 Dialysis and drying of clays

The clay suspension was transferred into a proper length dialysis tubing with the minimum volume of the suspension. After rinsing of all of the particles into the tubing, some air was added, and two knots were made to close the second end of the tubing. Filled tubing was immersed in the distilled water in a 4-liter beaker. Water was changed in the beaker every few hours and then about 3 times per day. Electrical conductivity was measured until it reached a value lower than 2 μS/cm. After this, the suspension was transferred into pre-weighed 50-mL centrifuge tube, the total weight was measured. The weight of clay was quantified by the gravimetrical method after drying an aliquot of the suspension at 105 ˚C.

3.1.9.5 Sand, silt, and clay samples' preparation for X-ray diffraction

First, a representative amount of the sand fraction was grained in an amount which is enough to fill the XRD powder holder. Both the sand and silt fractions samples were simply loaded in labeled holders.

For the clay sample, magnesium saturation and glycerol solvation were conducted. 50 mg of dried clays were mixed with 2-mL of $MgCl_2$ in the centrifuge tube using the vortex mixer. Then, more 0.5 M $MgCl_2$ was added (up to 15-mL mark), and the centrifuge tube was shaken for 20 minutes. After this, the tube was centrifuged for 10 minutes at 2000 rpm, and the upper clean solution was pipetted off. This Mg-washing procedure was repeated two more times.

Next, the Mg-saturated clay was washed three times with deionized water, mixed, shaken for 10 minutes, and centrifuged for 10 minutes at 2000 rpm. The solution was pipetted out. Then, the clay fraction was suspended in 1-mL of deionized water and transferred using a disposable pipet on a labeled glass disk. A sufficient amount was added to cover the entire disc. Then, the disc was covered with a watch glass and left for a few days to let the solution to evaporate.

The same procedure was used to prepare K-saturated clay films. 1 M KCl was used instead of 0.5 M $MgCl_2$.

These preparations are important for XRD analysis of the clay fraction because they help to orient specimens and have clear peaks as a result. A special technique for an interpretation of the XRD-patterns was used. The main principles of this technique are summarized in **Table 3.1** which were modified from Whittig (1965).

Table 3.1: The d(001)-spacings of phyllosilicate minerals after different cation saturation, solvation, and heat treatments

Saturation, solvation, heat	d(001)-spacing, (nm)					
	Kaolinite	Mica	Vermiculite	Smectite	Chlorite	HIV/HIS*
Mg, 25 ˚C	0.7	1.0	1.4	1.4	1.4	1.4
Mg-Glycerol	0.7	1.0	1.4	1.8	1.4	1.4
K, 25 ˚C	0.7	1.0	1.0-1.2	1.0-1.4	1.4	1.4
K, 330 ˚C	0.7	1.0	1.0	1.0	1.4	1.0-1.4
K, 550 ˚C	-	1.0	1.0	1.0	1.4**	1.0-1.4

* – Incomplete hydroxide interlayer vermiculite (HIV) or smectite (HIS) is an intermediate between chlorite and vermiculite or between chlorite and smectite.

** – The intensity of the 1.4 nm peak enhances with an accompanying loss in intensity of the higher order peaks.

3.1.10 Sample preparation for the Fourier Transform Infrared Spectroscopy analysis

1 mg of clay was weighed on a piece of weighing paper. Then, 300 mg of KBr was weighed and mixed thoroughly with the prepared clay. Then, the mixed sample was transferred into the pellet die chamber. The plunger was placed into the die, and the sample was spread uniformly. The assembled die was placed into the pellet press. Vacuum was applied for 5 minutes. Then, the pressure was increased up to 20,000 psi for 5 more minutes. After this, the pressure was released, and the die was obtained from

the press. The finished pellet was pressed out from the die and placed in a labeled glass vial which was placed in a desiccator.

3.1.11 Removing of iron oxides

Iron oxides can be a cementing material among aluminosilicates which causes difficulties with the dispersion and segregation of colloidal aluminosilicates. The technique of Mehra and Jackson (1960) was used in the laboratory, and it is the sodium dithionite-citrate-bicarbonate procedure. Sodium dithionite ($Na_2S_2O_4$) reduces ferric iron (Fe^{3+}) to ferrous iron (Fe^{2+}). This makes iron oxide be more soluble. The sodium citrate $Na_3[HOC(COO^-)(CH_2COO^-)_2]$ acts as a chelate and complexes the iron in the solution. The bicarbonate ion acts as a pH buffer to prevent a changing of the pH.

First, the sample and standards were weighed (no more than 2.5 g and 0.1 g, respectively) in duplicate 50-mL tubes. Then, 20 mL of 0.3 M Na-citrate and 2.5 mL of 1 M $NaHCO_3$ were added, and the solution was shaken using a vortex mixer until the particles were suspended. The samples were warmed in a water bath up to 75˚C (approximately 15 minutes). 0.5 g of $Na_2S_2O_4$ was added. The solution should be swirled. To promote flocculation, 2 mL of saturated NaCl should be added. Samples and standards were centrifuged for 15 minutes at 2000 rpm. The supernatant was collected in a 100-mL volumetric flask. This procedure was repeated two times.

After this, the solution was diluted with deionized water until there was 100 mL of total volume. Then, the bottles were shaken. After this, the solution was diluted 100 times, and both concentrated and diluted solutions were transferred to pre-labeled plastic bottles.

3.1.12 Cation exchange capacity evaluation

Cation exchange capacity (CEC) is a measure of the quantity of readily exchangeable cations neutralizing negative charge in the sample. Objectives of this work are to determine the CEC and to estimate the amount of highly charged clay minerals in the sample.

First, four 50-mL plastic centrifuge tubes were marked and weighed (two for samples and two for standards). Then, 7.3 mL (approximately 100 mg of clay) of prepared and homogenized clay suspension were added to a pre-weighed centrifuge tube. 100-mg of standard were added to another 50-mL plastic centrifuge tube. Then, two more tubes with standard and sample were prepared in the same way. After this, all of the samples were washed with a 0.5 M $CaCl_2$ solution. Tubes were filled until the 20-mL mark and shook for 15 minutes. Then, they were centrifuged at 1500 rpm for 10 minutes. The supernatant was pipetted out and preserved. This washing procedure with a high $CaCl_2$ concentration was repeated for 3 times in total. Then, each sample was washed three more times with 0.005 M $CaCl_2$ to complete the saturation of the cation exchange sites with Ca^{2+} ions. Then, the supernatant was removed. After this, each tube was weighed with sample and interstitial solution.

The next part of the work is a washing of the samples and standards with 0.5 M $MgCl_2$ to exchange Ca^{2+} ions with Mg^{2+} ions. For this purpose, the centrifuge tubes were filled with 0.5 M $MgCl_2$ to the 15-mL mark, and then, they were shaken for 15 minutes. After this, a centrifugation at 1500 rpm for 10 minutes was done. Afterwards, the supernatant was transferred to the 100-mL flasks. This washing procedure was repeated

for four times in total. Then, the supernatant was diluted with 0.5 M $MgCl_2$ up to 100-mL mark and mixed. Next, 20 mL of the solution was transferred to another 100-mL flask and diluted up to 100 mL with distilled water. After this, both the concentrated and diluted solutions were poured into the marked 20-mL plastic vials.

The last step is to determine the weight of the clay residue. To remove the excess of $MgCl_2$, the tubes were filled with distilled water up to 14 mL and shaken using a vortex mixer. After centrifugation at 1500 rpm for 10 minutes, the supernatant was discarded, and the tubes with the clay residue were placed in the oven at 60 ˚C. After cooling in the vacuum, the desiccator tubes were weighed (W4 in the **Formula 3.9**).

After this, the exact concentrations of Ca in the 0.005 M $CaCl_2$ solution and in the 0.5 M $MgCl_2$ solution were determined using an atomic absorbance spectroscopic analysis.

3.1.13 SEM and TEM analysis

A FEI QUANTA 600F field emission scanning electron microscope (SEM) was used to construct scanning electron micrographs of the silt fraction. A point-to-point measurement strategy was used. The sample was platinum coated prior to the analysis to enhance conductivity. Samples were mounted on a flat surface of a SEM stub with help of an adhesive tab. Surface mineral morphology and EDS were used in mineral identification.

TEM permits morphology viewing, chemically analyzing (EDS), and structurally analyzing (electron diffraction) sub-micron particles. It is also important to have a visual image of each particle to understand the properties and structures of minerals better.

During the TEM analysis, data of different types was obtained: morphology, selected area electron diffraction (SAED), energy dispersive spectrum (EDS), and lattice fringes. For mounting of the clay, a holey-C grid was used. It could be stated that TEM data complements XRD data, and it is a good technique for confirming previous results.

3.1.14 Total K determination

The evaluation of the total amount of potassium cations is a popular technique for the determination of mica in clay samples. The presence of K-feldspars is the principal source of errors in such an estimation; however, for samples that don't have exchangeable K^+, this method could be useful. It is important to replace any exchangeable K^+ by another cation. For this purpose, 60 mg of the oven dried clay sample and standard (New York Ca-Illite clay) were weighed and emptied into the 50-mL Nalgene volumetric flasks. Two mL of aqua regia and 3 mL of 50% HF were added into each volumetric flask. Volumetric flasks were capped tightly using parafilm and shaken. After shaking, the saturated boric acid was added to the solution up to the 50-mL mark. After the reaction, the samples were diluted 1:10 with 0.05 NaCl to prevent the ionization of K in the flame during atomic absorbance/emission analysis. A subsample of the solution was taken and reserved for the determination of K concentration of the solution using the AAS unit.

3.2 Results and Discussion

3.2.1 Preliminary evaluation of the sample

The results of the moisture content quantification experiment and calculations are shown in **Table 3.2**.

Table 3.2: Moisture quantification

Replication	Dish weight, gram	Dish+air dry sample, gram	Dish+oven dry sample, gram	Moisture, %
1	1.3288	2.4241	2.3876	1.5287
2	1.3257	2.3514	2.324	1.1790
3	1.3263	2.4046	2.3735	1.3103
			Average	1.34

A reaction of the sample with HCl didn't occur. It should be noticed that the surface of the sample is hydrophobic which can be seen noticeably in **Figure. 3.2**. This is one of the reasons that the sample wasn't reacting with HCl. Some amount of aluminosilicates together with calcite should be present in the sample as a cementing material which was found by a previous analysis. They should react with HCl, but there is an idea that the sample's particles are covered with oil and other organic materials which are working as a barrier between the minerals and HCl. The sample in hydrogen peroxide showed positive responses, but the reaction wasn't with vigorous bubbling, even though the sand sediment is rich in oil. A small amount of gas was evolved (**Figure 3.3**).

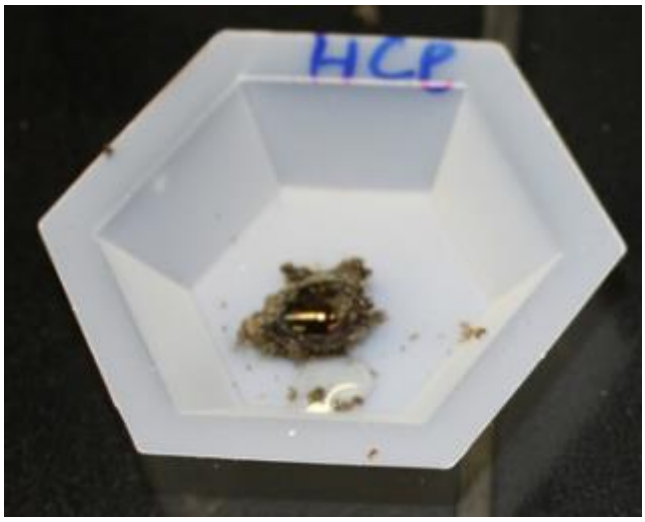

Figure 3.2 – Reaction with HCl

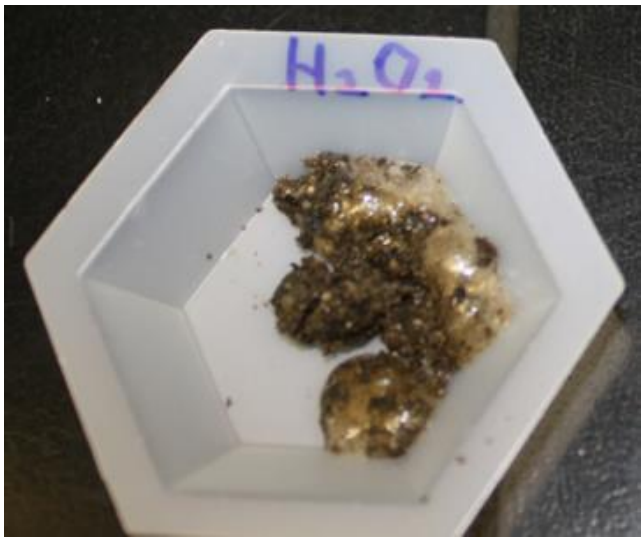

Figure 3.3 – Reaction with H_2O_2

No magnetic minerals were found with the magnetic bar. The results of the reactions of supernatant with Acetone, $BaCl_2$, and $AgNO_3$ are shown in **Figure 3.4**.

After reacting with acetone, the solution was slightly cloudy, so a very small amount of gypsum can present. After the reaction with $BaCl_2$, the supernatant became a little cloudier, and it indicates some amount of sulfate ions (SO_4^{2-}) is in the sample. The supernatant became most cloudy after the reaction with $AgNO_3$ which identifies some chloride ions Cl^-.

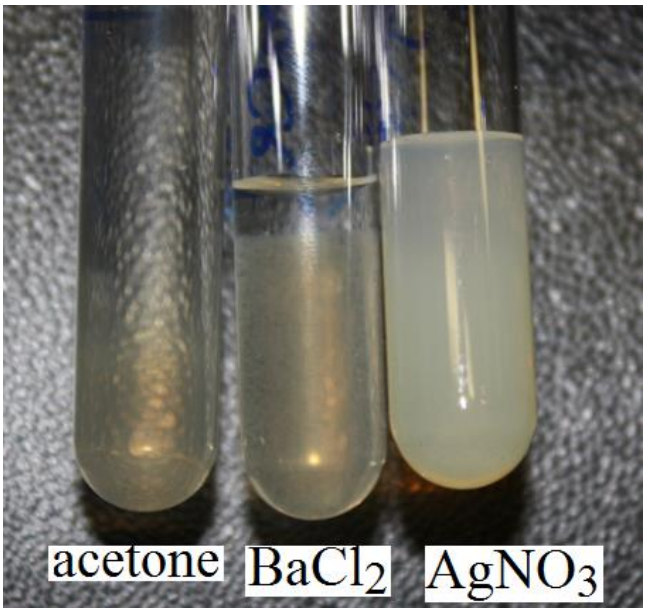

Figure 3.4 – Evaporate minerals evaluation

The EC result was measured to be 165.5 μS/cm which indicates that some soluble salts are in the solution. The pH was measured to be 7.206. This may imply the possibility of having a small amount of calcite as a cementing material in the sample.

A preliminary examination of the sample is summarized in **Table 3.3**:

Table 3.3: Preliminary examination summary

Sample #	Reaction with		Magnetic minerals	Tests with			EC (μS/cm)	pH
	1M HCl	30% H2O2		Acetone	$BaCl_2$	$AgNO_3$		
1	Evaluation scale: 0 – none, 5 – vigorous/abundant						165.5	7.2
	0	1	0	1	2	3		

The XRD results for the bulk sample are shown on **Figure 3.5**. Quartz is the most abundant mineral for this sample. Some other peaks were interpreted using EVA software. Calcite was shown by three main peaks, but they are not very intense. It should be noted that mineral identification using XRD is a difficult task for the bulk sample because of the presence of numerous cementing and organic materials which make invisible tiny particles. That is why, in the next stages, the sample will be pretreated and separated in fractions prior to XRD analysis.

Feldspar and illite were checked based on the previous experience of work with these samples. The peaks are not exactly matching at some points and should be further proved, additionally. Calcite was identified based on the three main peaks observed. These materials are usually cement for sandstone reservoirs. That is why they are present in a much smaller amount in comparison with quartz.

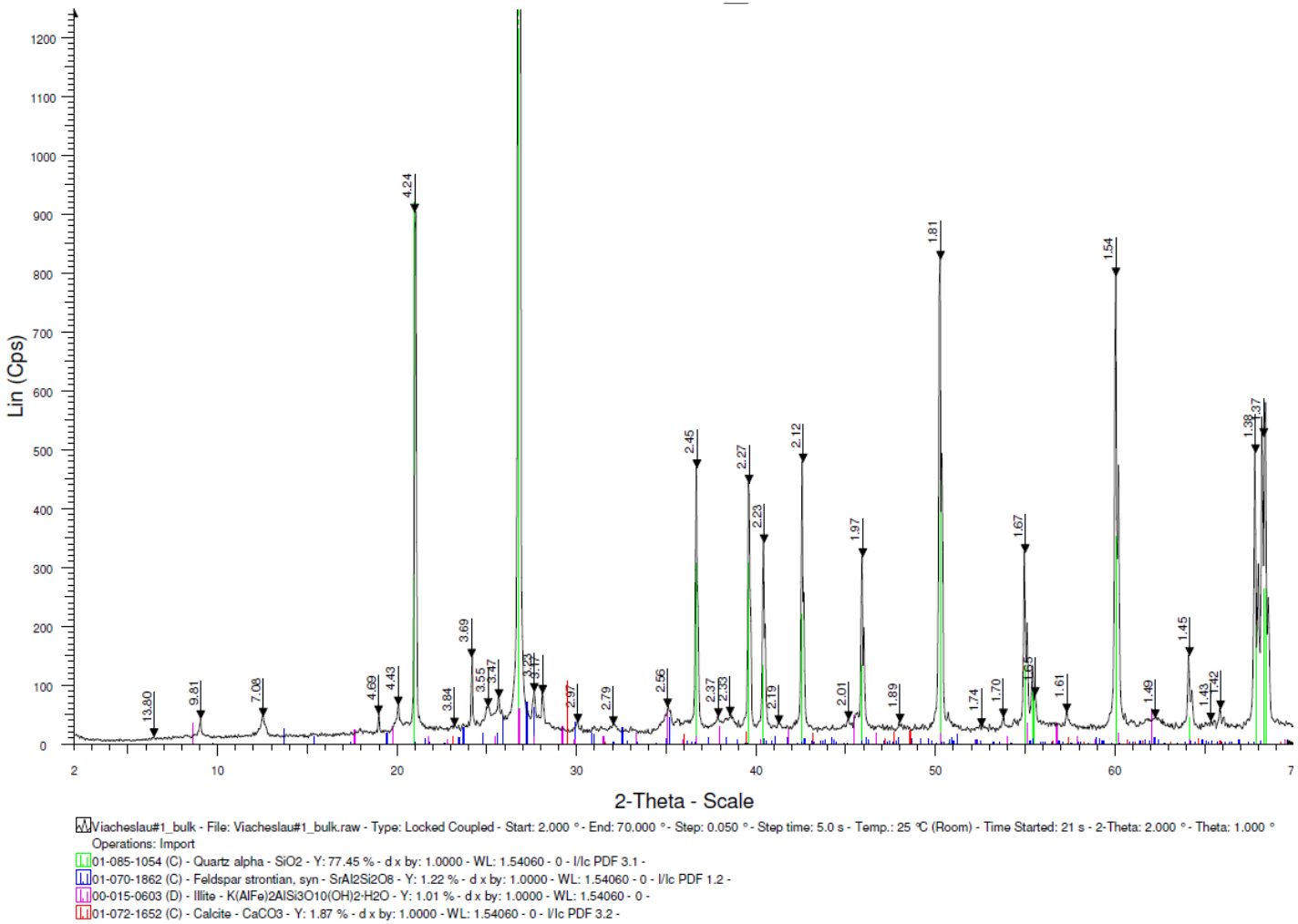

Figure 3.5 – XRD results for the bulk sample

After adding sodium acetate for the removal of calcite and dolomite, some bubbles were presented, but they weren't vigorous. The procedure was repeated 3 times until the amount of bubbles decreased significantly. However, probably all of the calcite and dolomite still weren't removed.

Based on the observations during the organic matter treatment, it could be concluded that the sample was saturated with oil and other organic materials. A large amount of these materials was floating on the surface of the suspension and was removed with a spoon during the heating process. The supernatant was clear but discolored, which indicates the presence of dissolved organic materials or iron without soil particles in the solution.

3.2.2 Sample fractionation

The results of separation and mass measurements for sand, silt fractions presented in **Table 3.4**. The actual weight of the clay sample was determined based on the content of clay in the suspension which was determined to be 1.369 wt% (**Table 3.5**).

Table 3.4: Weight of the sand and silt fractures

Sample	Dish weight, g	Dish+fracture, g	Weight of the fracture, g
Sand	1.0306	13.1834	12.1528
Silt	1.0233	4.4803	3.4570

Table 3.5: Clay content in the suspension

Dish weight, g	Dish+1 ml clay suspension, g	Dish+clay (oven dry), g	Content of clay, %
1.0134	2.0136	1.0271	1.369 %

After dialysis, the clay sample was kept in the water solution (**Table 3.6**). The weights of the organic matter, sand, silt, and clay fractions were used to summarize the initial content of the oil sand sample (**Figure 3.6**).

Table 3.6: Clay fraction

Container weight, g	Container + clay suspension, g	Weight of suspension, g	Weight of clay, g
34.9875	101.9810	66.9935	0.9176

The bulk sample is mainly composed of quartz. Sand size particles are abundant, but silt and clay particles are also present in the sample. It should also be noted that organic materials are the biggest part of the sample by weight. Quantitatively, sand takes more than 30 % of the sample. Silt fraction is almost 9 %, and clay is slightly higher than 2 %. Almost 59 % out of the 40 grams of the initial sample weight is organic material.

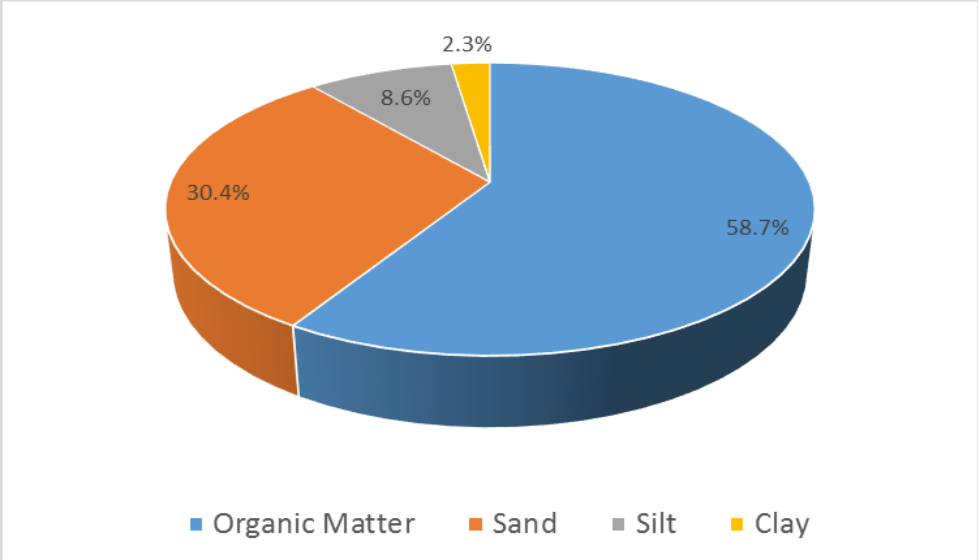

Figure 3.6 – Fractions distribution for the oil sand sample

3.2.3 XRD results analysis

It should be mentioned that pretreatment and fractionation of the sample are important and useful procedures because it aids to identify more minerals than just for a bulk sample which was discussed previously. First of all, the sand fraction was analyzed. The sample was taken from the oil sands which means it mainly consists of the silicon oxide. **Figure 3.7** shows that sand fraction is composed by almost pure quartz.

Next, the silt fraction was analyzed (**Figure 3.8**). Quartz was found to be the main component here again, but a large amount of other peaks were identified too. Based on these peaks, kaolinite is presented in this sample. Some of the peaks fit very well with an illite pattern. Another mineral which has a good agreement with the pattern is muscovite. The presence of some of these minerals were also proved by the XRD

results for clay fracture and FTIR which again shows that a complex analytical approach is sometimes better than just one whole-sample test.

The clay sample was analyzed at different conditions as it was mentioned before. This fraction showed a lot of different peaks (**Figure 3.9**). First, the peaks from 9.91 up to 10.02 Å are mica (Muscovite). These peaks are around 10 Å (=1 nm) for all types of saturations and temperatures. Then, the peaks from 7.13 up to 7.18 Å are for kaolinite. It is true because there is no peak for K at 550 ˚C. It is interesting to note that there are some peaks, 7.84 – 7.89 Å, in between mica and kaolinite. These are most probably a regularly interstratified mica/kaolinite. Interesting mineral specie is presented by peaks from 10.65 up to 11.01 Å. This is an incomplete hydroxide interlayer smectite which is an intermediate between smectite and mica. It should be noted that peaks 5.52 Å and 4.97 – 5.00 Å are (002) peaks for an incomplete hydroxide interlayer smectite and mica respectively. Peaks with d-spasing 3.95 Å are probably (002) peaks for a regularly interstratified mica/kaolinite. High peaks, 3.56 – 3.57 Å, are (002) peaks for a kaolinite. (003) peak for an incomplete hydroxide interlayer smectite which is presented by 3.69 – 3.7 Å peaks. Another very common mineral presented in the clay fraction is quartz which is determined by 3.33 – 3.34 Å and 4.24 – 4.25 Å peaks. The uncommon mineral was checked and identified because of some TEM observations. It is rutile which is shown by 3.24 Å peaks. There are also some peaks which are still under discussion, and they are the 4.70 – 4.74 Å peaks.

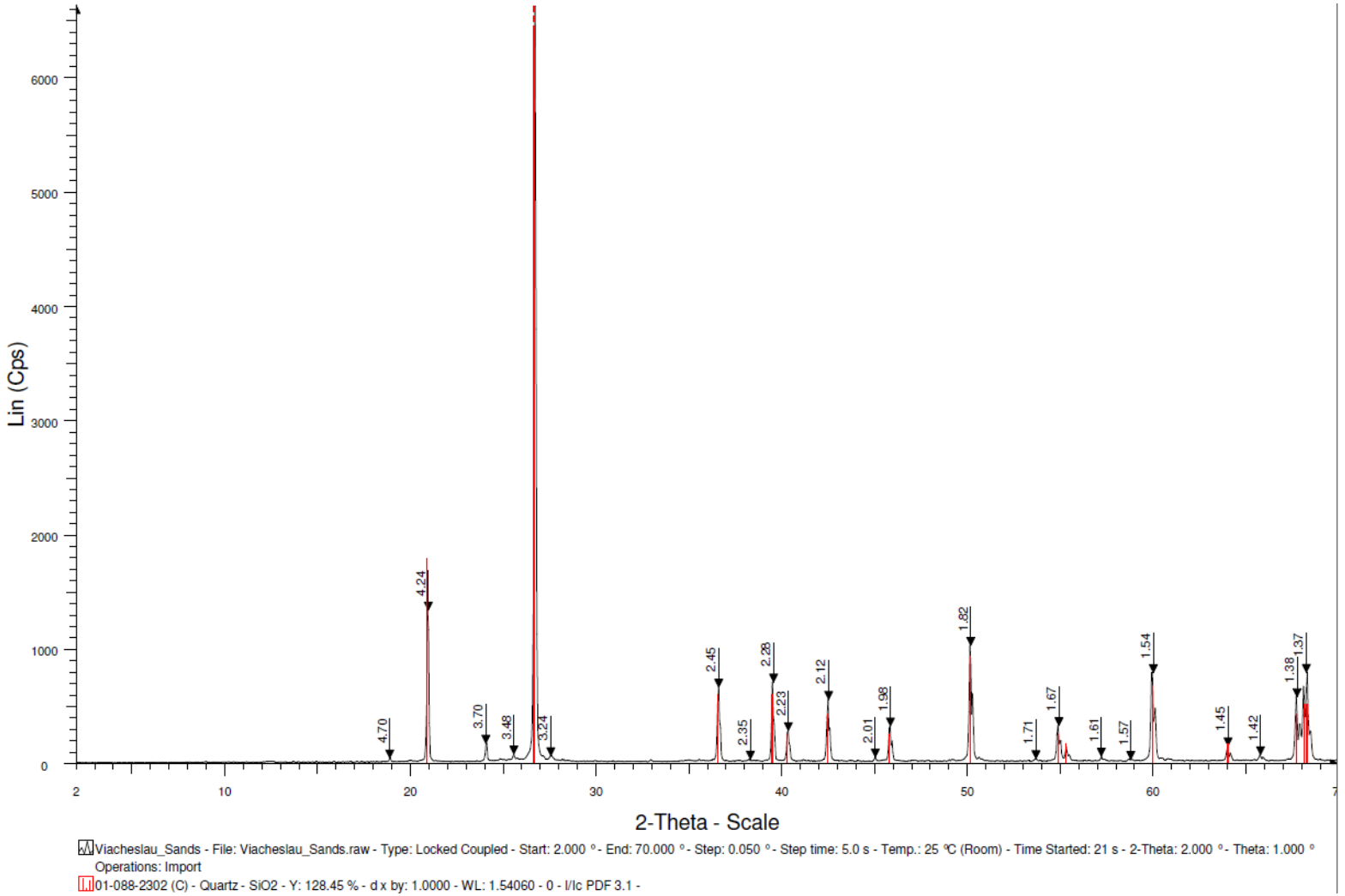

Figure 3.7 – Results of the XRD analysis for the sand fraction

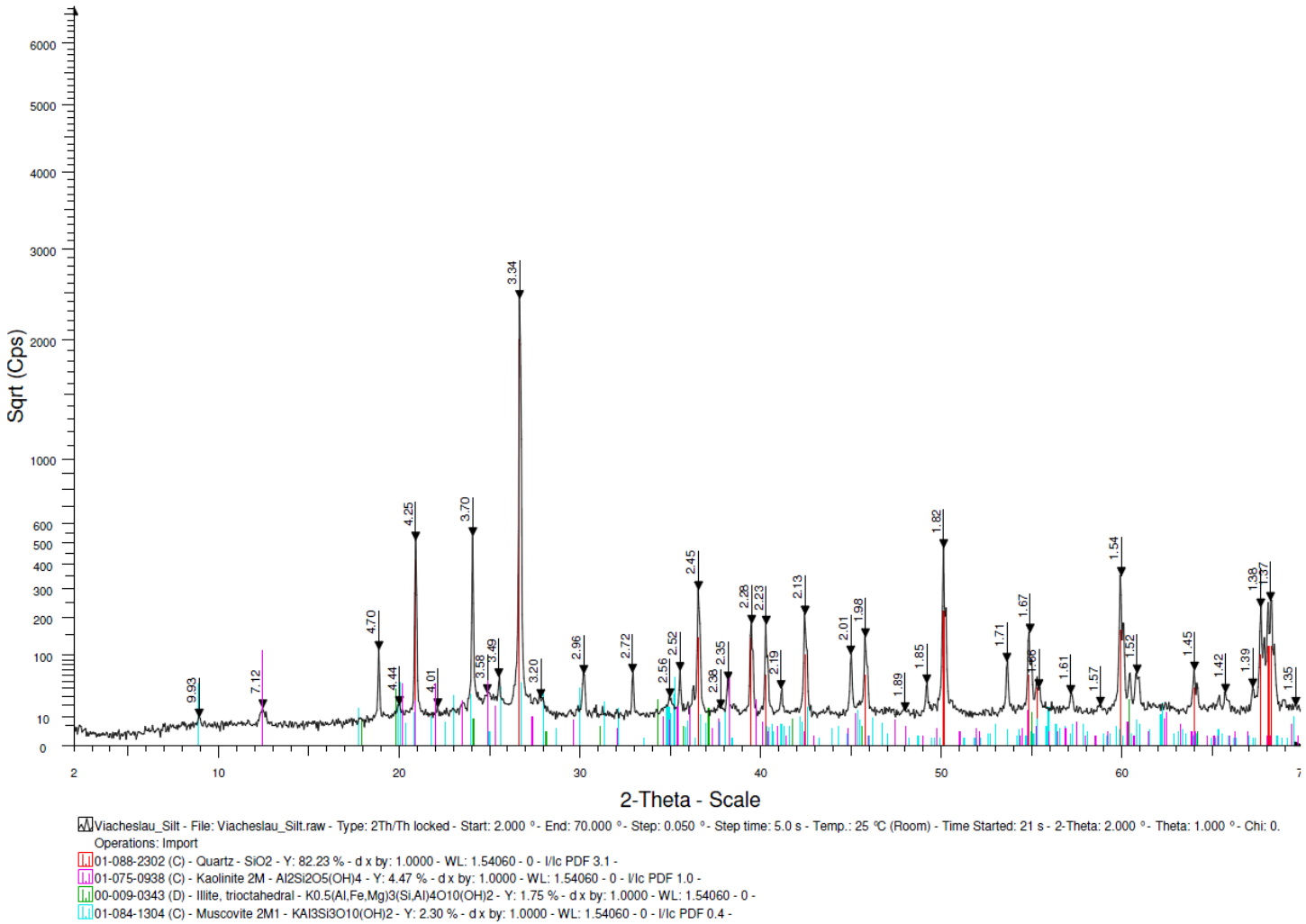

Figure 3.8 – Results of the XRD analysis for the silt fraction

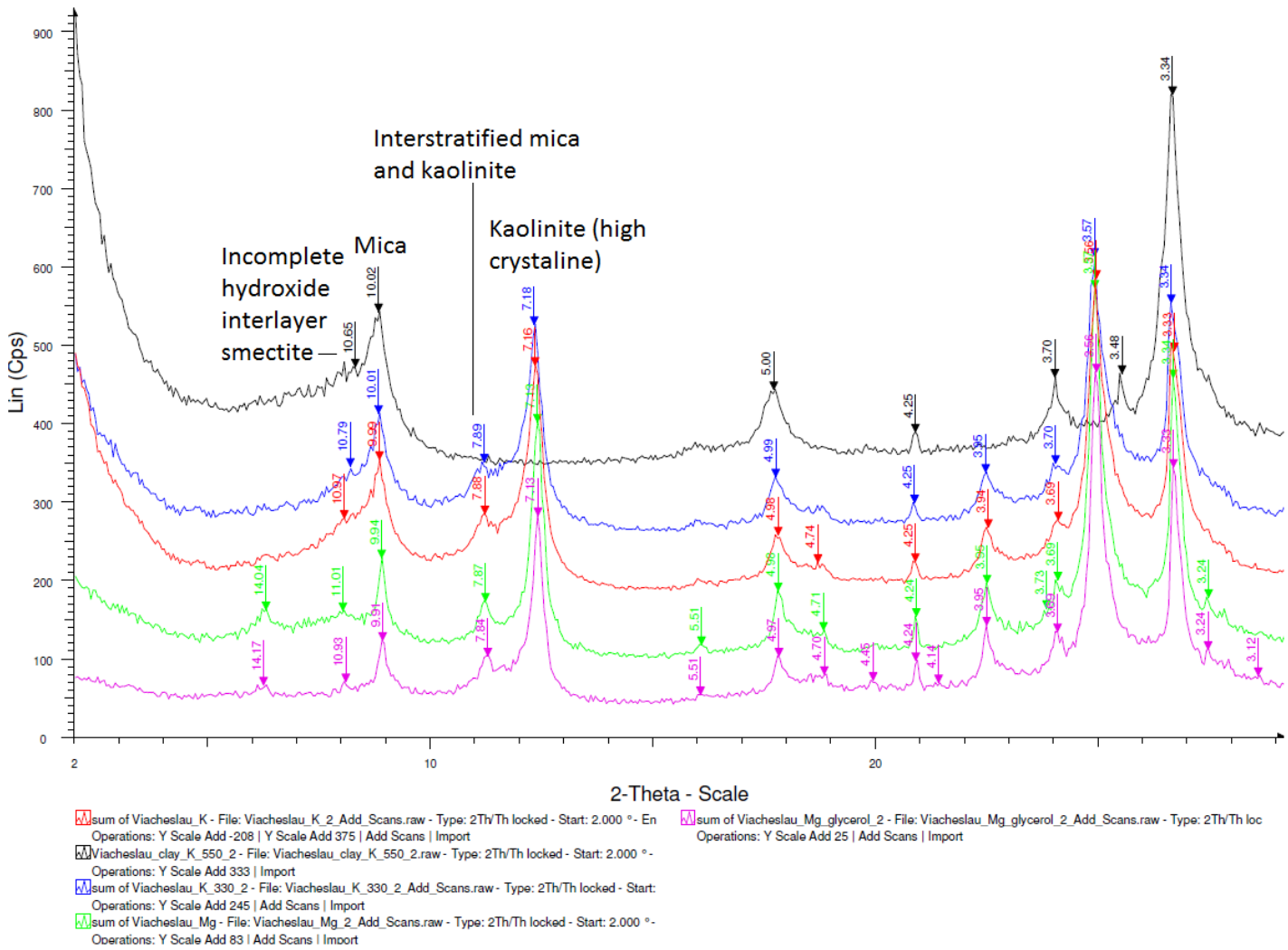

Figure 3.9 – Results of the XRD analysis for the clay fraction

3.2.4 FTIR results analysis

A Fourier Transform Infrared Spectroscopy (FTIR) analysis was done on bulk and clay samples (**Figures 3.10 – 3.12**). This technique usually helps to check and confirm the results of XRD.

First, FTIR was done for a bulk sample. A high wavenumbers analysis (Figure 3.11) doesn't give a lot of information about the common minerals. However, Figure 3.10 is more useful for such purposes. Wavenumbers 3696, 3649, and 3620 cm^{-1} (OH bond) identify kaolinite which is in good agreement with the XRD results. 756 cm^{-1} and 827 cm^{-1} are probable numbers for muscovite which was definitely identified during the XRD analysis. There are some peaks around 780-800 cm^{-1} which can be a sign of quartz (Si-O bond). 2922, 2952, and 2853 cm^{-1} are most probably a sign of organic materials.

Next, the analysis of the clay fraction was conducted. Results are shown in Figure 3.12. These results are supporting the previous conclusion from XRD analysis. Wavenumbers 3698, 3648, and 3621 cm^{-1} present kaolinite. 1162, 799, 697, 536, and 470 cm^{-1} are signs of quartz. Muscovite was expected to be found, and 1032, 753, 536, and 436 cm^{-1} proved these expectations. It should be noted that it is very hard to remove all organic material from the sample because even after treatments, 2953, 2925, and 2854 cm^{-1} were identified.

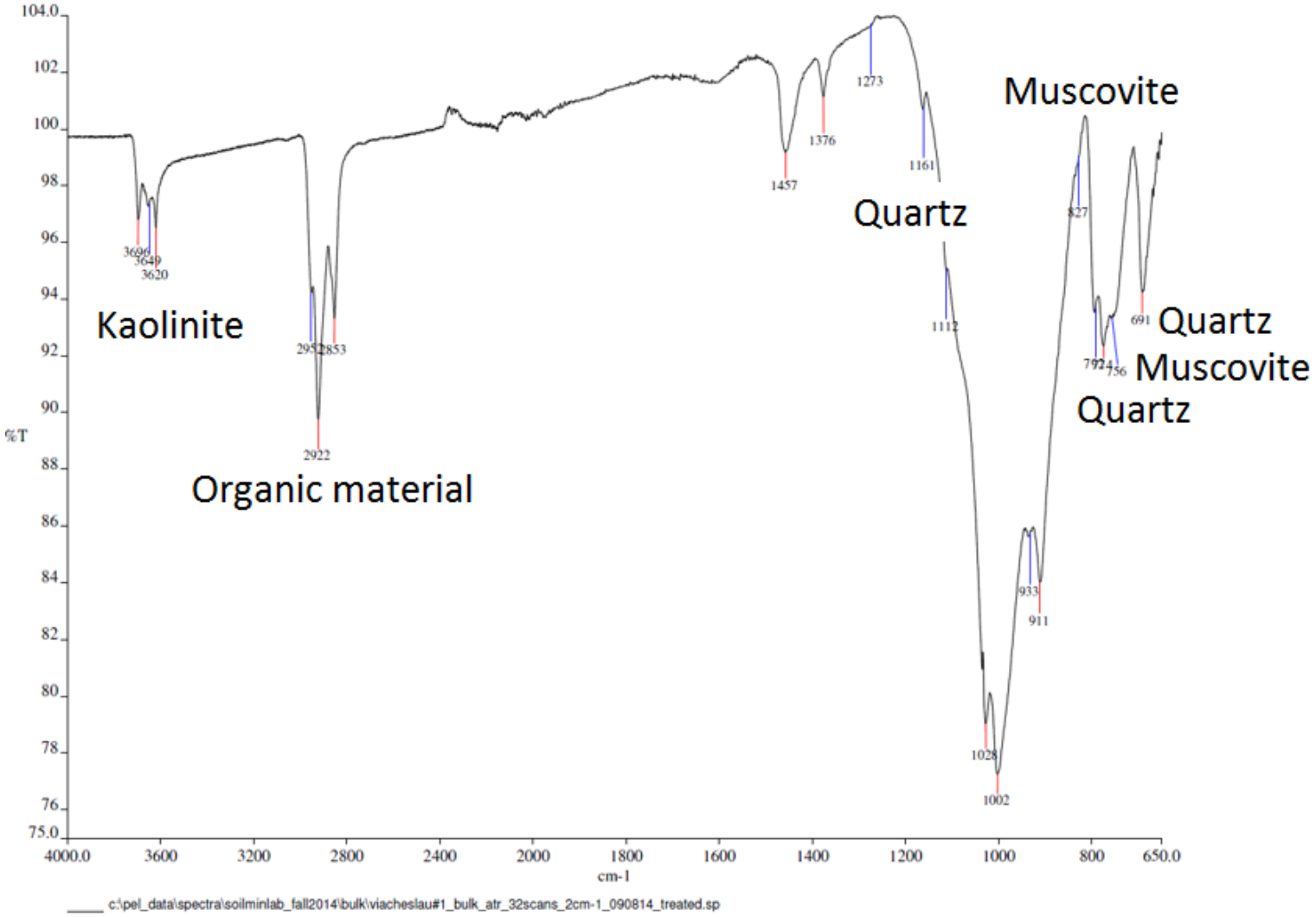

Figure 3.10 – Results of the FTIR analysis for the bulk sample

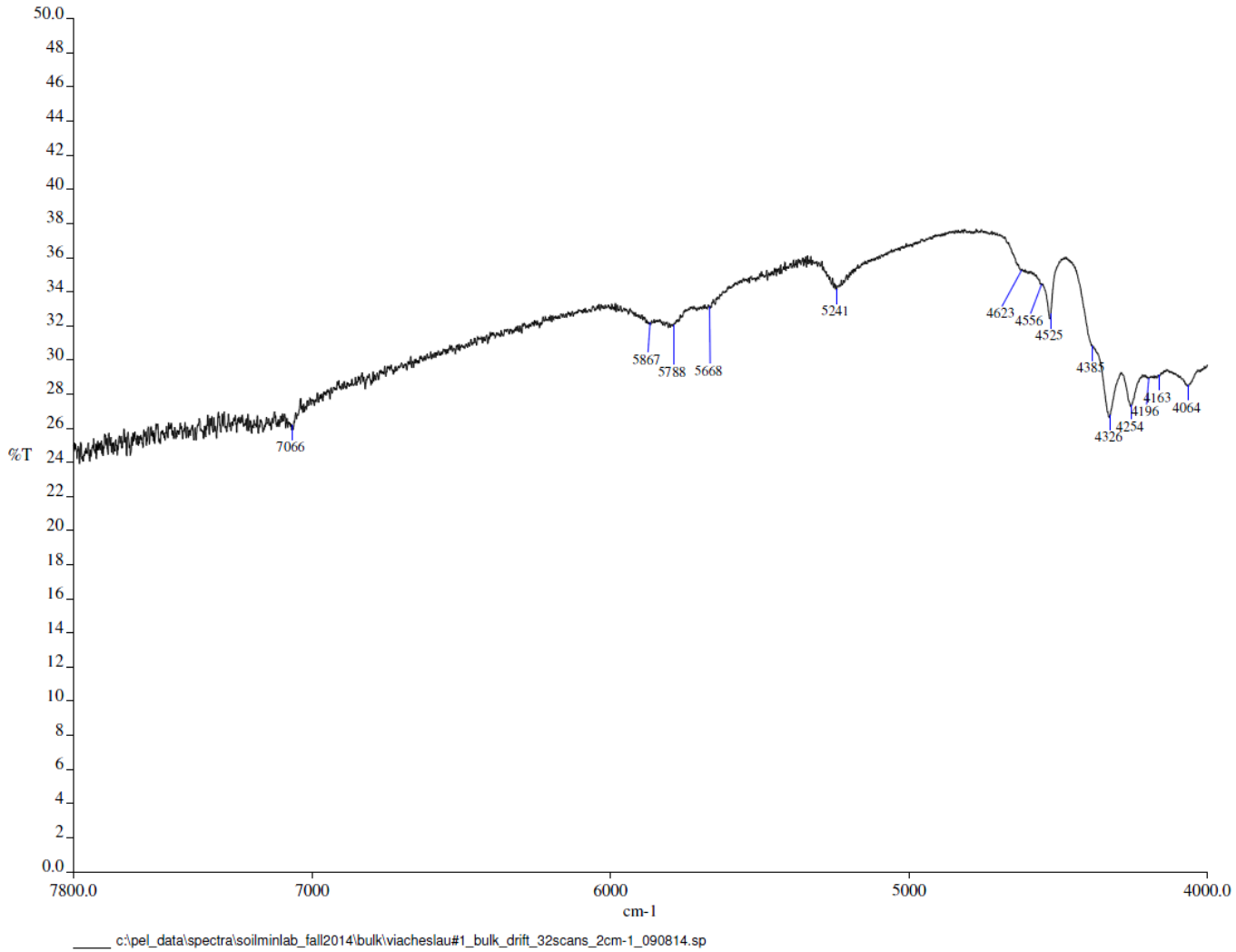

Figure 3.11 – Results of the FTIR analysis (high wavelengths) for the bulk sample

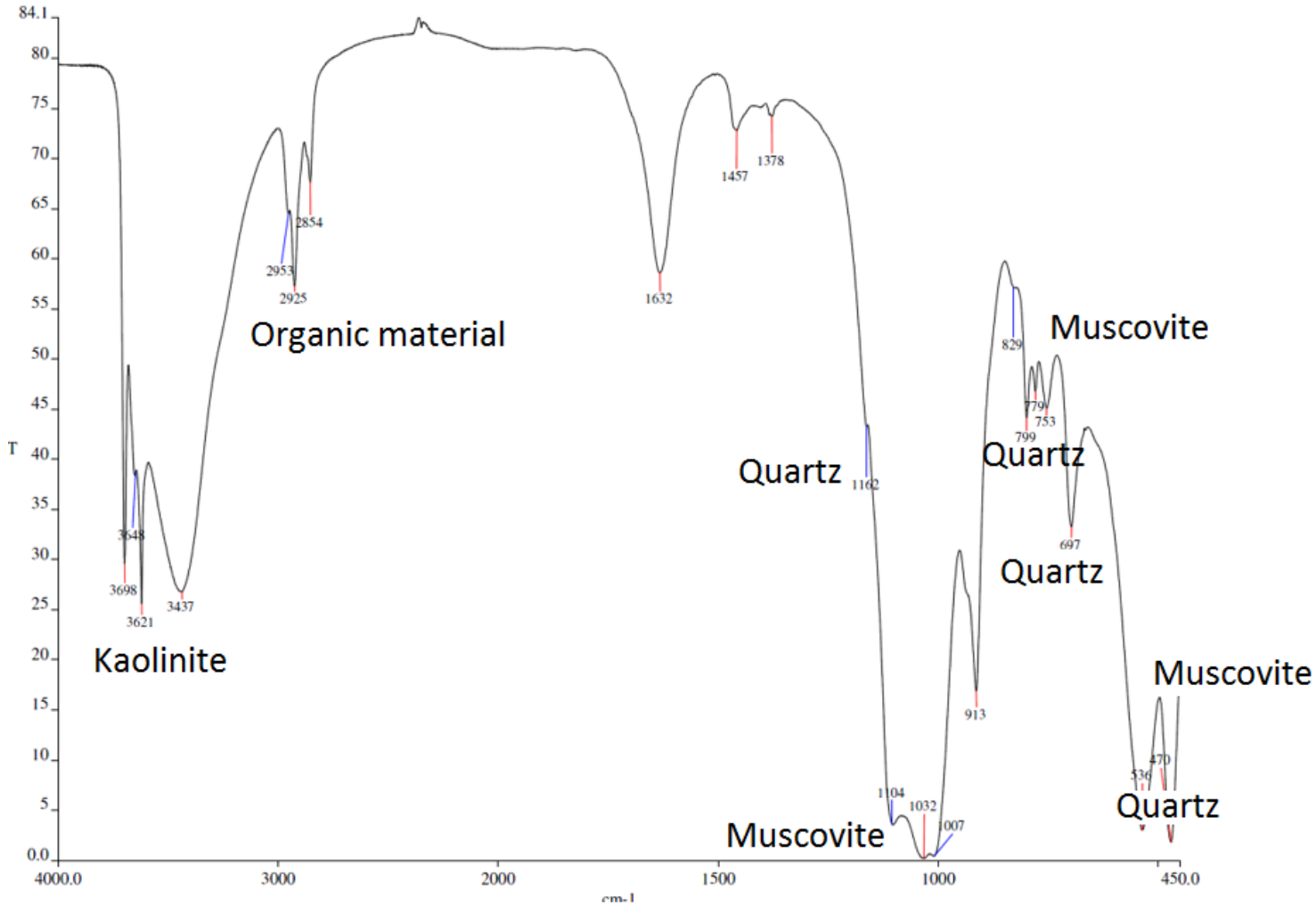

Figure 3.12 – Results of the FTIR analysis for the clay fraction

3.2.5 Iron oxides results analysis

The results of the iron oxides determination are summarized in **Table 3.7** and include weight measurements and atomic absorbance spectroscopic analysis results.

Table 3.7: Quantification of free iron oxides

	Sample-1	Sample-2	Standard 1	Standard 2
Air dry weight (g)	2.4246	2.4207	0.1009	0.1017
Fe in diluted solution (ppm)	0.1395	0.1078	0.9633	0.9949
Total Fe (g)	0.0014	0.0011	0.0096	0.0099
% Fe in soil	0.0575	0.0445	9.5466	9.7831
% Fe_2O_3 in soil	0.0823	0.0637	13.6517	13.9898
Average %	0.0730		13.8208	

Calculations were performed using the following equations and conversions (Deng et al. 2009):

$$ppm = mg/l \quad \ldots\ldots(3.3)$$

$$\text{Total Fe (g)} = \text{Fe (ppm)}/100 \quad \ldots\ldots(3.4)$$

$$\%Fe = \text{Total Fe (g)}/\text{Sample wt. (g)} * 100\% \quad \ldots\ldots(3.5)$$

$$\%Fe_2O_3 = 1.43 * \%Fe \quad \ldots\ldots(3.6)$$

3.2.6 CEC results analysis

The CEC of the clay fraction is given in the **Table 3.8**.

Table 3.8: Cation Exchange Capacity results

	Sample 1	Sample 2	Standard 1	Standard 2
W1 (g): Centrifuge tube	12.9945	12.9862	12.9077	12.9227
W2 (g) (for dry sample only)	13.2982	13.2909	13.0073	13.0225
W3 (g): tube + clay + interstitial $CaCl_2$	13.6184	13.5908	13.3611	13.3962
W4 (g) tube + dry clay	13.0870	13.0768	12.9954	13.0098
Ca_S (ppm)	0.4590	0.4290	3.1210	3.2100
Ca_I (ppm)			200.796	
Calculations results				
A	0.2295	0.2145	1.5605	1.6050
B	0.0643	0.0602	0.0710	0.0750
CEC	8.9122	8.4974	84.7483	87.6526
Average CEC	8.7048		86.2005	

Where Ca_I = ppm of Ca in 0.005 M $CaCl_2$ and Ca_S = ppm of Ca in supernatant from the sample.

Formulas used for these calculations are shown below (Deng et al. 2009):

$$A = Ca_S * (1 \text{ mg Ca} / 1000 \text{ mL}) * (500 \text{ mL}) = Ca_S / 2 \quad \ldots\ldots\ldots\ldots\ldots\ldots (3.4)$$

Where A = weight of exchangeable and interstitial Ca in mg.

$$B = Ca_I * (1\ mg\ Ca / 1000\ mL) * (W3 - W2) * (1\ mL / 1\ g\ H_2O) \quad \ldots\ldots\ldots (3.5)$$

Where B = weight of interstitial Ca in mg, (W3 – W2) is the weight of the interstitial solution in grams.

$$CEC = (A\text{-}B)mg / [(200.4\ mg/cmol) \times OD] \times (1000\ g / 1\ kg) \quad \ldots\ldots\ldots\ldots (3.6)$$

Where CEC = Cation Exchange Capacity in cmol/kg, 200.4 mg is the equivalent weight of 1 cmol Ca, and OD is (W4 – W1).

3.2.7 SEM results analysis

A scanning electron microscopy analysis was performed under the guidance of Dr. Deng to produce micrographs and an elemental analysis of selected silt particles present in the sample. The results indicate similar findings to that of the XRD.

In **Figure 3.13**, a particle of k-feldspar is shown. Two points were analyzed by EDS and both of them have approximately 1:1:3 Al:K:Si ratio. This particle most probably is microcline. **Figure 3.14** shows two different shaped particles. The quartz particle has a more flat surface, and the particle is round. EDS confirmed this idea and showed silicon oxide. The second particle has K and Al peaks which are about 0.3 times as intense as Si. Most probably, this is microcline. A small amount of Na can be a substitution, so it is also could be sanidine. It should be stated that quartz is the most abundant mineral. This is proved by **Figure 3.15** in which several different shapes of quartz particles could be observed. Some of them are subangular. Some are angular, but all of them are silicon oxides. **Figure 3.16** presents some particles with a platy morphology. Some of them have an Al peak almost equal to Si with a small amount of K. These particles are kaolinite with possible interstratified micas. Some particles have

the same morphology but include more K, so they are muscovite particles. In a backscatter image of **Figure 3.17**, some particles are brighter than the other ones. This means they have a higher density. EDS shows that these are – zircon ($ZrSiO_4$) and rutile (TiO_2). Zircon is a very stable mineral. Rutile has the same EDS pattern as anatase, but, based on prismatic morphology of the particle, it is most probably rutile. Rutile morphology is shown better in **Figure 3.19**. Other minerals here are muscovite with a platy morphology and relatively high K content and quartz. In **Figure 3.18**, some interesting results are shown. There are some very rare elements: Nd, La, and Ce. Along with phosphorus, they show that this is a phosphate mineral (La, Ce, Nd) PO_4 - Monazite-(La). This result explained what could be a source of phosphorus in the flowback samples which will be described in the next chapter. **Figure 3.19** shows a prismatic morphology of the rutile particle, platy shaped and worm-like shaped kaolinite morphology, and big platy muscovite particle. It is interesting to conclude that most of the time, mica and kaolinite were stuck together and were sharing K. This fact is additional prove of the random interstratification of these two minerals. It is also interesting to note that some feldspars are also present in the sample. It is difficult sometimes to differentiate feldspar and mica particles by EDS results only because both of them can contain K, but morphology gives additional details to make a conclusion. For this case, platy morphology is common for muscovite, while a rough surface is more common for weathering based feldspars. Very interesting worm-like morphology was observed for one kaolinite particle (**Figure 3.20**). This particle has a size of only a few micrometers.

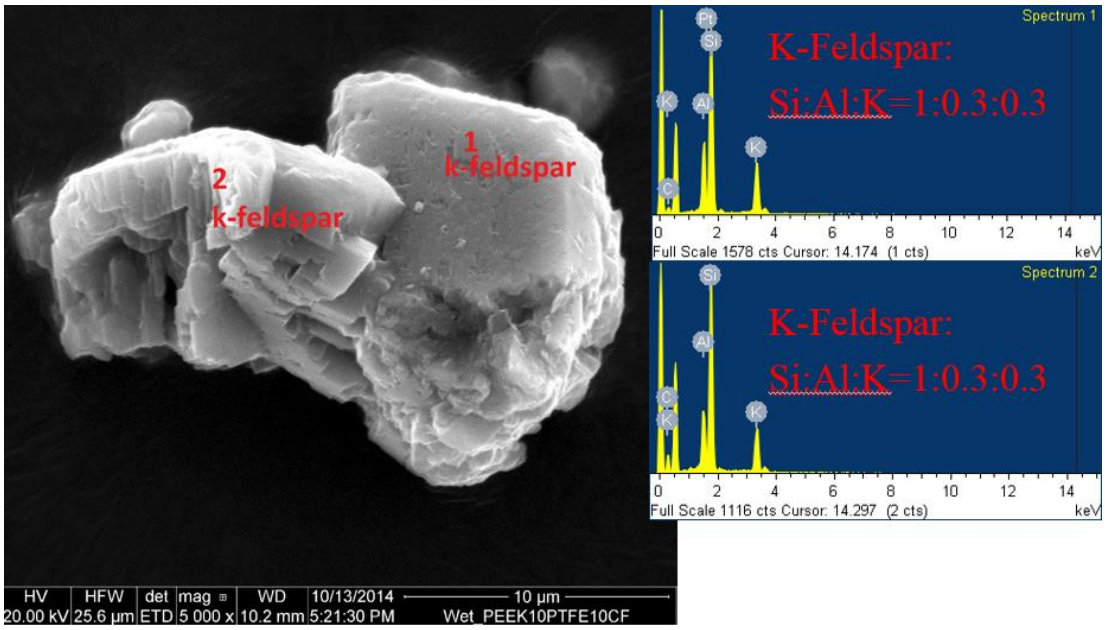

Figure 3.13 – K-Feldspar particle and EDS spectra

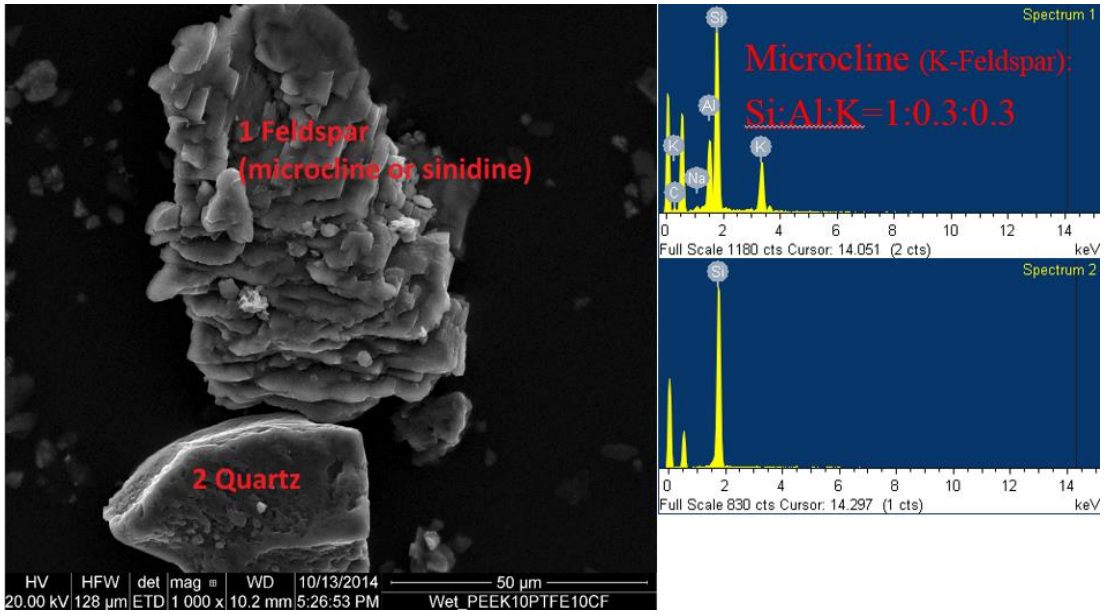

Figure 3.14 – Feldspar and quartz particles with EDS spectra

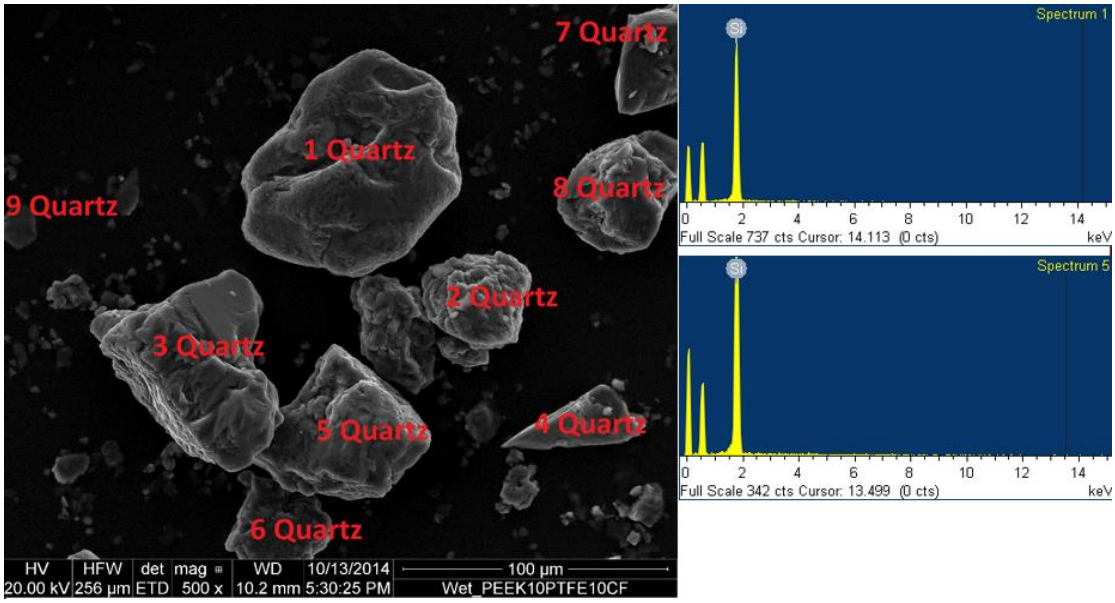

Figure 3.15 – Quartz particles and some of the EDS spectra

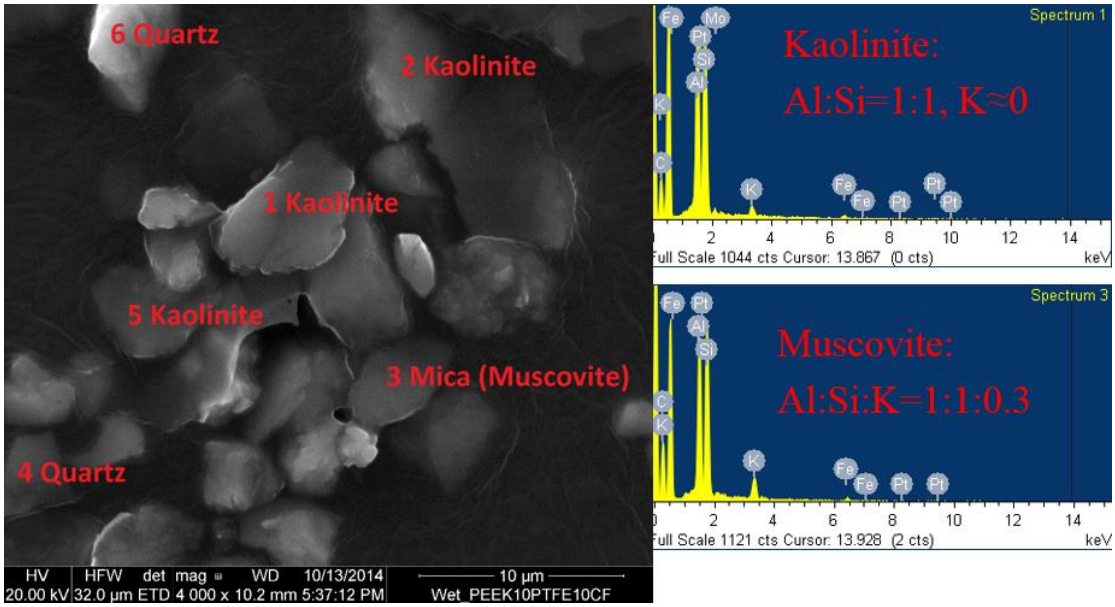

Figure 3.16 – Kaolinite and quartz particles and some of the EDS spectra

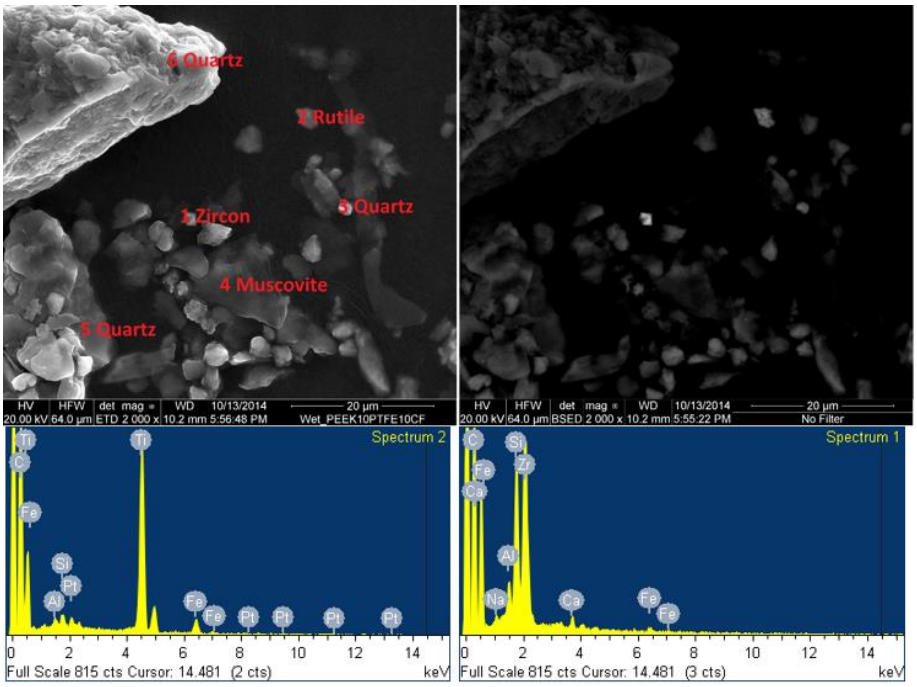

Figure 3.17 – Zircon, rutile, and quartz particles with backscatter image and EDS

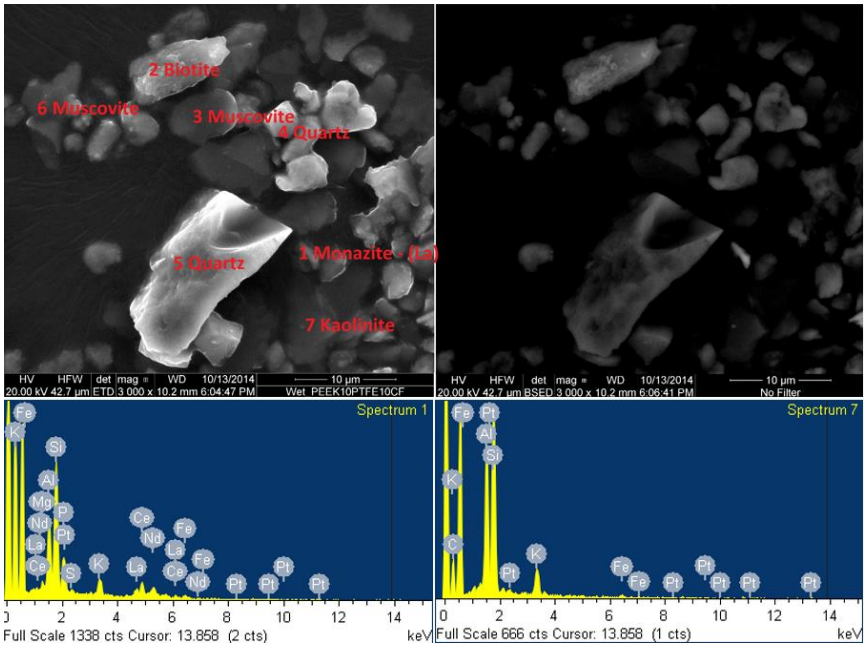

Figure 3.18 – Monazite-(La) and others with backscatter image and EDS

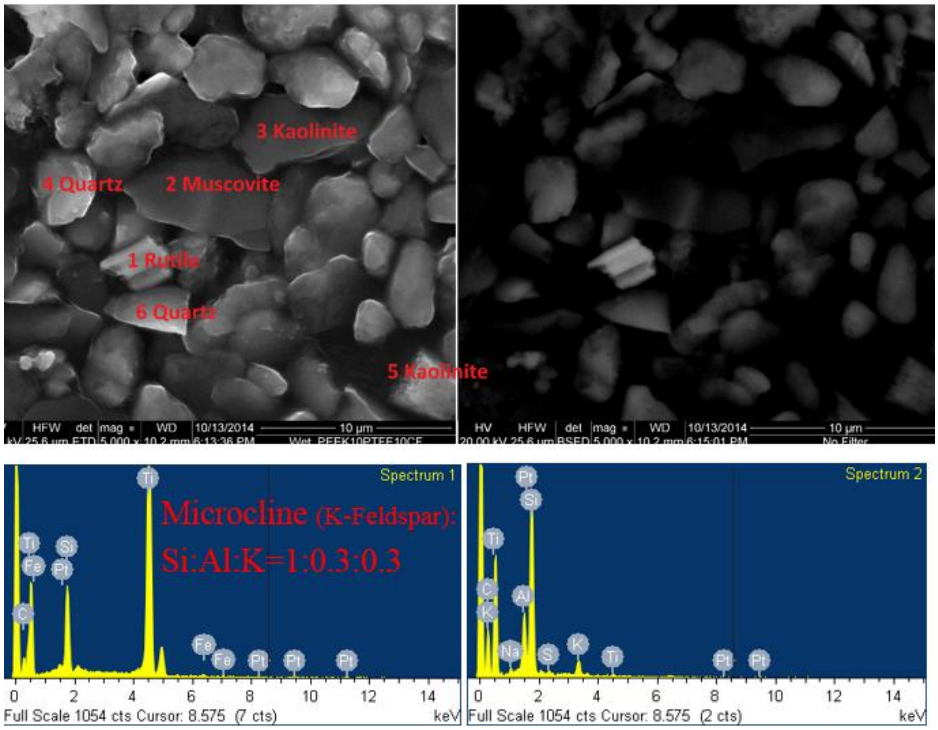

Figure 3.19 – Rutile, kaolinite, and others with backscatter image and EDS

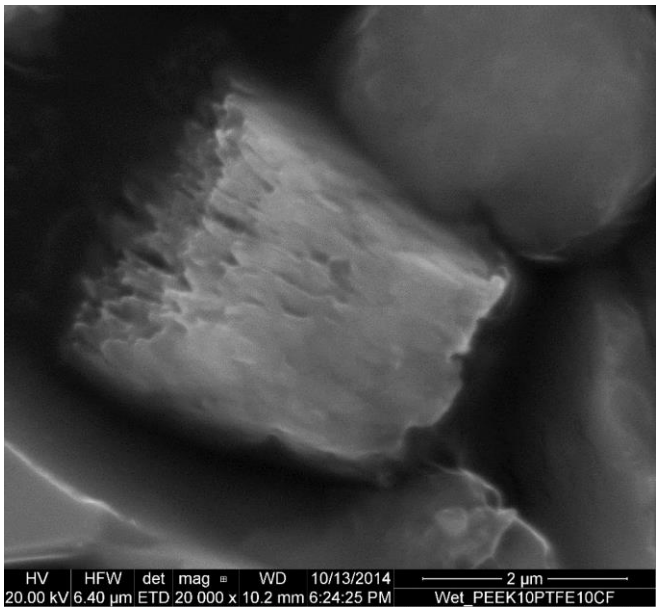

Figure 3.20 – Enlarged worm-like kaolinite particle

3.2.8 TEM results analysis

The analysis of the clay sample using the transmission electron microscope provides a great opportunity to observe the tiniest layers of the smallest particles. These results confirmed previous observations that muscovite, kaolinite, and ilmenite are present in the clay fraction of the sample. The frame with a mica particles and EDS results is shown in **Figure 3.21**.

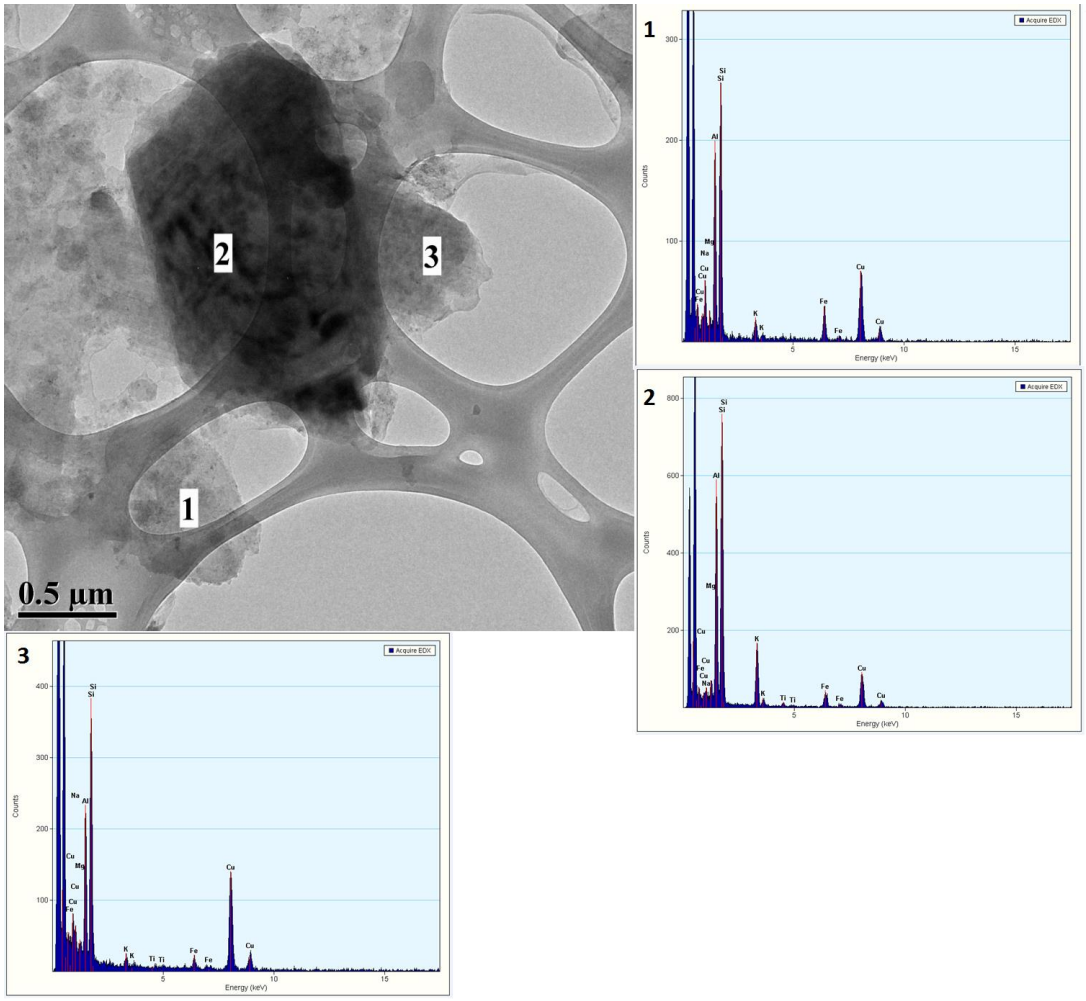

Figure 3.21 – Mica particles and EDS results for each location

Figure 3.21 consists of a pattern of light and dark areas corresponding to different amount of mica layers. The term “transmission” implies that the image is produced by electrons passing through the sample which means that light areas in the image correspond to not very electron dense regions. This means that the dark region consists of more layers of mica than those of the light layers in **Figure 3.21**.

In **Figure 3.22**, different minerals are shown. Titanium oxide is ilmenite based on the ratio of Ti:Fe. A few kaolinite particles were also identified there. A small amount of K was identified by EDS, but this amount is smaller than 0.3 out of the Al or Si peak as in muscovite.

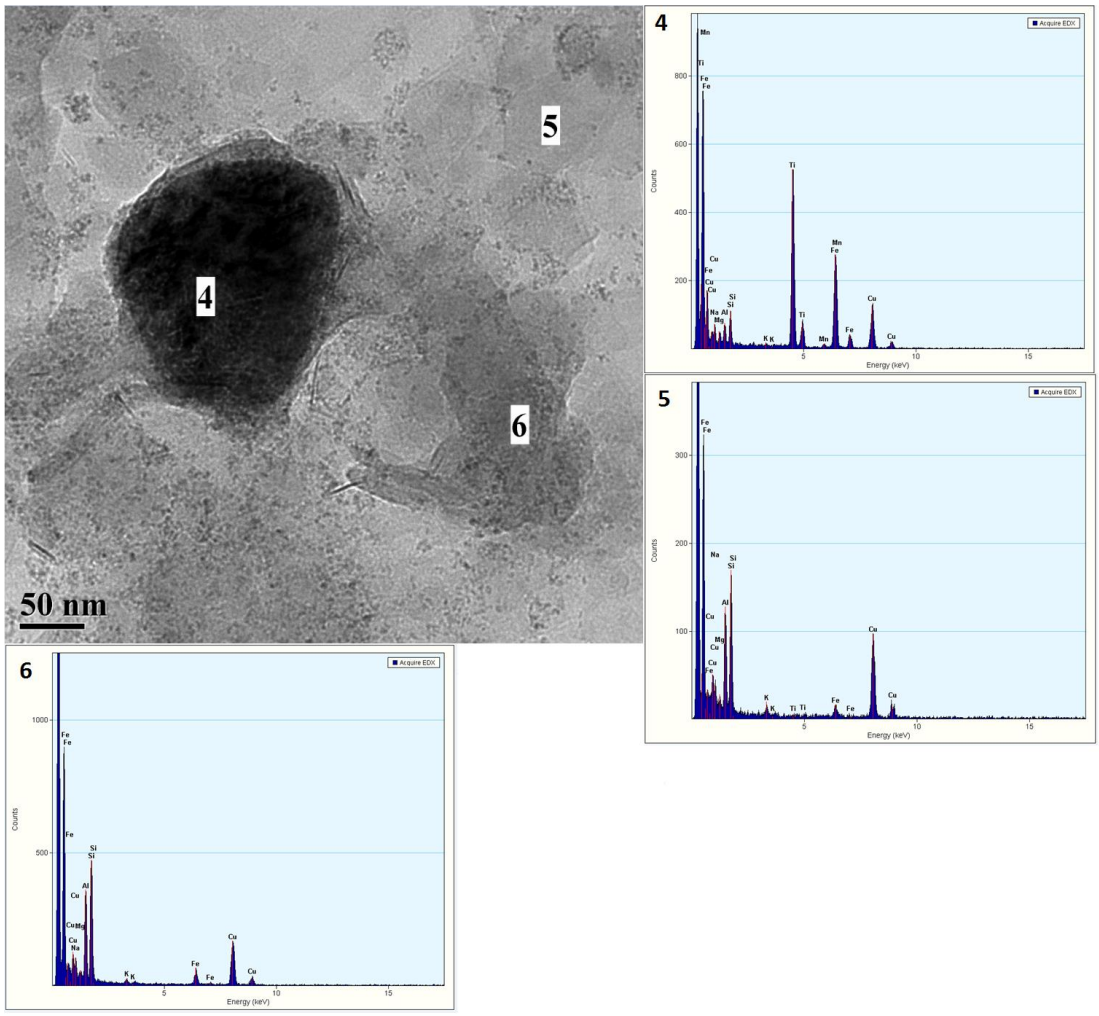

Figure 3.22 – Ilmenite and kaolinite particles and EDS results for each location

Figure 3.23 shows a phyllosilicate particle with small amount of K. Based on morphology, this particle is kaolinite even though the Al:Si ratio is not equal to 1.

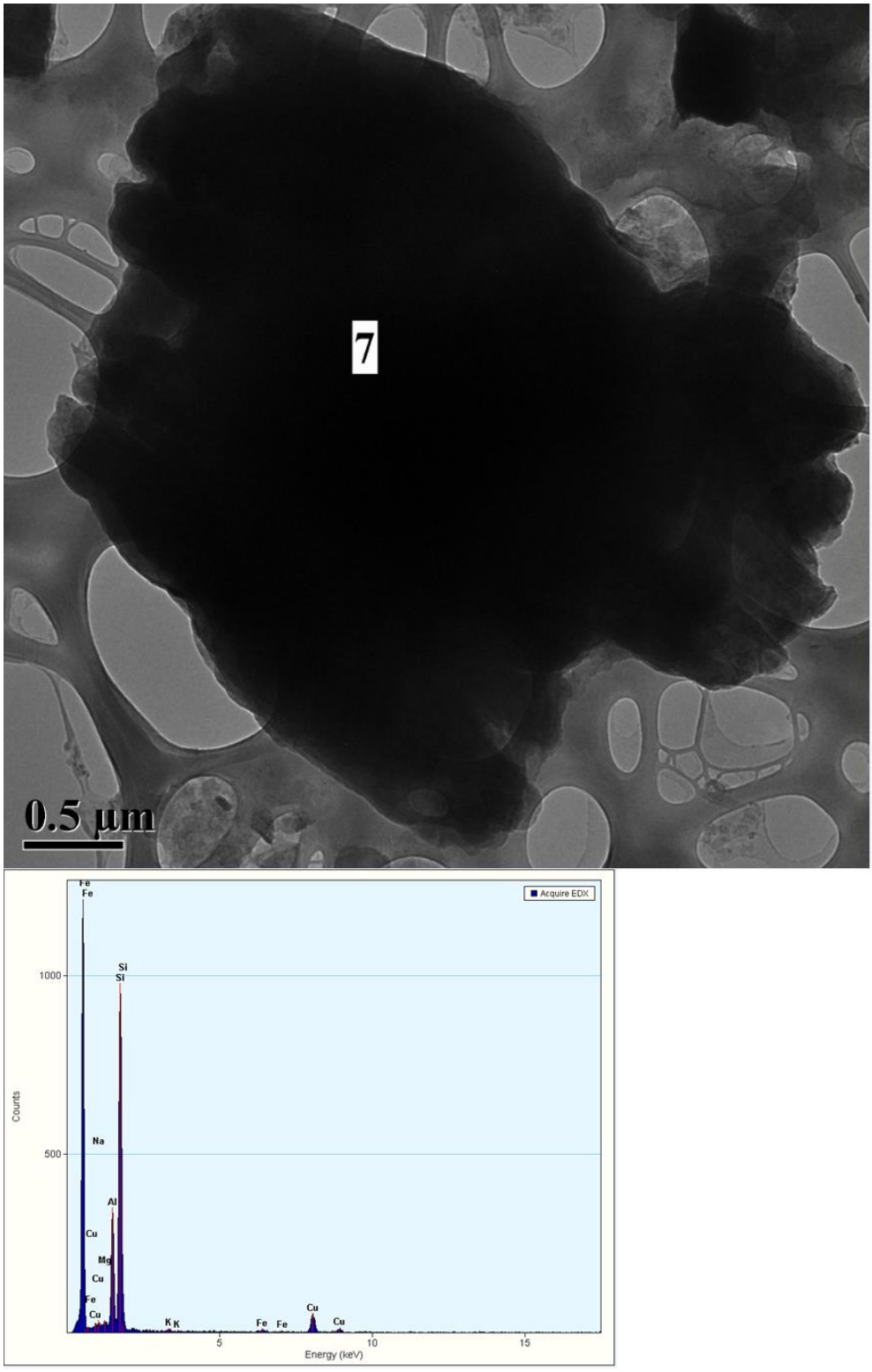

Figure 3.23 – Kaolinite particle

In **Figure 3.24**, a particle of kaolinite aggregate is shown. Because of the electron beam energy on the right part of the picture, some changes in the layers could be observed. Most probably, these changes are result of dehydration of the kaolinite.

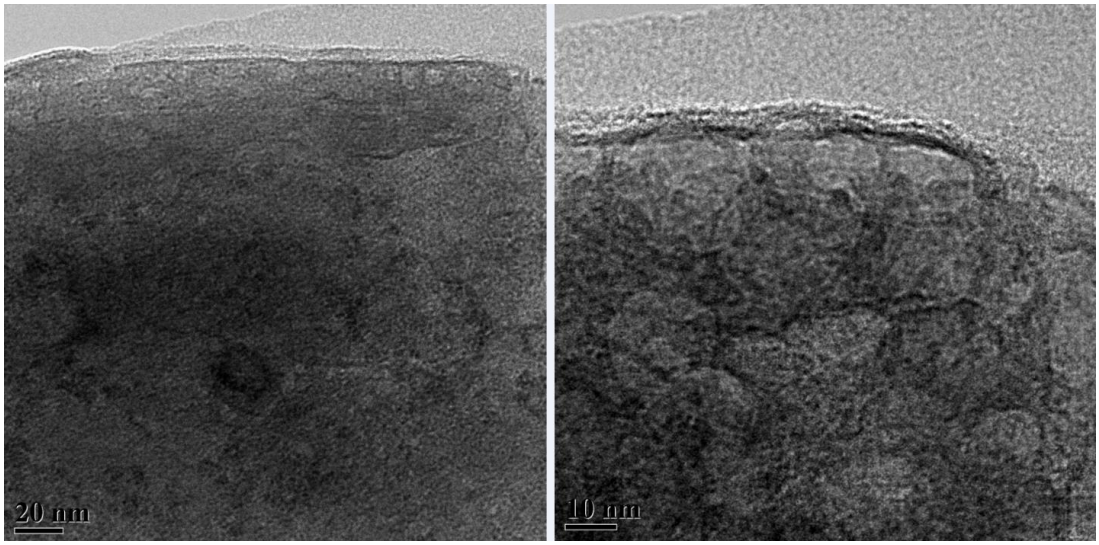

Figure 3.24 – Dehydration of the kaolinite particle

An interesting result is shown in **Figure 3.25**. Based on EDS, the Al peak is almost equal in height to the Si peak, and no significant K is there which is an indicator of the kaolinite particle. A high diversity of the layered materials in the top part of the micrograph can be also observed. Also, unclear lattice fringes could be observed in the top right part of the dense dark area.

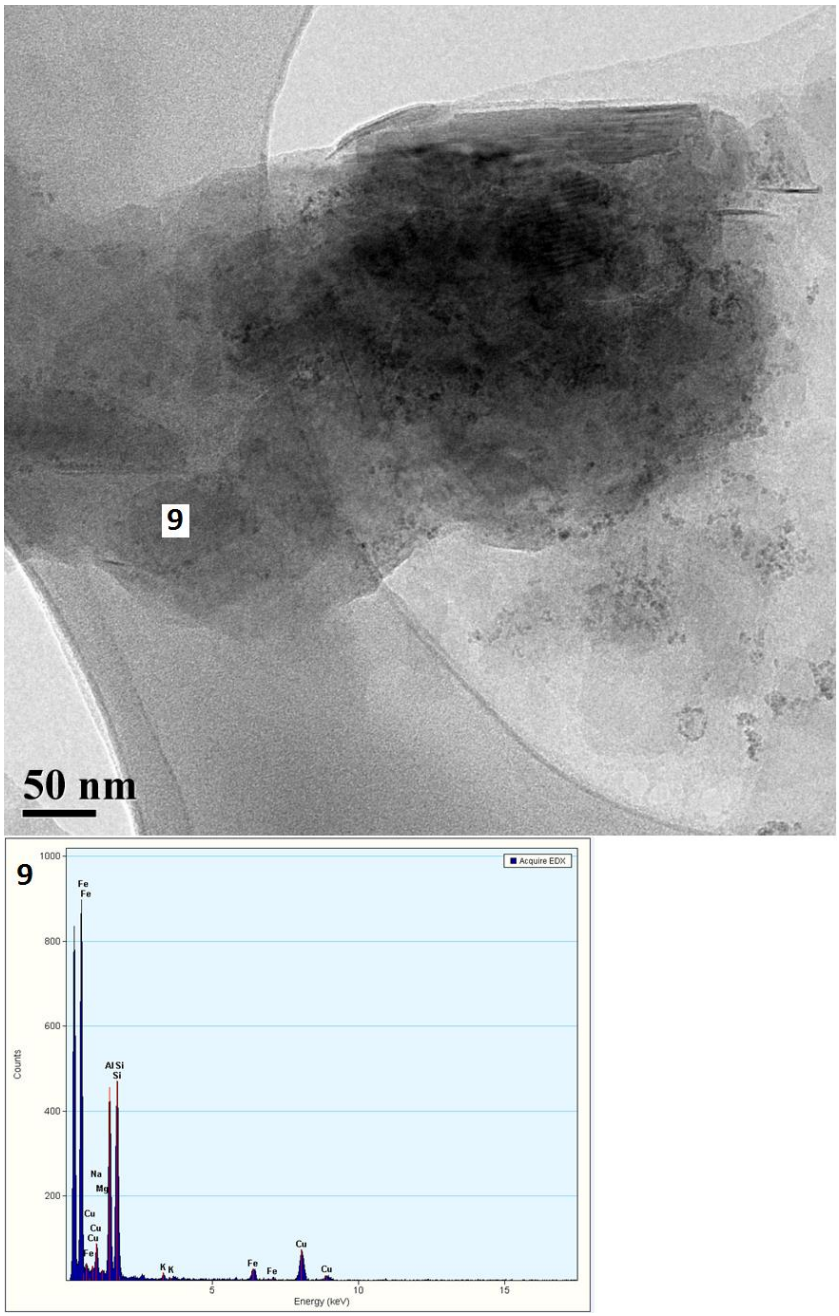

Figure 3.25 – Layered kaolinite particles with EDS results

Selected area electron diffraction (SAED) images were also analyzed for each particle. **Figure 3.26** shows a SAED image for location 1 from **Figure 3.21**. This picture identifies a crystalline material of both single crystal (symmetrical lines) and multiple crystals (radial symmetry) (**Figure 3.26**).

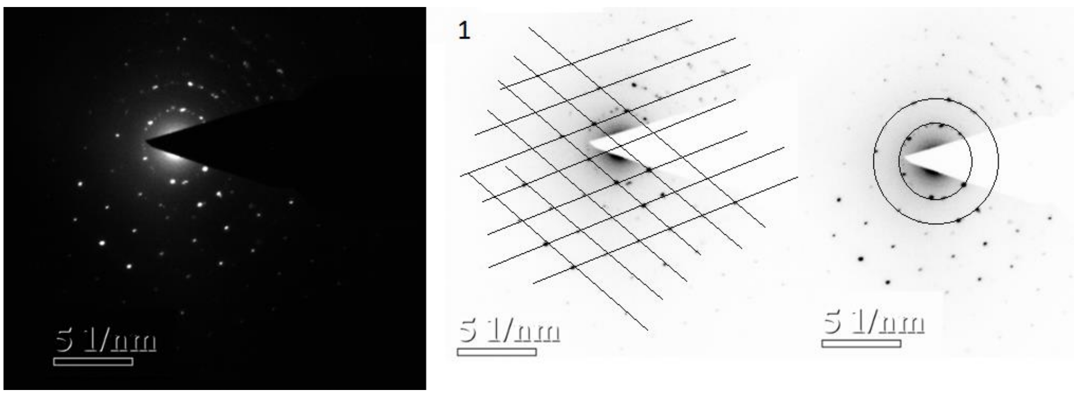

Figure 3.26 – SAED picture for the particle from location 1

It is interesting to note that SAED images could be also used for the determination of the d-spacings of the mineral. This could serve as an additional tool to double check the EDS results and morohology pictures. The identification of r_x for the same particle from spot 1 is shown in **Figure 3.27**. Not all points are marked in the figure since some of them are symmetrical relative to the center. The formula used for calculations of d-spasing (d_x) is shown below:

$$d_x = (r_s/r_x) * d_s \qquad (3.7)$$

Where $1/d_s = 5nm^{-1}$ (magnification of the **Figure 3.27**), d_s=0.2 nm, and the real size of the line is r_s = 28.5 mm.

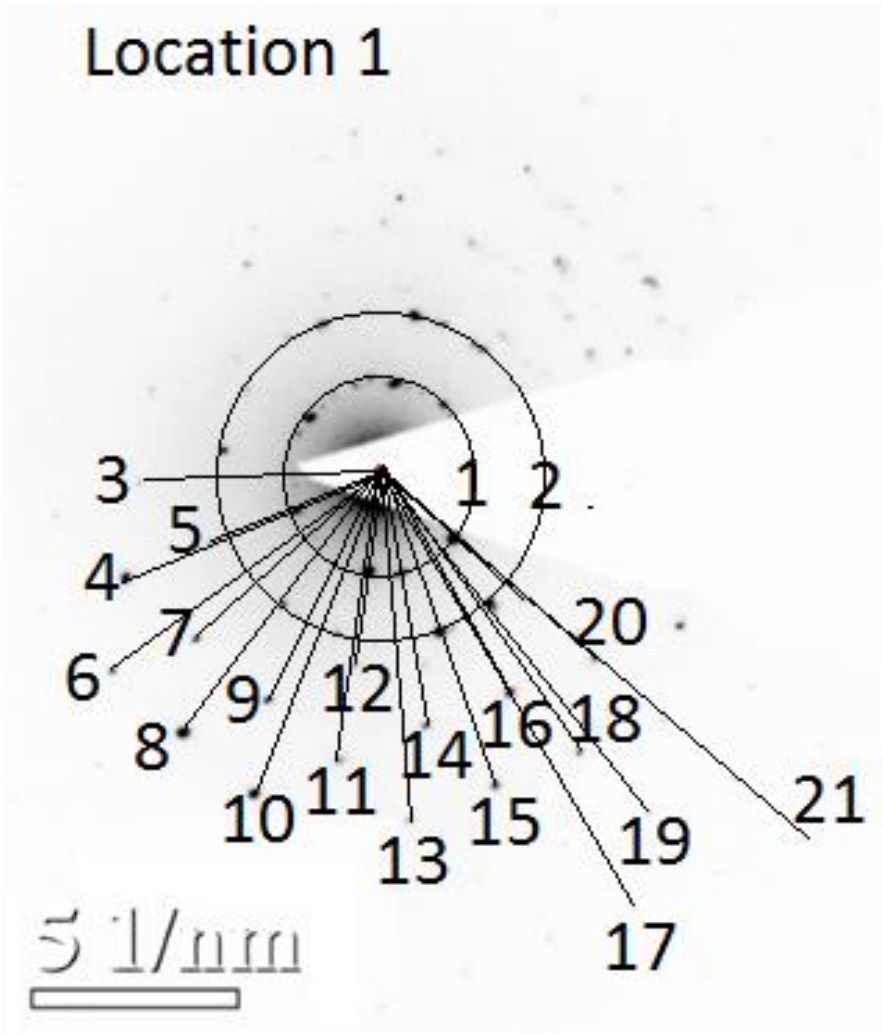

Figure 3.27 – Measurements of the r_x for the first spot

Table 3.9 presents the results of the calculations. This particle presents one of the micas based on the determined d-spacing and previously obtained EDS data.

Table 3.9: Calculations of d-spacing for the first spot

Point	Radius rx (mm)	dx (nm)	dx (Å)
1	12	0.475	4.75
2	22	0.259	2.59
3	33	0.173	1.73
4	38	0.150	1.5
5	25.5	0.224	2.24
6	46	0.124	1.24
7	34.5	0.165	1.65
8	45.5	0.125	1.25
9	35.5	0.161	1.61
10	43	0.133	1.33
11	40	0.143	1.43
12	27	0.211	2.11
13	48	0.119	1.19
14	36	0.158	1.58
15	46	0.124	1.24
16	35	0.163	1.63
17	69	0.083	0.83
18	47	0.121	1.21
19	59.5	0.096	0.96
20	39	0.146	1.46
21	77	0.074	0.74

3.2.9 Total K determination results analysis

The XRD peaks of orthoclase, sanidine, and microcline were compared with the XRD results for the clay fraction. The XRD data of clay fraction doesn't indicate the presence of k-feldspars in the clay fraction. TEM and EDS results for the clay fraction were also checked. They also didn't indicate k-feldspars. This means that mica content could be calculated directly using the following equations (Deng et al. 2009):

$$\text{Total solution K (mg)} = \text{ppm K}/2 \quad \ldots\ldots\ldots\ldots\ldots\ldots\ldots\ldots\ldots\ldots (3.8)$$

$$\%K = (\text{Solution K}/\text{ Sample Wt}) * 100\% \quad \ldots\ldots\ldots\ldots\ldots\ldots\ldots\ldots\ldots\ldots (3.9)$$

$$\%Mica = 12.046 * Total\ K\% \quad \ldots\ldots\ldots\ldots\ldots\ldots\ldots\ldots\ldots\ldots (3.10)$$

Table 3.10 presents results of the measurements and calculations for mica evaluations. It should be mentioned that the average percentage of mica in the sample is almost two times lower than those in standards. This could be explained by fact that the dominant mineral in the clay fraction of the oil sand sample was determined to be kaolinite.

Table 3.10: Total K and mica content evaluation

	Sample 1	Sample 2	Standard 1	Standard 2
Sample weight Wt (mg)	60.200	60.000	61.000	60.000
K (ppm) in solution	2.484	2.496	5.469	5.354
Total K (mg) in digestion solution	1.242	1.248	2.735	2.677
%K in sample	2.063	2.080	4.483	4.462
%Mica in sample	24.852	25.056	54.000	53.745
Average %Mica	24.954		53.872	

3.3 Conclusions

The oil sand sample was preliminary analyzed and separated for sand, silt, and clay fractions. A significant amount of the sample was determined to be an organic material which was removed during the preparation stage of the analysis.

XRD results for the bulk sample showed that the main component is quartz which is an expectable result for the sandstone reservoir. However, the main interest

presents minerals which serve as a cementing material of the rock. Particles of these minerals could be very small in size, and, sometimes, they are insignificant in total mineralogical content. However, detailed mineralogy of the reservoir should be always taken into consideration for acid treatment design purposes. It is a critical issue because, sometimes, a very small inclusion of minerals with unexpected cations or structures could cause insoluble precipitates which usually lead to serious formation damage.

A complex treatment approach which includes different cation saturation, solvation, and heat treatments was successfully applied during the XRD analysis. This helped to identify minerals in the clay fraction such as quartz, muscovite, kaolinite, an incomplete hydroxide interlayer smectite, and a randomly interstratified mica/kaolinite. These interlayering and interstratifications are usually explained by mineralogists as a result of weathering processes. It could be suggested that steam interactions with reservoir fluids and rocks play a significant role in the shift of balance and cause mineral's transformations. This could be checked by an analysis of the samples from the same reservoir which wasn't treated by steam. It is very clear that cores which were previously treated by steam are much more unconsolidated in comparison with pre-steam cores (**Figure 3. 28**). This deconsolidation with time could also lead to fines migration and formation damage. The investigation of these transformations and reactions could provide some useful insights in the formulation of SAGD optimization strategies and formation damage prevention. These topics could be considered for future research. Silt fraction was mainly presented by quartz, muscovite, kaolinite, and illite. Sand fraction was determined to be almost pure quartz.

Figure 3.28 – Sandstone reservoir rock samples before and after steam injection

Basically, these results are very important in order to not damage the target zone during the acid treatment. Sandstone reservoirs are very complex. Even fresh water injected in the sandstone would cause formation damage because of the destabilization and migration of clays. Hydrochloric acid is the most popular treatment for stimulation and formation damage removal. However, it is very strong acid, and, even at low concentrations, the corrosion rates are very high, especially at 400 ˚F. Also, HCl reacts with cementing material of the sandstone and can cause sand production. Every sandstone reservoir contains clays at some amount. Illite is a very acid sensitive clay mineral, which causes formation damage. A similar effect could be caused by zeolite

minerals which have a very highly reactive area. Hydrofluoric acid could be usually used for the removal of formation damage caused by silicates or bentonite. However, HF is a weak acid and causes numerous precipitations when spent (secondary and tertiary reactions). Additionally, HF causes water insoluble precipitations when reacted with calcite and dolomite. HF reacts with clays first because of the bigger reactive area in comparison with those of silt and sand fractions. For the particular target zone, HF should not be used because of the presence of potassium ions from the muscovite ($KAl_2(AlSi_3O_{10})(OH)_2$). Hexafluorosilicic acid (from the secondary reaction) causes water insoluble precipitations while reacting with K^+. Smectite also contains ions which cause formation damage in case of reaction with HF or H_2SiF_6 (Ca^{2+}, Mg^{2+}, K^+). This means that well-known mud-acids (traditionally 12% HCl + 3% HF) could not be used in this reservoir mainly because of corrosion issues and threat of formation damage. However, organic mud acid or chelating agent could be considered for the treatment of the well.

A FTIR analysis was conducted after XRD. The results for a bulk sample and clay fracture provided additional proof for previously identified minerals. It could be stated that these results are in good agreement with the XRD data. Additionally, FTIR identified some organic materials which weren't fully removed during the treatment with peroxide. This once again shows how complex the interactions between organic matter and minerals are, and how hard it is to reach a full oil recovery for oil sands.

The average iron oxide content of the oil sands was calculated to be 0.08%. In comparison with the standard which has an average Fe_2O_3 content of 13.9%, it can be

stated that there is very little iron oxides present. This means that the source of iron for actual rust samples, which were analyzed in chapter 2, is not a reservoir rock, but the liners themselves.

The average CEC of the sample was measured to be 8.7 cmol/kg which is almost ten times lower in comparison with the standard that had a CEC of 86.2 cmol/kg. This result could be explained by the domination on the kaolinite in the clay fraction.

SEM and TEM with EDS analysis helped with description of the morphology and chemical composition of the sample. Both silt and clay fractions were carefully analyzed. Common SEM recognition criteria were applied. The ideas about interstratification of kaolinite and mice were supported by figures and EDS data. Overall, the most common minerals are quartz, some kaolinite, and mica. Other minerals present in limited quantities include: feldspars, muscovite, biotite, illite, monazite-La, zircon, ilmenite, and rutile.

4. GLDA TREATMENTS AND FLOWBACK SAMPLES ANALYSIS

Acidizing of sour, heavy oil, weakly consolidated sandstone formations under steam injection is a real challenge. Fines migration, sand production, inorganic scale, corrosion products, and damage due to asphaltene precipitation are some of the common concerns with these sandstone reservoirs. They cause a decline in the productivity of the wells, and there is always a need to stimulate these wells to restore their productivity. Furthermore, the complexities of sandstones require a mixture of acids and several additives, especially at temperatures up to 400°F. Seven acid treatments were performed in a different horizontal production wells.

A typical field treatment included pumping a foaming agent to have proper rheological characteristics and a better controlled pumping process, followed by the main stage of the treatments. The treatment fluids were displaced into the formation by pumping produced water and were allowed to soak for 4 or 6 hours. Then, the well was put on production, and samples of flowback fluids were collected. The concentrations of key cations were determined using ICP, and the chelate concentration of the GLDA was measured utilizing a titration method using a ferric chloride solution.

The treatments using GLDA were successful, and the well's productivity increased significantly. It is important to note that these treatments were applied in the field without encountering any operational problems. A significant gain in oil production was achieved without adversely impacting the water cut, causing sand production, clay swelling, or fines migration. The analysis of flow back samples indicated that iron was

the main cation which shows that the chelating agent mainly dissolved corrosion products.

In this chapter, the results of the field applications will be described and evaluated using results of the analysis of the flowback fluids after the treatments. Emulsion rates and pressure drawdowns will also be explained for evaluation of the feedback from production point of view.

4.1 Field Case

As they were mentioned before, seven treatments of different wells were conducted with full range of flowback analysis. In this chapter, one treatment case and followed flowback analysis will be described in details.

4.1.1 Field case description

A SAGD production well had an increase in pressure drawdown due to steam-reservoir interaction, and the blocking of the slotted production liner is due to scale deposition. There was a need to stimulate this well to decrease the drawdown pressure and increase the well production rate. The sand particles in this reservoir are cemented by clay minerals and an insignificant amount of calcite and dolomite. The target zone contained sand, K-feldspar, and some kaolinite, illite, and smectite with an average porosity of 35.9 vol% and a permeability of 1194.7 mD. The mineralogy of the target zone is mainly composed by quartz with some inclusions of illite, smectite, kaolinite, K-feldspars, and other minerals.

The well is equipped with a slotted liner, and the length of the target zone is 2000 ft. The wellbore volume is from 15 to 30 m^3. Steam with 99 % quality was used to decrease the viscosity of oil. The well produces oil-water emulsion at a water cut of 45 vol%, and the concentration of key ions in produced water are given in **Table 4.1**. It should be noted that the concentrations of the main cations were measured both in the field and in laboratory conditions. The well tubulars and liner were mainly made of low-carbon steel L-80. An electrical submersible pump is used to produce from this well. The depth of the target zone is nearly 2300 ft.

Table 4.1: Concentrations[1] of main cations in the produced water from the treated well

Cations						
Na	K	Ca	Mg	Ba	Sr	Fe
360	20.6	2.68	0.6	0.03	0.05	0.25

1. All concentrations are expressed in ppm.

4.1.2 Corrosion testing of GLDA

Nasr-El-Din et al. (2012) examined the corrosion behavior of GLDA on low carbon steel. They have conducted 6-hour metal loss experiments and concluded that GLDA is gentler to low carbon steel than other alternative stimulation fluids such as HEDTA, acetic acid, citric acid, and formic acid. It was also shown that a very small amount of corrosion inhibitor is enough to protect the low carbon steel against a 20 wt% GLDA solution (pH 3.8) and keep the corrosion rate below the acceptable corrosion

limit even at high temperatures and in the presence of high concentrations of H_2S and CO_2.

The corrosion rates for chelating agent B are negligible because it is a high pH fluid. The maximum anticipated weight loss for uninhibited 1 wt% hydrochloric acid at 356˚F was measured to be 0.0778 lb/ft^2 for 6 hours of soaking time.

4.1.3 Treatment program

This well was treated before with a different degree of success. This field case represents a real challenge because of the following reasons. High bottomhole temperature (400 ˚F) causes a high corrosion rate, instantaneous uncontrolled reaction for HCl, and degradation for some chelating agents. A relatively high formation permeability and a long production horizontal section can cause flow of the acid into the reservoir instead of the acid placement in the whole length of the well in order to treat scale within the slots. Chemicals, which were used for the treatment, are given in **Table 4.2**. GLDA was first diluted with produced water in a 1 to 1 ratio. Next, a diluted chelating agent was mixed with a foaming agent for a better product placement. The foamed chelating agent was injected in the well. The produced water was injected at the end to displace the treatment into the target zone.

Table 4.2: Chemicals used for the field treatment

Pumping stage	Chemical	Volume (m^3)	Function
1	Foaming agent	30	To create a proper rheology, to be able to control the injection process, and place acid through the whole horizontal well interval
	15 m^3 of 20 wt% chelating agent (GLDA) diluted with 15 m^3 of produced water	30	Remove blocking materials (corrosion products, iron sulfides, carbonates, and silicon-based scales accumulation) from the slots
2	Produced water	30	To displace the treatment fluids into the target zone

The well flowback was started after six hours soaking time. Samples of the produced fluids were collected as a function of the volume of the returned fluid and were analyzed to assess the outcome of the treatment. A total of 70 samples were collected during a 435 minute time period with a total flowback volume of 150 m^3. Pressurized samples were also taken before and after the treatment (**Figure 4.1**).

Figure 4.1 – Flowback samples

Each plastic bottle contained data about the date and time when the sample was taken, pH of the sample, oxidation-reduction potential, temperature, and cumulative liquid volume as shown in **Figure 4.2**.

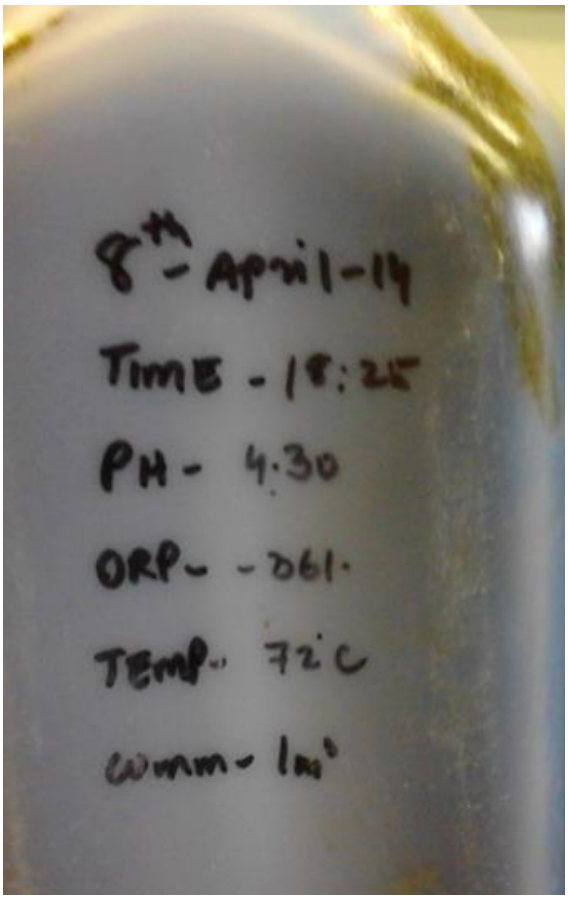

Figure 4.2 – Data on the bottles with a flowback sample

4.2 Flowbback Samples Analysis

4.2.1 Visual inspection and separation

Flowback samples presented a mixture of GLDA, produced water, and heavy oil. First of all, most of the heavy oil was removed using the gravimetrical separation method. However, some samples presented a very strong emulsion. Even after a few days in a separation funnel, the boundary between phases could not be observed for such

samples. These samples were separated by density multiple times. Almost all of the samples at the end of the separation stage presented black watery liquid because of the big amount of oil films remaining in the water-acid mixture. Only a few samples were clear after the separation stage, and they mainly had dark a green color (**Figure 4.3**). These colors indicate the presence of various iron species.

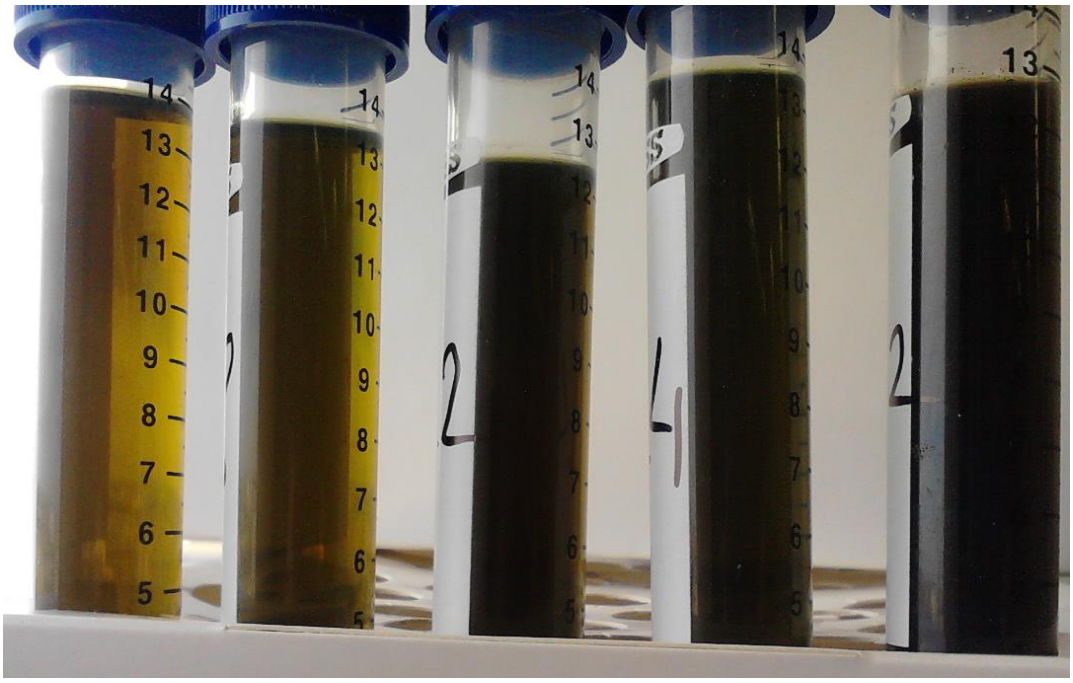

Figure 4.3 – Clear samples after the separation stage

To continue the separation of the oil films, a centrifugation machine was used, and each sample was processed for 5 minutes with a rotational velocity of 4500 rpm (**Figure 4.4**).

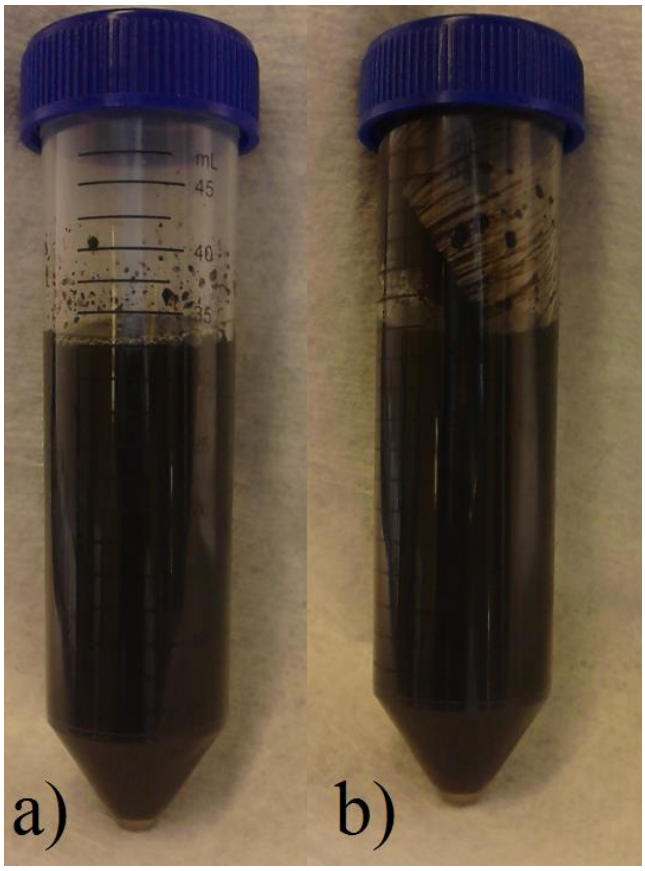

Figure 4.4 – Emulsion sample before (a) and after (b) centrifugation

4.2.2 Emulsion breaking

Most of the samples remained dark after centrifugation. Different methods were tried in order to break the emulsion and prepare samples for ICP. Mutual solvent was added and mixed but didn't show any visible results except for foaming (**Figure 4.5**).

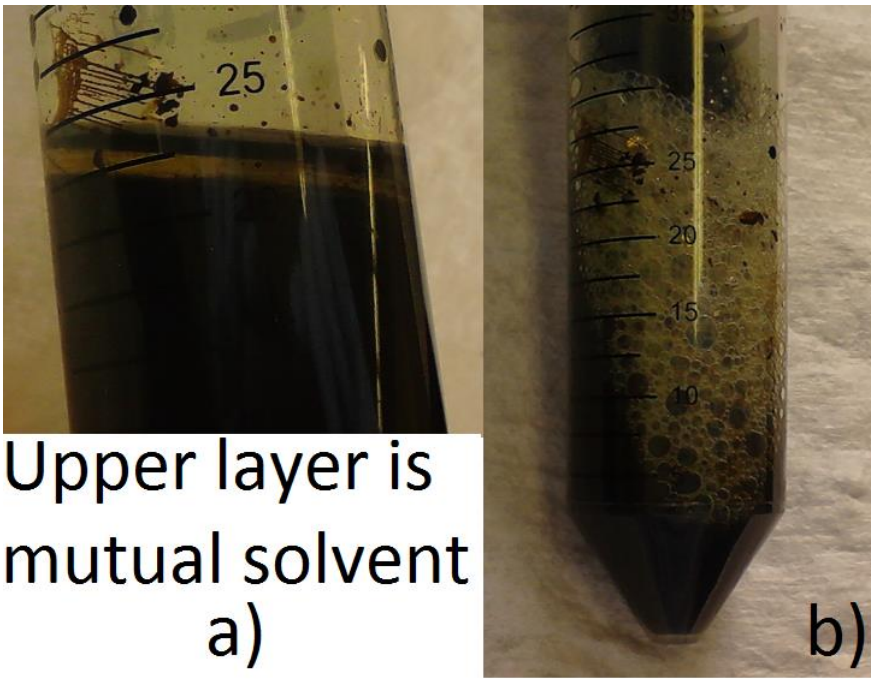

Figure 4.5 – Emulsion sample before (a) and after (b) mixing with mutual solvent

Hydrochloric acid was also tried for emulsion breaking (**Figure 4.6**). It reacted immediately, and the solution became clear. Also, black precipitations were formed and precipitated with time (**Figure 4.7**).

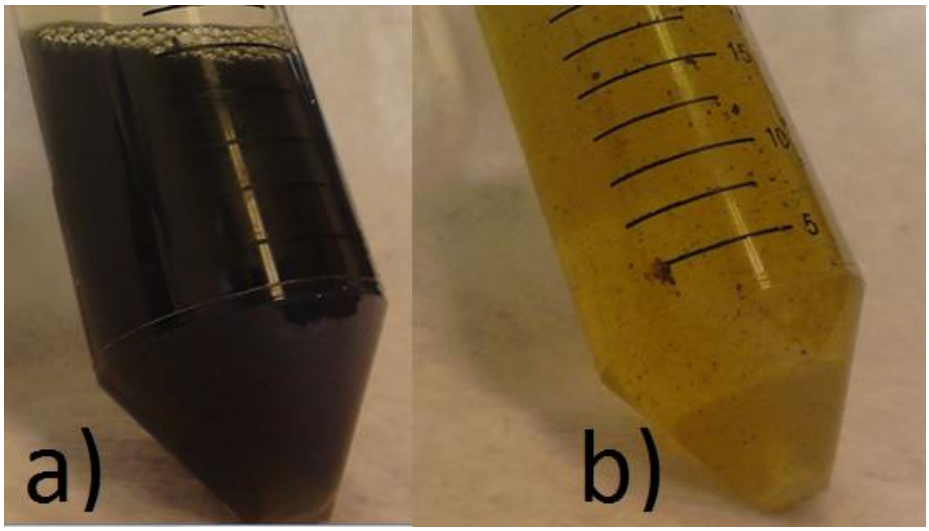

Figure 4.6 – Emulsion sample before (a) and after (b) reation with 1 ml of 15 wt% HCl

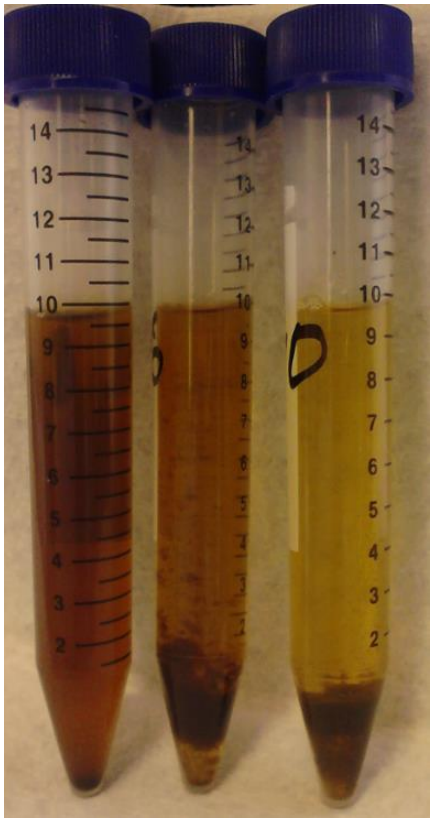

Figure 4.7 – Emulsion samples after the reaction with 1 mL of 15 wt% HCl

Both solutions were filtered, and the concentrations of the main cations were determined using ICP. The only significant change in concentration for the HCl samples before and after the reaction was iron (**Figures 4.8**).

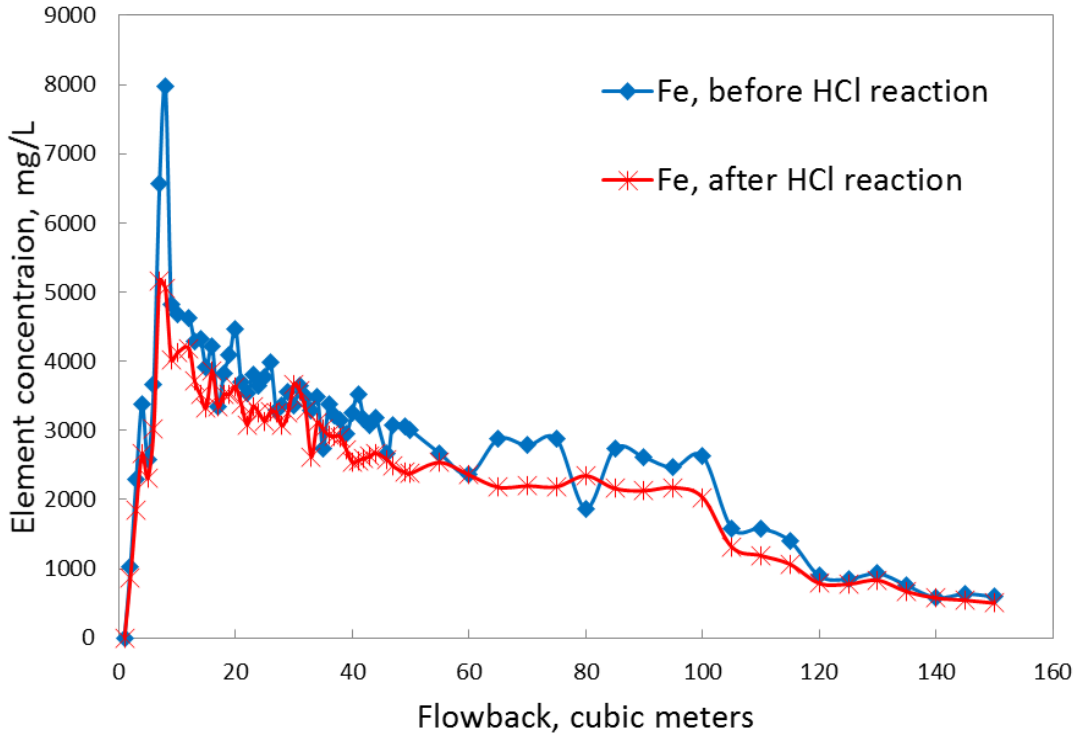

Figure 4.8 – Iron concentration before and after the reaction with HCl

It was determined that the samples presented a strong emulsion, and even after few stages of separation, they contain some tiny oil films. Liu et al. (2006) stated that the black sulfide solid particles in the form of FeS can be suspended in water, and some of the FeS solid particles can attach to oil particles, forming a solid/oil drops emulsion. As

a result, they form a FeS layer at the oil/water contact, and the produced emulsion becomes very stable. This concept was checked using reactions of flowback samples with HCl. The fact is that after adding of few drops of 20 wt% HCl, precipitation was formed. It could be explained by the reaction of the acid with iron which removed the barrier between water and oil bubbles, and, as a result, the emulsion was broken. However, in order to be able to apply titration method using the ferric chloride solution, these samples should not contain iron. The addition of NaOH increases the pH of the sample and causes precipitation of iron which is shown in **Figure 4.9**. The concentration of iron was measured to be zero after the reaction with NaOH.

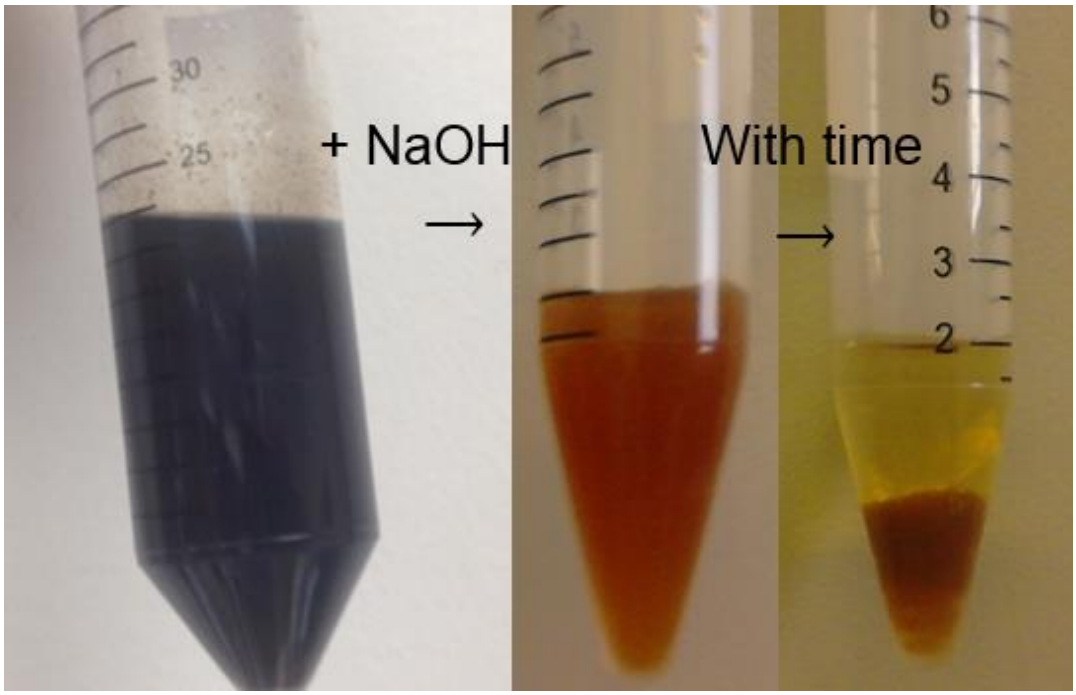

Figure 4.9 – Typical reaction of the flowback sample with NaOH

4.2.3 ICP analysis

In order to prepare the samples for ICP, all of the solid particles should be removed. The filtration of the centrifuged samples was conducted using a 1 μm pore size filter paper. It should be noted that a lot of oil films were removed together with solids separation (**Figure 4.10**).

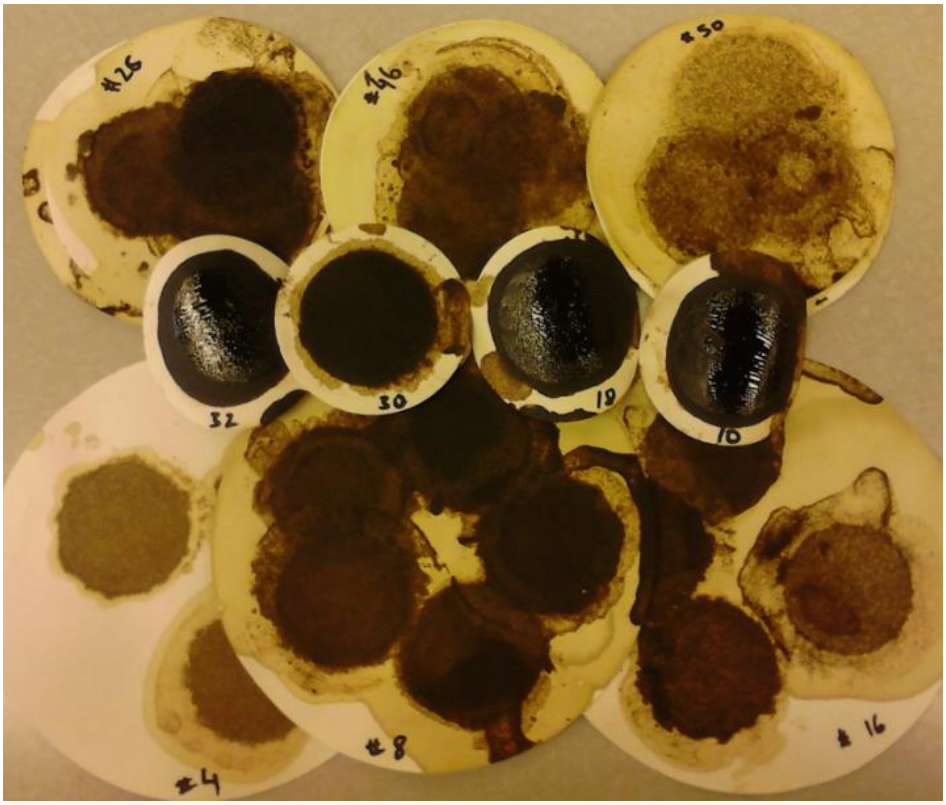

Figure 4.10 – Used filter paper

Additionally, the pH of the filtered samples were measured and compared with onsite data (**Figure 4.11**). The pH measured onsite started at nearly 4, increased up to 6

and even almost 7 for some points, and then it remained constant at approximately 6-6.5. This range of pH shows that the produced fluids were still slightly acidic after the treatment.

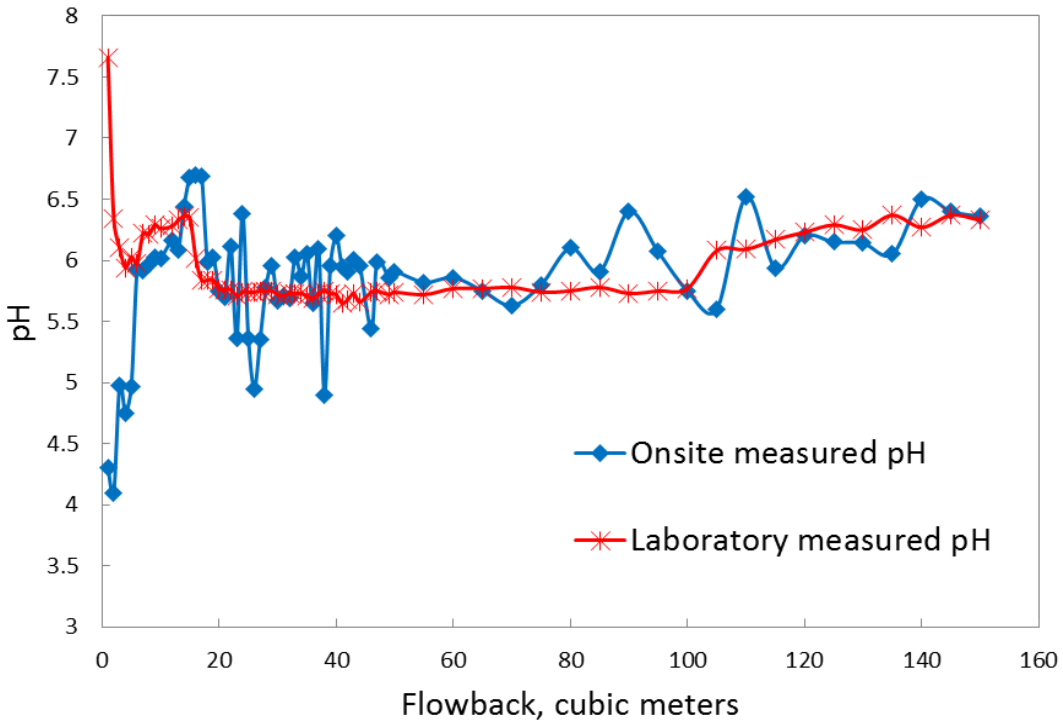

Figure 4.11 – Onsite and laboratory measured pH

After the filtration, the samples were diluted with deionized water in a ratio of 1:500 (**Figure 4.12**).

Figure 4.12 – Filtered (a) and diluted (b) emulsion sample

Inductively coupled plasma emission spectroscopy (ICP-ES) was used to determine the concentrations of key cations.

The concentration of sodium is shown in **Figure 4.13**. The main source of sodium in the treating fluids was the chelating agent. Mono-sodium GLDA was used for the treatment, and, therefore, sodium concentration in the flowback samples can be used to track the flow of the treating fluid and its reaction with the reservoir minerals. Figure 4.13 shows that initially the sodium ion concentration was 15,685 ppm, and then it

gradually decreased to the level which is close to the concentration of sodium ions in the produced fluid.

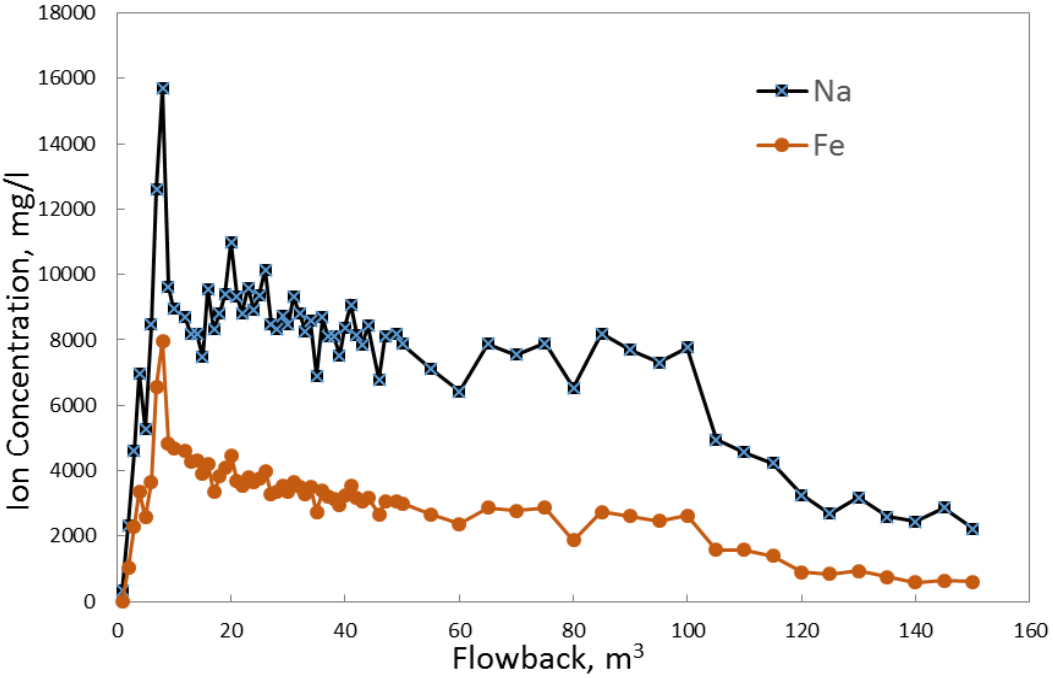

Figure 4.13 – Concentrations of sodium and iron ions in the flowback samples

NaGLDA was used to dissolve the rust and scale from the liners, surface and slots and to remove the damaging materials from the target zone. Flowback samples were saturated with iron (**Figure 4.13**). The highest concentration of the iron ions is 7970 ppm. The dependence of iron ions concentration is very similar to sodium, and the peaks of these two lines are consistent. The main source of the iron is iron sulfide scales inside of the slots and tubing. Another source of iron ions is connected with corrosion of

the tubing. There are also some carbonate and dolomite in the reservoir and chlorite in the scale which were dissolved during the treatment. **Figure 4.14** shows the variations of calcium, magnesium, and aluminum ions in the flowback samples. The concentrations of these elements are in good agreement with each other and with iron ions. The main sources of calcium and magnesium are smectites, feldspars, and other minerals with isomorphous substitution. Calcite and dolomite which also cement quartz in the sandstone reservoirs are not abundant in this case. There are a lot of sources for aluminum such as clays and feldspars which could be destabilized because of the equilibrium shift not only during the treatments, but also during the steam injection and production processes.

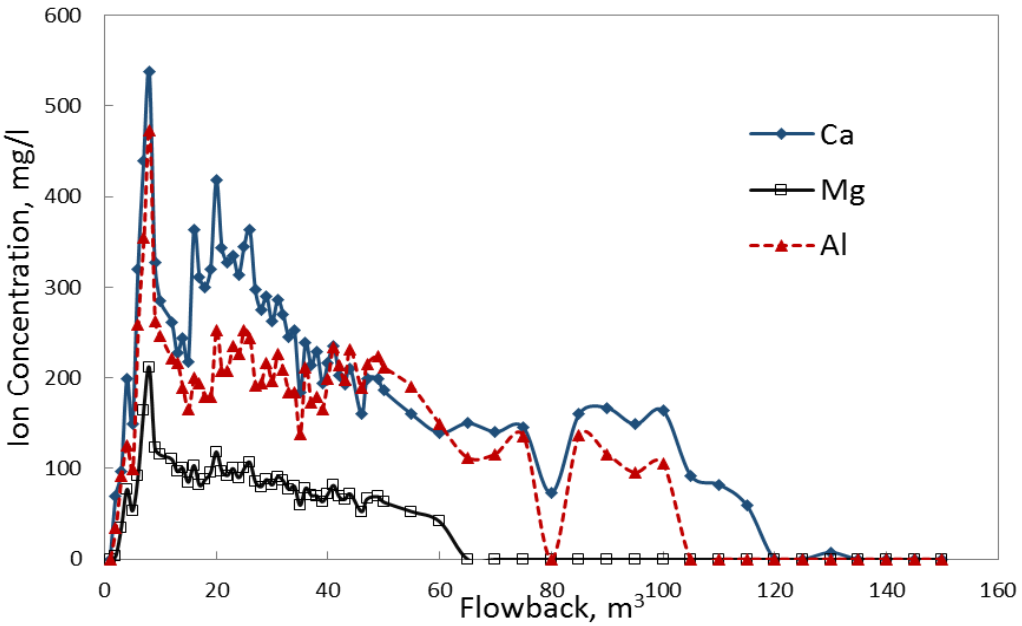

Figure 4.14 – Concentrations of calcium, magnesium, and aluminum ions in the flowback samples

Figure 4.15 shows the concentrations of ions that are related to corrosion. The main ions of interest for L-80 tubing, connectors, and joints are nickel, chromium, manganese, and molybdenum. Iron's ion concentration could not be used because it mainly comes from the dissolved scale. All of these ions were presented in the flowback samples. Manganese's ion variation is consistent with the variation of other ions, but the concentration is very small. This similarity in trends of iron and manganese means that some corrosion did happen because of high downhole temperatures, but it is insignificant damage based on the concentration. Other ions concentration is only in tracer amount. These results are in good agreement with the corrosion testing for mono-sodium GLDA, which shows that the treatment had no significant impact on the integrity of the well tubulars.

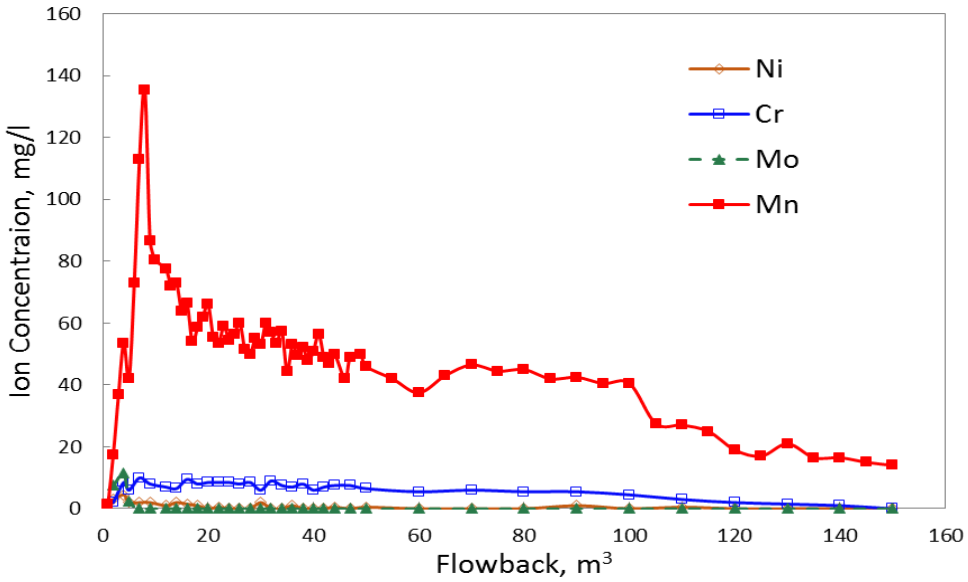

Figure 4.15 – Concentrations of manganese and zinc ions in the flowback samples

4.2.4 Titration and analysis of GLDA

The concentration of GLDA in the flowback samples is an important parameter which describes behavior of the treatment fluid at the downhole conditions. The GLDA concentration in the aqueous phase of each sample was measured by titration with a $FeCl_3$ solution (Sokhanvaian et al. 2012). An extensive preparation was conducted on the flowback samples because they should be de-ironized for the application of this method. As it was explained previously, sodium hydroxide was used to precipitate $Fe(OH)_3$. Subsequently, the solution was filtered and buffered at a pH of 3 to make sure that all of other metal ions will be replaced by Fe^{3+} during the titration. The initial concentration of the GLDA in the treatment prior to dilution was 20 wt%. **Figure 4.16** shows the concentration of GLDA in the produced fluids (assumed density is 1.265 g/cc, and molar mass is 2.85 g/mole). This concentration is significantly lower than the one in the treatment which can be explained by the dilution of the treatment fluid with the pumped afterwards water and the formation brine. It also should be noted that a high bottomhole temperature (390˚F) can cause the decomposition of the GLDA. As a result, the concentration of the GLDA in the flowback samples gradually decreased from 4-5 wt% and reached 1-2 wt% for the last sample. This tendency is in an agreement with the time needed for the dissolved ions to reach similar levels in the production fluid. For each point, the amount of complexed GLDA was calculated based on the ICP data for di- and trivalent cations. It shows that, initially, approximately 90 % of GLDA was complexed. With time at a higher produced back volume, the amount of complexed GLDA gradually decreased to 20 %.

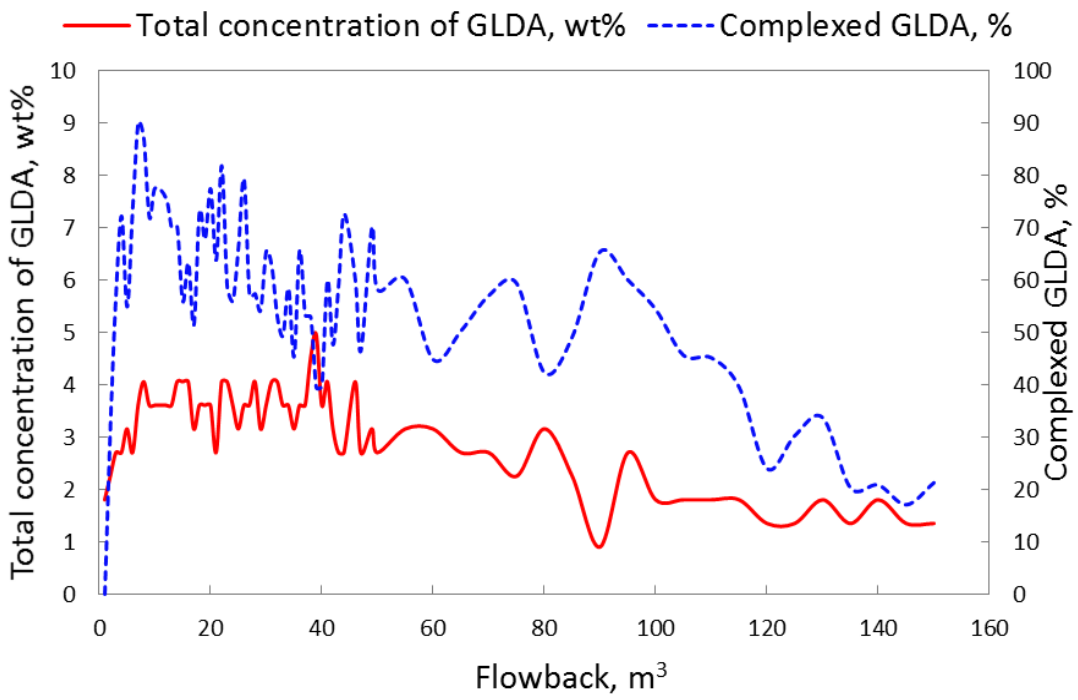

Figure 4.16 – Concentrations of GLDA in the flowback samples

4.2.5 Decomposition products analysis

The initial concentration of GLDA was 20%. After dilution in a ratio of 1 to 1 by volume with production water, additional dilution was done with pumped afterwards production water, and the actual concentration of the GLDA became lower than 10%. Additionally, this GLDA was diluted in the reservoir by formation brine. However, the concentration of GLDA in flowback samples was found to be less than 5%. This fact could be explained by the decomposition of GLDA during the treatment which lasted almost 6 hours.

Figure 4.17 shows the DTS (distributed temperature sensing system) log for the well before and after the application of GLDA. It must be noted that when the well is not running during the application, there is a slight temperature drop. At the depth of the target zone, the temperature prior to the treatment is almost the same as for the well while it is running well. However, a cooling effect is observed after injecting 30 m^3 of the treatment fluid, but the degradation of the chelating agent at this temperature is less severe even at the chosen soaking time.

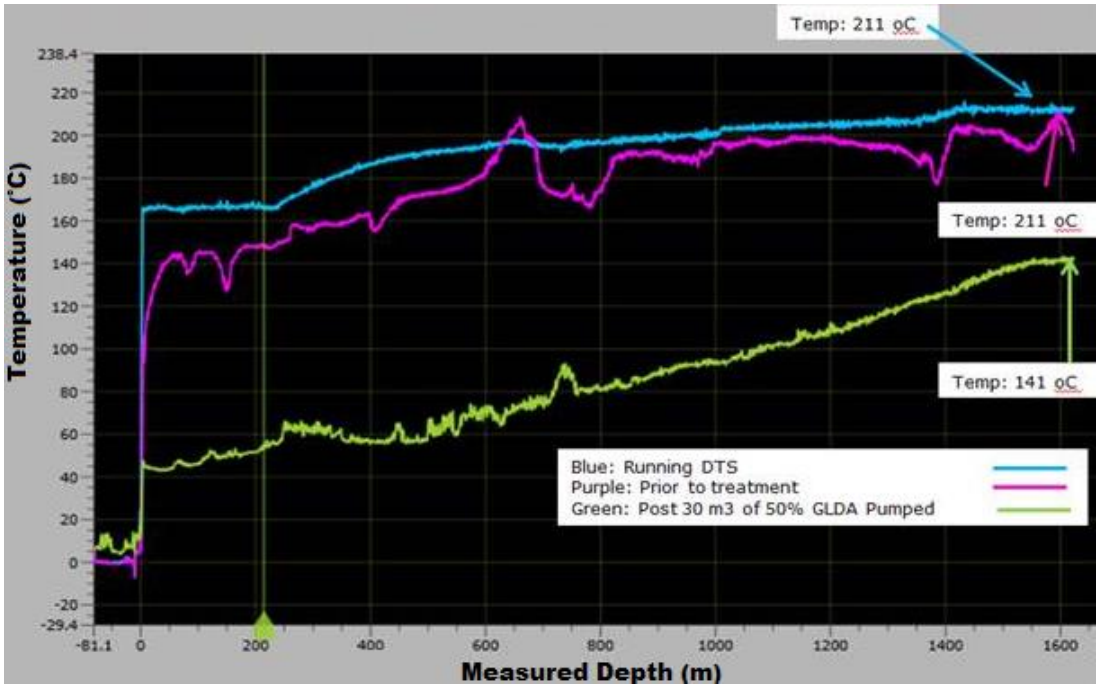

Figure 4.17 – Temperature profile

However, Sokhanvarian et al. (2012) reported that at 400˚F for 6 hours of soaking time, the stability of the NaGLDA is less than 30 %. An extensive analysis was conducted on the aqueous phase present in the well flowback samples to determine whether there was a thermal degradation to the chelate under bottomhole conditions. First, 20 wt% NaGLDA was aged at 400˚F for 6 hours to mimic bottomhole conditions. It should be noted that the temperature ramp wasn't the same as during the real treatment. Two aging cells were pressurized and placed in the oven. The volume of the sample was approximately 70 cm^3 each which means that they reached the target temperature of 400˚F quickly. However, in real conditions, the volume of the fluid is much higher and heating process lasts longer. As a result of the aging, change of the color, cloudiness, and precipitations formation indicate a decomposition of the chelate (**Figure 4.18**). The next step is to identify the decomposition products.

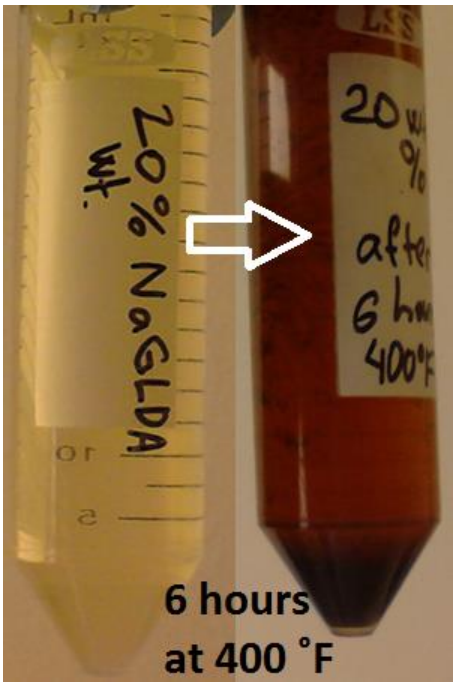

Figure 4.18 – Result of the aging of GLDA in oven at 400˚F for 6 hours

A gas chromatography-mass spectrometry (GC-MS) analysis was used to identify the decomposition products of GLDA. For the GC-MS analysis, three flowback samples were chosen: the first flowback sample, the sample with the highest iron concentration, and the last flowback sample (marked red in **Figure 4.19**). This distribution of samples was used to investigate the dependence of GLDA to decompose based on the time and position in the liner. For the first sample, the decomposition product was found to be a phosphoric acid. It should be noted that the sources of phosphorus can be some minerals from the target zone such as: apatite, monazite, and xenotime which were previously found in the target zone. For example, **Figure 3.18** shows the SEM and EDS results for the sample of rock from the target zone. The

presence of very rare elements - Nd, La, and Ce along with phosphorus, show that this is Monazite-(La).

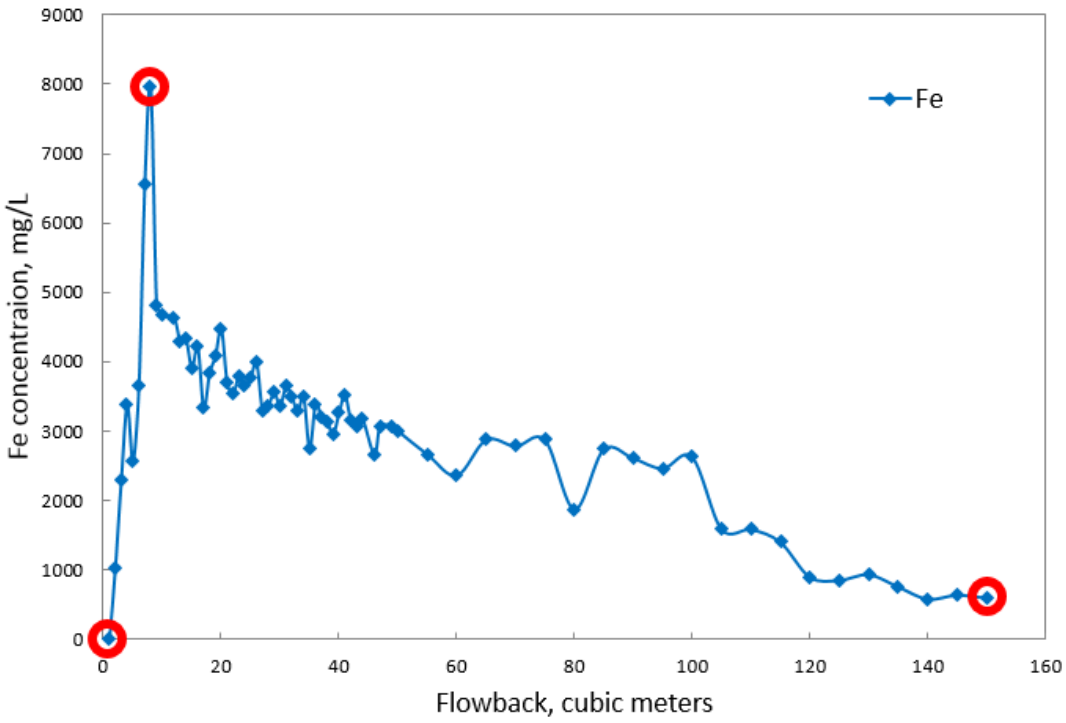

Figure 4.19 – Flowback samples chosen for GC-MS analysis

The other two flowback samples have the same decomposition products. These products are glutaric and iminodiacetic acids (**Figure 4.20**). The peak for a retention time of 17.33 minutes wasn't fully interpreted, but it most probably presents heavy hydrocarbons. Electrospray ionization (ESI) was conducted to confirm the results of GC-MS. ESI identified hydroxyglutaric and iminodiacetic acids as well as another common peak which was found previously (**Figure 4.20**). It should be also noted that

hydroxyglutaric and iminodiacetic acids were previously identified as decomposition products for H_4GLDA (Sokhanvarian et al. 2012). Peak interpretation work is a hard task, and it requires further investigation. However, these tests are important to answer the question about the degradation of chelating agents. The results obtained will help to improve the methodology of further treatments.

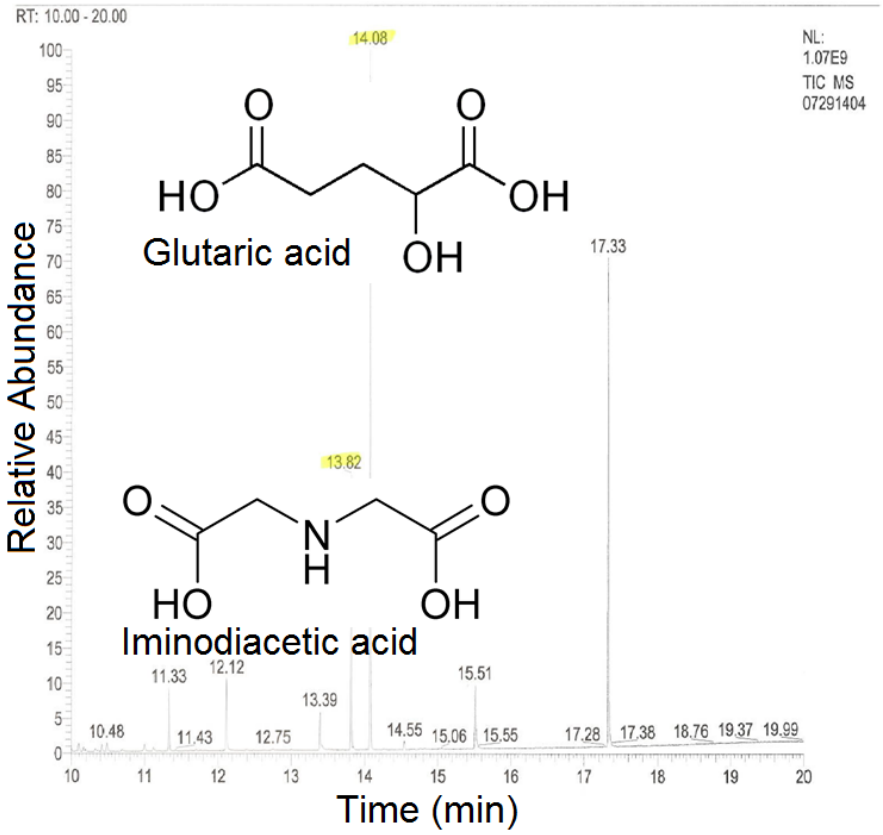

Figure 4.20 – GC-MS results for the flowback sample with the highest iron ion concentration

Both **Figures 4.20** and **4.21** show the GC-MS and ESI results for the sample with the highest iron concentration. The last sample has almost the same results. The results show that for the first produced flowback sample decomposition is less severe. Most probably, this observation is connected with cooling down of the near wellbore area during the injection of the treatment fluids and soaking time difference.

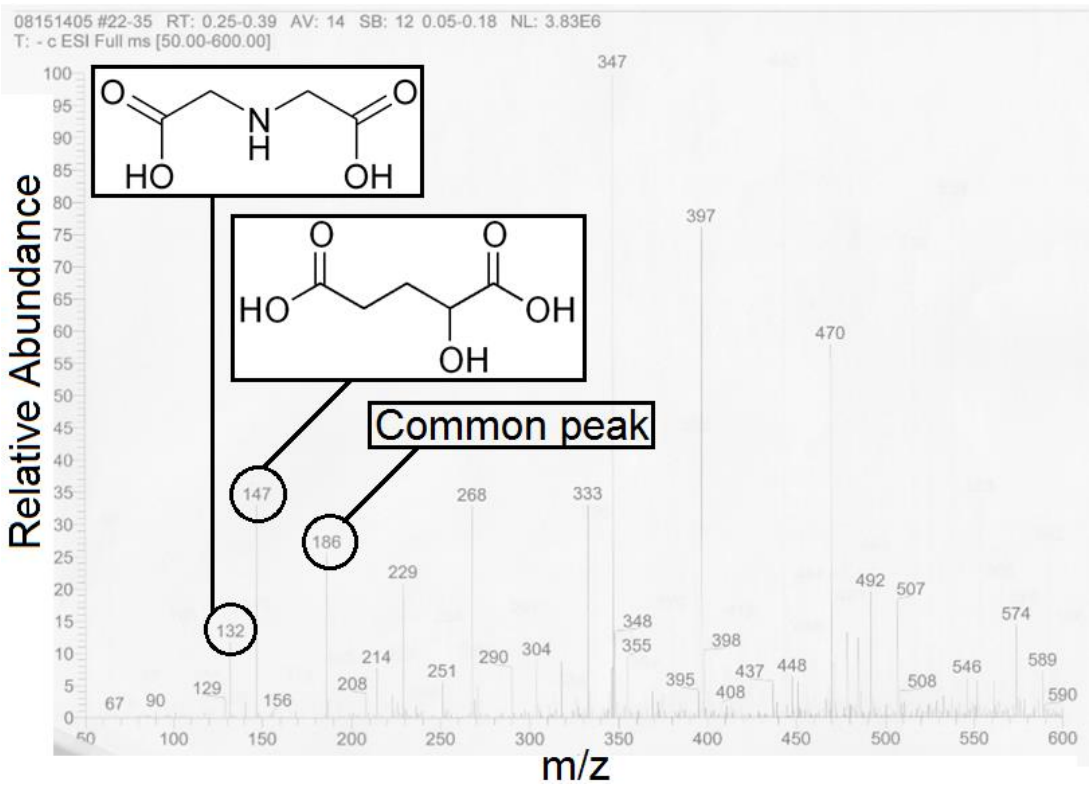

Figure 4.21 – ESI results for the flowback sample with the highest iron ions concentration

It should also be mentioned that geochemical modeling was conducted for these flowback samples. Its purpose was to analyze the distribution of GLDA complexes in flow back samples and estimate the effectiveness of a GLDA treatment. Another aim of the modeling was to determine optimum dosage amounts and pH values for specific conditions prior to a treatment (Ameur et al. 2015).

4.2.6 Solids in the flowback

The flowback samples contained a very minor amount of sand particles which wasn't higher than in the usual production fluid. This observation indicates that GLDA was compatible with sandstone minerals, and it did not cause fines migration problems or additional sand production. However, for some other wells which were treated by GLDA, solid particles were separated from the pressurized samples. These solids will be analyzed and explained in future work.

4.2.7 Summary of flowback analysis

Extensive analysis of flowback analysis was performed. The preparation of the flowback samples for analysis is a significant part of the work and requires multiple centrifugation and separation phases. Based on the concentrations of main ions, it could be stated that scaling materials were dissolved, and the integrity of well tubulars wasn't affected. Titration results showed that decomposition of the chelant wasn't significant, despite the high temperature of the formation. Analysis of the decomposition products proved the necessity of reduction in soaking time which was successfully applied during the treatments of other wells.

4.3 Production Data Analysis and Conclusions

4.3.1 Production data

It should be stated that the well was treated numerously previously. Just in the last 5 months before the NaGLDA treatment, this well was treated with HCl and a high pH chelating agent. In order to compare the production rate results after all three treatments, they were plotted together. The dimensionless emulsion rate is shown in **Figure 4.22**. This is a normalized rate expressed in percentage as a ratio of a production rate at different time moments to a minimum production rate, which was reached at approximately 4 months after the well was treated with HCl. This point has a normalized rate equal to 100%. Based on the graph, it is clear that blocking materials were removed significantly enough, and the permeability was restored very well which resulted in the fast growth of the production rate up to 160% which is 30% higher than before the treatment. Additional to the production increase after the treatment, there was no increase in the water cut (**Figure 4.23**). More than three months after the treatment, a significant increase of the oil production was observed.

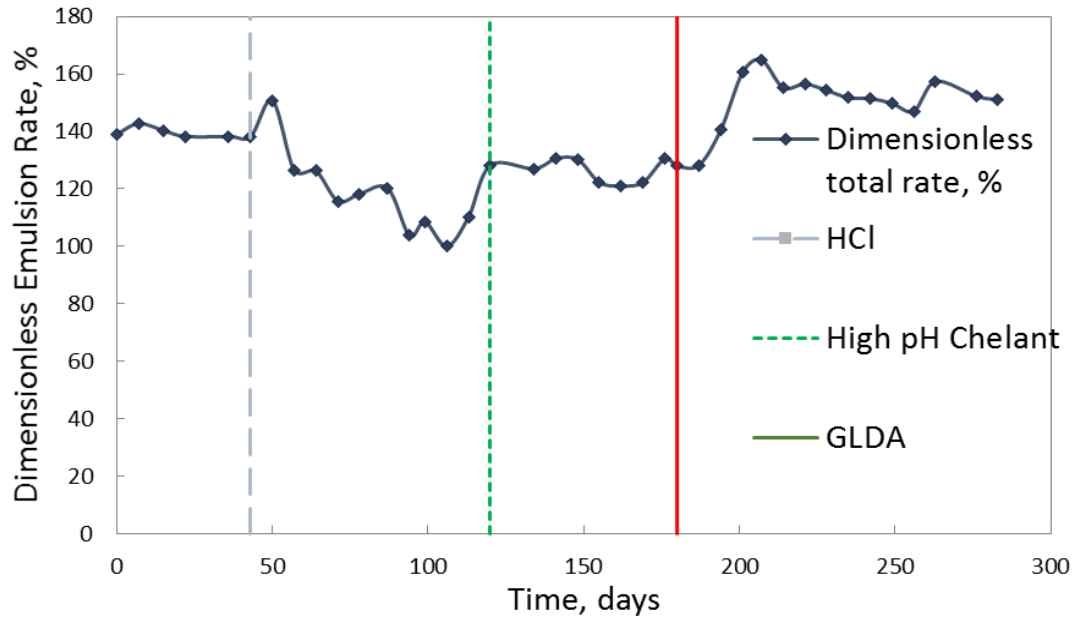

Figure 4.22 – Dependence of normalized emulsion rate on time

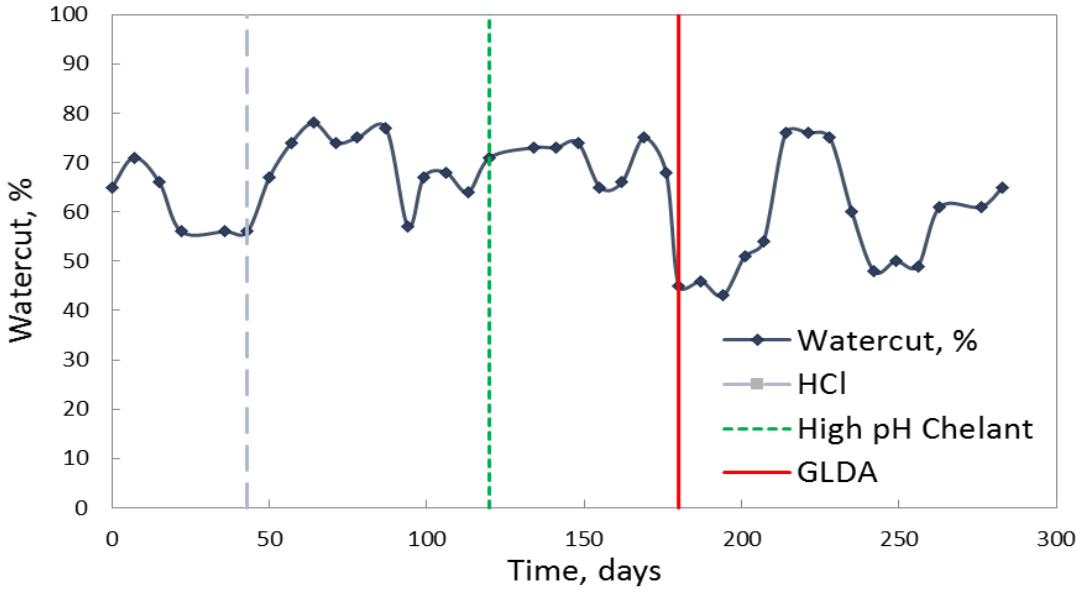

Figure 4.23 – Dependence of watercut on time

It also should be noted that the treatment didn't cause incompatibility problems with formation fluids, sand production, fines migration, or asphaltenes precipitation. This treatment maintained the integrity of the tubulars at almost 360˚F which is also a very impressive result. Based on both the geochemical and production analysis of the chelating agent (GLDA), the application was deemed successful.

Flowback samples analysis and production data confirmed that the treatment was performed successfully. However, there are some improvements which should be considered based on the gained experience. First of all, it was shown that GLDA can degrade at high temperatures and long soaking time. This could decrease the performance of the treatment fluid and cause formation damage by degradation products. Since it is not easy to control temperature in the reservoir, the soaking time should be adjusted to minimize possible negative effects. It should be mentioned that such an improvement was made. After reducing the soaking time down to 4 hours, the concentration of GLDA in the flowback samples was determined to be higher.

It should be noted that corrosion inhibitors were not used during the treatment. However, for each particular treatment in the future, such additives should be carefully evaluated and applied if needed. This is especially important for cases when GLDA is less diluted with produced water prior the treatment.

Some treated wells were found to have H_2S. Because of the dissolution of iron sulfide scales, hydrogen sulfide could be released which is a serious environmental and safety issue. That is why experiments for choosing and applying H_2S-scavengers for

each particular soar well should be taken seriously and considered as a future improvement.

Overall, it could be stated that there were numerous amounts of fluids that were developed for sandstone acidizing. Even just among the group of organic acids and chelating agents, some new treatment fluids could be considered and tested which could give an opportunity to treat the well more efficiently. This means that future investigations could provide useful insights in order to improve the design and cost effectiveness of treatments.

5. SUMMARY AND FUTURE WORK

In this chapter, all of the previous conclusions will be summarized. The author's vision of the future work and possible improvements will be also described.

5.1 Blocking Materials Analysis

Experimental work on liners provided some interesting results. First of all, it is clear now that problems with drawdown pressure are caused by different types of materials. It is important to understand the sources of each type of blocking materials. Some of them were formed in the liner because of a pressure or temperature drop, some of them were transferred in the liner from the reservoir, and some of these materials were injected or caused by injected fluids.

Corrosion products together with iron sulfides and sulfates cover the inner walls of liners, and, sometimes, these species are also present in the slots. Additionally, there are also some minerals from the serpentine group that were found in the slots. Further investigation is needed in order to understand whether these minerals were formed in the slots or migrated there from the reservoir. Overall, more actual samples of blocking materials from the slots should be collected and analyzed in detail from the mineralogy point of view to determine features of their formation. Also, different treatment fluids should be applied for dissolution tests at high temperatures in order to find the best fit for dissolution of scale from the slots for a particular liner or target zone. There are also numerous silicon-based species. Hydrofluoric acid could be considered to treat them, but only with a reasonable preflush stage. Organic acids, chelating agents, or even

hydrochloric acid could be used together with HF, but corrosion inhibitors should be used accordingly. Additional to the chemical methods, many authors published their mechanical methods of scale removal. The combined effect of a coiled tubing jetting system and chemical treatment could be developed and applied in order to improve the well's performance.

It is important to note that solubility tests should be performed in realistic conditions. An aging cell or reactor should be designed in order to be able to conduct solubility tests not only with a scale samples and coupons, but also with the actual section of the liner. It will mimic real conditions better because the reactions will occur on the inner and outer surfaces at the same time. It will also show how essential the effect of corrosion is in comparison with blocking materials and scale dissolution.

Another recommendation should be made concerning organic material layers which cover a liner's surfaces and block slots. These materials also consolidate scaling and rust and make it harder to remove. Except the cementing effect, organic barriers also prevent the reaction between the minerals' surface and acid. All of these facts were discussed and proved during the experiments. This means that the removal of organic materials prior to an acid job could affect of the treatment to be much more significant. That is why the author wants to point out that organic solvent could be used during the preflush stage. Of course, this addition should be adjusted to be in agreement with the rest of the treatment program. Also, this improvement is only proposed for the liners where these organic layers were observed to be a significant issue.

In this work, only production wells were analyzed. In fact, drawdown pressure also depends on the blockage in the injectors. In further work, scale samples from the injectors could be collected and investigated in order to design a treatment for these wells. It is interesting to compare what minerals precipitate as a scale in injectors and producers. This data could be used for the overall optimization of the steam injection technique.

Questions concerning the optimal slots geometry remained untouched in this work. However, it is important to understand what slot geometry would be the best in order to prevent precipitation of particular minerals. This topic is also considered as a possibility for future work.

5.2 Mineralogical Analysis of the Target Zone

The mineralogy of a reservoir is a very important parameter not only in terms of the treatment design, but also in the overall prevention of the blockage and production problems. There are a lot of publications proving the importance of the interactions in the reservoir system: rock-brines-steam. That is why, the author would like to share the author's vision of a possible long term strategy to solve the problem of scaling and blocking of the production liners. Mineralogy analysis could be useful for the determination of the main reactive minerals and forecasting of their transformations in changed conditions. These minerals' reactions could be modeled and, as a result, provide a useful insight into a precipitations prevention technique. This approach could be also amplified by the usage of clay stabilizers. Steam injection experiments could be used to

prove or disprove the theoretical approach. Different packing models and coreflood experiments could be useful tools in adjustments of all the needed additives.

From the other hand, injected fluids should be also prepared very carefully. Steam properties and purity are two of the most critical aspects to keep track of. Too high of a pH of the injected steam and excess of some cations proved to have a negative impact on minerals reactions. Additionally, every acid job or other treatments should be conducted without a negative impact on the assets' integrity. In this particular case, corrosion inhibitors are strongly recommended.

In case of a short term tactic to blockages, mineralogy is an even more important factor. It could be stated that the wells' treatments are used to take care of materials which were formed because of imperfections of prevention techniques. At the same time, treatments itself can cause a significant formation damage. It is especially true for sandstone formations, as it was discussed previously. For this particular case, the mineralogy analysis of the target zone was used not just to cause formation damage, but also the main aim was to remove the blocking materials from the slots and restore the liners' throughput capacity.

For the discussed case, the mineralogy analysis was performed in detail which helped to prevent formation damage. However, it is also recommended to conduct coreflood experiments to monitor permeability changes and identify the causes of them. This is particularly important for clay rich sandstones.

5.3 GLDA Treatments and Flowback Samples Analysis

The results described in the first two chapters were applied to design a stimulation treatments. Overall, seven treatments in five different wells were performed with positive results and performance improvements.

The technique of flowback samples analysis was developed and applied in order to describe the processes that occurred during the treatment. The preparation process includes multiple separations and centrifugation of the flowback emulsion. Based on the ICP results, it could be stated that GLDA dissolved a significant amount of rust and blockage materials which had a good impact on the production.

At the same time, titration and spectrometry results proved the partial decomposition of the chelant. This means that at a fixed reservoir temperature, the optimum time of the GLDA treatment should be determined. Also, the stability and reactions of the other types of chelants with blocking materials should be investigated.

As it was mentioned before, in order to determine the effect of the decomposition products on the reservoir permeability, coreflood experiments should be conducted. At the same time, a better understanding of the decomposition products should be developed. Precipitations obtained during the aging of the GLDA present amorphous organic material. The content of this material should be further investigated. The decomposition products should be determined qualitatively and quantitatively.

A better understanding of decomposition products will provide important data for geochemical modeling. This direction of work could be useful in an adjustment of

optimal parameters of the treatment fluid, such as chelant's volume, concentration, and pH.

It is also important to note that the analysis of the production data is a very important task. Drawdown pressure is a useful criteria in order to evaluate the degree of the blockage removal. Also, the emulsion rate should be monitored together with a watercut data. It should be mentioned that candidates for GLDA treatments were chosen among the wells which were treated numerously in the past. In order to evaluate the result of a particular treatment, it is important to have a well in production mode for a reasonable amount of time.

REFERENCES

Adenuga, O.O., Nasr-El-Din, H.A., and Sayed, M.A.I. 2013. Reactions of Simple Organic Acids and Chelating Agents with Dolomite. Society of Petroleum Engineers. http://dx.doi.org/10.2118/164480-MS

Al-Dahlan, M.N., Nasr-El-Din, H.A., and Al-Qahtani, A.A. 2001. Evaluation of Retarded HF Acid Systems. Society of Petroleum Engineers. http://dx.doi.org/10.2118/65032-MS

Ali, A.H.A., Frenier, W. W., Xiao, Z. et al. 2002. Chelating Agent-Based Fluids for Optimal Stimulation of High-Temperature Wells. Society of Petroleum Engineers. http://dx.doi.org/10.2118/77366-MS

Ali, S.A., Ermel, E., Clarke, J. et al. 2005. Stimulation of High-Temperature Sandstone Formations from West Africa with Chelating Agent-Based Fluids. Society of Petroleum Engineers. http://dx.doi.org/10.2118/93805-MS

Ameur, Z. O., Kudrashou, V. Y., Nasr-El-Din, H. A. et al. 2015. Stimulation of High Temperature SAGD Producer Wells Using a Novel Chelating Agent (GLDA) and Subsequent Geochemical Modeling Using PHREEQC. Society of Petroleum Engineers. http://dx.doi.org/10.2118/173774-MS

Armirola, F., Machacon, M., Pinto, C. et al. 2011. Combining Matrix Stimulation and Gravel Packing Using a Non-acid Based Fluid. Society of Petroleum Engineers. http://dx.doi.org/10.2118/143788-MS

Bennion, D.B., Thomas, F.B., and Sheppard, D.A. 1992. Formation Damage Due to Mineral Alteration and Wettability Changes During Hot Water and Steam Injection in Clay-Bearing Sandstone Reservoirs. Society of Petroleum Engineers. http://dx.doi.org/10.2118/23783-MS

Braun, W., de Wolf, C., and Nasr-El-Din, H.A. 2012. Improved Health, Safety and Environmental Profile of a New Field Proven Stimulation Fluid (Russian). Society of Petroleum Engineers. http://dx.doi.org/10.2118/157467-RU

Chakrabarty, T. and Longo, J.M. 1994. Production Problems in the Steam-stimulated Shaley Oil Sands of the Cold Lake Reservoir: Cause and Possible Solutions. Petroleum Society of Canada. http://dx.doi.org/10.2118/94-10-04

Davies, D.K., Vessell, R.K., Fu, R.Y. et al. 1996. Nature, Origin, Treatment and Control of Well-Bore Scales in an Active Steamflood Wilmington Field, California. Society of Petroleum Engineers. http://dx.doi.org/10.2118/35418-MS

Deng, Y.,White, G. N., and Dixon, J. B. (2009). Soil Mineralogy Laboratory Manual. 11th edition. Published by the authors, Department of Soil and Crop Sciences, Texas A&M University, College Station, Texas.

DeVine, C.S., Kalfayan, L.J., and Ali, S.A. 2002. Method for Proper HF Treatment Selection. Petroleum Society of Canada. http://dx.doi.org/10.2118/2002-288

Erno, B.P., Chriest, J., and Miller, K.A. 1991. Carbonate Scale Formation in Thermally Stimulated Heavy-Oil Wells Near Lloydminster, Saskatchewan. Society of Petroleum Engineers. http://dx.doi.org/10.2118/21548-MS

Feng Bo, Yi-ping Lu, Qi-ming Feng, Peng Ding, Na Luo. Mechanisms of surface charge development of serpentine mineral, Trans. Nonferrous Met. Soc. China 23(2013) 1123 − 1128.

Fredd, C.N. and Fogler, H.S. 1997. Chelating Agents as Effective Matrix Stimulation Fluids for Carbonate Formations. Society of Petroleum Engineers. http://dx.doi.org/10.2118/37212-MS

Fredd, C.N. and Fogler, H.S. 1998. The Influence of Chelating Agents on the Kinetics of Calcite Dissolution. J Colloid Interface Sci. 204 (1): 187-97.

Frenier, W., Brady, M., Al-Harthy, S. et al. 2004. Hot Oil And Gas Wells Can Be Stimulated Without Acids. Society of Petroleum Engineers. http://dx.doi.org/10.2118/86522-MS

Frenier, W.W., Fredd, C.N., and Chang, F. 2001. Hydroxyaminocarboxylic Acids Produce Superior Formulations for Matrix Stimulation of Carbonates at High Temperatures. Society of Petroleum Engineers. http://dx.doi.org/10.2118/71696-MS

Frenier, W.W., Rainey, M., and Wilson, D. 2003. A Biodegradable Chelating Agent is Developed for Stimulation of Oil and Gas Formations. Society of Petroleum Engineers. http://dx.doi.org/10.2118/80597-MS

Gallup, D.L. and Hinrichsen, C.J. 2008. Control of silicate scales in steam flood operation. Society of Petroleum Engineers. http://dx.doi.org/10.2118/114042-MS

Gdanski, R.D. 1985. AlCl3 Retards HF Acid for More Effective Stimulation. OGJ, 111 - 115.

Gill, J.S. 1998. Silica Scale Control. NACE International.

Guan, H. 2013. Selection of Scale Inhibitor for Geothermal Applications. NACE International.

Hajdo, L.E. 1994. Formation Damage of an Unconsolidated Reservoir During Steamflooding. Society of Petroleum Engineers. http://dx.doi.org/10.2118/27385-MS

Hein, F.J., Cotterill, D.K., and Berhane, H. Earth Sciences Report 2000-07. An Atlas of Lithofacies of the McMurray Formation, Athabasca Oil Sands Deposit, Northeastern Alberta: Surface and Subsurface.

Hower, W.F. 1974. Influence of Clays on the Production of Hydrocarbons. Society of Petroleum Engineers. http://dx.doi.org/10.2118/4785-MS

Kia, S.F., Fogler, H.S., and Reed, M.G. 1987. Effect of Salt Composition on Clay Release in Berea Sandstones. Society of Petroleum Engineers. http://dx.doi.org/10.2118/16254-MS

Kumar, M. and Hong, K.C. 1992. Effects of Wellbore Steam Segregation on Steamflood Performance. Society of Petroleum Engineers. http://dx.doi.org/10.2118/18086-PA

Li, L., Nasr-El-Din, H.A., Chang, F.F. et al. 2008. Reaction of Simple Organic Acids and Chelating Agents with Calcite. International Petroleum Technology Conference. http://dx.doi.org/10.2523/12886-MS

Lim, K.T., Ramey, H.J., and Brigham, W.E. 1992. Steam Distillation and Oil Quality Change During Thermal Oil Recovery. Society of Petroleum Engineers. http://dx.doi.org/10.2118/23718-MS

Liu, D., Zhang, H., Chen, X. et al. 2006. Field Tests of Sulfide Removing Biologically in Surface Systems. Society of Petroleum Engineers. http://dx.doi.org/10.2118/102696-MS

Mahmoud, M.A., Nasr-El-Din, H.A., and DeWolf, C.A. 2011. Removing Formation Damage and Stimulation of Deep Illitic-Sandstone Reservoirs Using Green Fluids. Society of Petroleum Engineers. http://dx.doi.org/10.2118/147395-MS

Mehra, O. P. and Jackson, M. L. (1960). Iron oxide removal from soils and clays by dithionite-citrate system buffered with sodium bicarbonate. Clays and Clay Minerals, 7.

Nasr, T.N., Golbeck, H., Korpany, G. et al. 1998. SAGD Operating Strategies. Society of Petroleum Engineers. http://dx.doi.org/10.2118/50411-MS

Nasr-El-Din, H.A., de Wolf, C.A., Bouwman, A. et al. 2012. A New, Low Corrosive Fluid to Stimulate Wells with Carbon Steel Tubular and Internals. Society of Petroleum Engineers. http://dx.doi.org/10.2118/160849-MS

Nengkoda, A., Mandhari, M.S., Ahmed, D. et al. 2008. Scaling Mitigation and Strategy for First Full Field Steam Injection Qarn Alam: History Matching and Modelling. Society of Petroleum Engineers. http://dx.doi.org/10.2118/113392-MS

Okoye, C.U., Onuba, N.L., Ghalambor, A. et al. 1990. Characterization of Formation Damage in Heavy Oil Formation During Steam Injection. Society of Petroleum Engineers. http://dx.doi.org/10.2118/19417-MS

Okoye, C.U., Onuba, N.L., Ghalambor, A. et al. 1991. Formation Damage in Heavy-Oil Formation During Steamflooding. Society of Petroleum Engineers. http://dx.doi.org/10.2118/22980-MS

Okoye, C.U., Onuba, N.L., Ghalambor, A. et al. 1992. An Experimental Investigation of Formation Damage in Heavy Oil Reservoir During Steam Injection. Society of Petroleum Engineers. http://dx.doi.org/10.2118/23781-MS

Ostroff, A.G. 1981. Injection Water Problems Identified By Laboratory Analysis. Society of Petroleum Engineers. http://dx.doi.org/10.2118/9632-MS

Ouled Ameur, Z. and Husein, M.M. 2012. Salting-Out Induced Aggregation for Selective Separation of Vanadyl-oxide Tetraphenyl-porphyrin from Heavy Oil. Energy & Fuels 26 (7): 4420-4425.

Parkhurst, D.L. and Appelo, C.A.J. 2013. Description of input and examples for PHREEQC version 3 — A computer program for speciation, batch-reaction, one-dimensional transport, and inverse geochemical calculations: U.S. Geological Survey Techniques and Methods, book 6, chap. A43, 497 p., available only at http://pubs.usgs.gov/tm/06/a43.

Parkinson, M., Munk, T.K., Brookley, J.G. et al. 2010. Stimulation of Multilayered High-Carbonate-Content Sandstone Formations in West Africa Using Chelant-

Based Fluids and Mechanical Diversion. Society of Petroleum Engineers. http://dx.doi.org/10.2118/128043-MS

Rabie, A., Mahmoud, M.A., and Nasr-El-Din, H.A. 2011. Reaction of GLDA with Calcite: Reaction Kinetics and Transport Study. Society of Petroleum Engineers. http://dx.doi.org/10.2118/139816-MS

Rae, P., and Di Lullo, G. 2003. Matrix Acid Stimulation - A Review of the State-Of-The-Art. Society of Petroleum Engineers. http://dx.doi.org/10.2118/82260-MS

Reyes, E.A., Smith, A.L., and Beuterbaugh, A. 2013. Properties and Applications of an Alternative Aminopolycarboxylic Acid for Acidizing of Sandstones and Carbonates. Society of Petroleum Engineers. http://dx.doi.org/10.2118/165142-MS

Rogers, B.A., Burk, M.K., Stonecipher, S.A. 1998. Designing a Remedial Acid Treatment for Gulf of Mexico Deepwater Turbidite Sands Containing Zeolite Cement. Society of Petroleum Engineers. http://dx.doi.org/10.2118/39595-MS

Schechter, R.S. 1992. Oil Well Stimulation, Chapter 18, 528-547. Eaglewood Cliffs, New Jersey: Prentice-Hall.

Smith, R.M., Martell, A.E., and Motekaitis, 2004. NIST Critically Selected Stability Constants of Metal Complexes database version 8.0 for Windows. NIST Standard Reference Database 46, U.S. Department of Commerce, Technology Administration, National Institute of Standards and Technology , Standard Reference Data Program , Gaithersburg, MD 20899, http://www.nist.gov/srd/nist46.cfm

Sokhanvarian, K., Nasr-El-Din, H.A., Wang, G. et al. 2012. Thermal Stability of Various Chelates That Are Used In The Oilfield And Potential Damage Due To Their Decomposition Products. Society of Petroleum Engineers. http://dx.doi.org/10.2118/157426-MS

Stolyarov, S. and Alam, A. 2013. Overcoming Challenges while Acidizing Sandstone Formation Successfully in the Gulf of Cambay, Offshore India. Society of Petroleum Engineers. http://dx.doi.org/10.2118/164631-MS

Thomas, R.L. and Crowe, C.W. 1978. Single-Stage Chemical Treatment Provides Stimulation And Clay Control In Sandstone Formations. Society of Petroleum Engineers. http://dx.doi.org/10.2118/7124-MS

Thomas, R.L., Nasr-El-Din, H.A., Lynn, J.D. et al. 2001. Precipitation During the Acidizing of a HT/HP Illitic Sandstone Reservoir in Eastern Saudi Arabia: A Laboratory Study. Society of Petroleum Engineers. http://dx.doi.org/10.2118/71690-MS

Thornton, S.D. and Radke, C.J. 1988. Dissolution and Condensation Kinetics of Silica in Alkaline Solution. Society of Petroleum Engineers. http://dx.doi.org/10.2118/13601-PA

Wang, S., McMahon, J., and Wylde, J. 2010. Scale Inhibitor Solutions for High Temperature Wells In A Steam Drive Reservoir. NACE International.

Whittig, L. D. (1965). X-ray diffraction techniques for mineral identification mineralogical composition. In Black, C. A., editor, Methods of soil analysis. Part

1. Physical and mineralogical properties, including statistics of measurements and sampling. American Society of Agronomy, Madison, WI.

Yang, F., Nasr-El-Din, H.A., and Harbi, B.A. 2012. Acidizing Sandstone Reservoirs Using HF and Organic Acids. Society of Petroleum Engineers. http://dx.doi.org/10.2118/157250-MS

Young, B.M., McLaughlin, H.C., and Borchardt, J.K. 1980. Clay Stabilization Agents - Their Effectiveness in High-Temperature Steam. Society of Petroleum Engineers. http://dx.doi.org/10.2118/7895-PA

Zhou, L. and Nasr-El-Din, H.A. 2013. Acidizing Sandstone Formations Using a Sandstone Acid System For High Temperatures. Society of Petroleum Engineers. http://dx.doi.org/10.2118/165084-MS